

Towards H₂ selective porous inorganic membranes: Pore size control through combined Sol-Gel and Atomic Layer Deposition Processes

PROEFSCHRIFT

ter verkrijging van de graad van doctor

aan de Technische Universiteit Delft,

op gezag van de Rector Magnificus prof. ir. K.C.A.M. Luyben,

voorzitter van het College voor Promoties,

in het openbaar te verdedigen op vrijdag 16 december 2011 om 10.00 uur

door

Thi Hoang Yen TRAN

Master en Chimie appliquée à la Formulation & aux Traitements de Surface,

Université Besançon, France

Geboren te Da Lat, Vietnam

Dis proefschrift is goedgekeurd door de promotor:

Prof. Dr. J. Schoonman

Copromotor: Dr. W.G. Haije

Samenstelling promotiecommissie:

Rector Magnificus	Voorzitter
Prof. Dr. J. Schoonman	Technische Universiteit Delft, promotor
Dr. W. G. Haije	Technische Universiteit Delft, copromotor
Prof. Dr. B. Dam	Technische Universiteit Delft
Prof. Dr. F. Kapteijn	Technische Universiteit Delft
Prof. Dr. Ir. A. Nijmeijer	Technische Universiteit Twente
Prof. Dr. C. Filiatre	UFR des Sciences & Techniques de Université Besançon
Dr. H. Schut	Technische Universiteit Delft

The research described in this thesis was carried out in *Materials for Energy Conversion and Storage (MECS) group*, Chemical Engineering, Faculty of Applied Science, at Delft University of Technology. Financial support is provided by the Stanford Global Climate and Energy Project (GCEP) in the framework of “Advanced Membrane Reactors in Energy Systems; A carbon-free conversion of fossil fuels”, subcontract number: 15619740-34891.

ISBN 978-94-6108-243-5 Copyright ©2011 by T.H.Y. Tran. All rights reserved.

Printed by Gildeprint Drukkerijen, Enschede, The Netherlands.

This thesis is dedicated to my grandmother

CHAPTER 361

STRUCTURAL CHARACTERIZATION AND POROSITY ANALYSIS IN SELF-SUPPORTED POROUS ALUMINA-SILICA THIN FILMS61

3.1	INTRODUCTION	62
3.2	EXPERIMENTAL DETAILS.....	63
3.2.1	<i>Thin film synthesis</i>	63
3.2.2	<i>Characterization</i>	64
3.3	RESULTS AND DISCUSSION	67
3.4	CONCLUSIONS.....	74

CHAPTER 479

HYDROGEN SEPARATION PROPERTIES OF A SOL-GEL DERIVED ZIRCONIA MEMBRANE WITH PORE SIZES TUNED USING ATOMIC LAYER DEPOSITION OF ALUMINA79

4.1	INTRODUCTION	80
4.2	EXPERIMENTAL DETAILS.....	82
4.2.1	<i>Preparations of zirconia thin-films and membranes</i>	82
4.2.2	<i>Alumina deposition using TMA and H₂O precursors</i>	82
4.2.3	<i>Characterization</i>	83
4.2.4	<i>Gas permeation tests</i>	84
4.3	RESULTS AND DISCUSSION.....	85
4.3.1	<i>The effects of alumina deposition on the pore size of unsupported zirconia membranes</i>	85
4.3.2	<i>Membrane permeation and separation experiments</i>	90
4.3.3	<i>Membrane surface characterization</i>	93
4.3.4	<i>Pore size analysis on supported membranes</i>	93
4.4	CONCLUSIONS.....	94

CHAPTER 599

PLASMA-ENHANCED ATOMIC LAYER DEPOSITION OF TITANIA ON ALUMINA FOR ITS POTENTIAL USE AS A HYDROGEN-SELECTIVE MEMBRANE.....99

5.1	INTRODUCTION	100
-----	--------------------	-----

5.2	EXPERIMENTAL DETAILS.....	101
5.2.1	γ -Al ₂ O ₃ membrane preparation.....	101
5.2.2	Plasma-enhanced ALD of TiO ₂	102
5.2.3	Characterization.....	103
5.3	RESULTS AND DISCUSSION	103
5.3.1	Membrane surface characterization.....	103
5.3.2	Pore size analysis.....	105
5.3.3	Membrane permeation properties.....	106
5.4	CONCLUSIONS.....	111
CHAPTER 6.....		115
ATOMIC LAYER DEPOSITION OF TiO₂ FILMS ON PLANAR DENSE AND POROUS SUBSTRATES		115
6.1	INTRODUCTION	116
6.2	EXPERIMENTAL.....	117
6.2.1	Mesoporous titania membrane preparations.....	117
6.2.2	ALD of TiO ₂ using TiI ₄ and H ₂ O precursors	118
6.2.3	ALD of TiO ₂ using TDMAT and H ₂ O precursors.....	121
6.2.4	Porosity analysis and structural characterization.....	125
6.2.5	Gas permeation.....	125
6.2.6	Atomic Force Microscopy.....	126
6.2.7	Spectroscopic ellipsometry (SE)	126
6.3	RESULTS AND DISCUSSION	127
6.3.1	Sol-gel derived titania membrane.....	127
6.3.2	Gas separation behavior of modified membranes obtained via ALD of TiO ₂ by using TiI ₄ and H ₂ O as precursors	130
6.3.3	Growth kinetics of the TDMAT/ H ₂ O process.....	131
6.3.4	Gas separation behavior of modified membranes via ALD of TiO ₂ by using TDMAT and H ₂ O as precursors.....	136
6.4	CONCLUSIONS.....	138
CHAPTER 7.....		143
SUMMARY AND OUTLOOK.....		143

7.1	SUMMARY	144
7.2	OUTLOOK.....	146
SAMENVATTING EN VOORUITBLIK.....		149
7.3	SAMENVATTING	150
7.4	VOORUITBLIK	152
ACKNOWLEDGMENTS.....		155
LIST OF PUBLICATIONS		157
CURRICULUM VITAE		161

Chapter 1

General introduction

Abstract

The concept of a hydrogen (H_2) economy, a situation where besides electricity, H_2 is used as a clean energy carrier, is a hot topic because of its pollution-free characteristics, its production from diverse energy resources (both fossil and renewable sources), and easy and efficient conversion to electricity via fuel cells or directly in gas turbines. Currently, H_2 is primarily produced via coal gasification, steam methane reforming, and water gas-shift processes. During the transition to a non-fossil fuel-based energy economy, fossil fuels will continue to be at the basis of H_2 production. Carbon dioxide (CO_2) capture and storage is then necessary for the H_2 to be considered a “low-carbon” energy carrier.

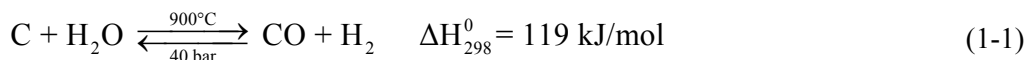
Membrane technology can play an important role in H_2/CO_2 separation. The key advantage for membrane applications is the possibility to go beyond the thermodynamic limits set by the equilibrium constant of the H_2 production reactions. The in-situ separation of H_2 from the gas mixture through membranes shifts the equilibrium toward higher production of H_2 , thereby preventing the back reaction. At the same time a pure stream of CO_2 is produced ready for storage in empty gas or oil fields, or aquifers.

This introductory chapter provides a more in-depth view of the potential application of membranes in H_2 separation from CO and CO_2 . It further presents the focus of the research in this thesis.

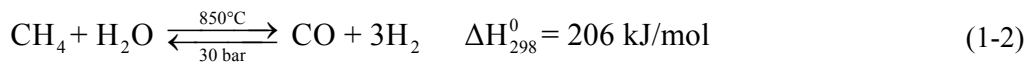
1.1 Introduction

The consequences of using fossil fuels for energy purposes are believed to have a strong adverse impact on the environment. The combustion of the fossil fuels releases greenhouse gases into the atmosphere. Carbon dioxide (CO₂) is such a greenhouse gas, which prevents heat radiation back to space, leading to a gradual temperature rise, hence climate change, and degradation of the natural environment ^[1]. The rapid growth in consumption of fossil fuels has furthermore accelerated the exhaustion of their reserves, especially oil and gas. Economic dependence on these fossil fuels intensifies the demand and leads to political tensions not only in the oil-rich regions, e.g., the Middle East ^[2, 3], but also between the oil suppliers and the Western world. Therefore, it is urgent to switch to alternative energy sources which are both clean and sustainable. The potential of hydrogen (H₂) as an environmentally clean energy carrier, i.e., the only combustion product being water, has attracted a lot of attention world-wide. Currently, H₂ is produced from steam reforming of coal, natural gas, hydrocarbons, biomass, and from water splitting. This diversification of sources significantly contributes to the security of energy and thus the H₂ supply. Thanks to technological maturity and the availability of the feedstock, there is already significant industrial scale H₂ production from coal gasification and steam reforming of natural gas (methane (CH₄) is its principal constituent) ^[2, 3]. Usually, the commercial production involves two main steps. The first step is the steam reforming of the fuel to the syngas, mainly consisting of carbon monoxide, CO, and H₂ as shown in the following chemical reactions:

(a) Coal gasification (CG)

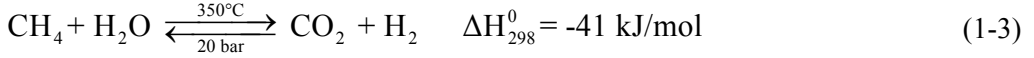


(b) Steam-methane reforming (SMR)

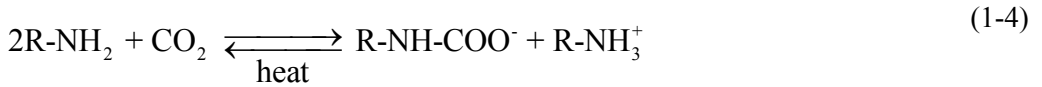


In the second step, CO in the syngas is converted into CO₂ and H₂ via the water-gas-shift (WGS) reaction:

(c) Water-gas-shift (WGS)



Regarding the abundance of coal reserves in the USA, Eastern Europe, South Africa, and China and a soaring price of natural gas, H₂ production from coal gasification (CG) can become competitive with steam-methane reforming (SMR). SMR contributes so far about 40% to the world's H₂ production. Where H₂ is produced from GC or SMR, CO₂ capture and storage (CCS) [4-6] is necessary for the H₂ processes to be considered a “carbon-free” energy supply. In power plants three main methods of CO₂ capture have been investigated as shown in Figure 1-1. These methods, namely post-combustion capture, pre-combustion capture, and oxyfuel-combustion [4-6] can be adopted in different types of power plants. In post-combustion capture, electricity is generated from the syngas and CO₂ in the flue gas is absorbed chemically by an amine-based sorbent. The amine-based sorbent reacts with CO₂ to form a carbamate as follows:



The weakly bonded carbamate is heated in which the original amine-based sorbent is recovered and the released CO₂ is ready for storage. For example, the heat in the CO₂-ethanolamine (CH₂CH₂OHNH₂) absorption system is ~ 2 MJ per kg CO₂ [7]. Since CO₂ is captured “end-of-the-pipe” from the flue gas, the process can be easily installed and the CO₂ obtained has a very high concentration (~ 98%). However, it requires a relatively high amount of heat to break down the carbamate in order to recover the sorbent and release CO₂. Therefore, post-combustion capture has a high energy penalty of ~ 12 percentage points. Application of CO₂ capture from pre-combustion systems can involve physisorption processes such a glycol-based absorbent called Selexol. This process is particularly integrated with gasification plants. After the CG and the WGS reactions, the syngas is sent to a Selexol unit where the CO₂ is absorbed into Selexol

and H_2 is combusted downstream to generate electricity. Unlike the carbamate in the post-combustion capture, the bonding between Selexol and CO_2 is relatively weaker, so it requires less energy to unload CO_2 from the adsorbent and leads to an energy penalty of ~ 10 percentage points. Another approach is oxyfuel combustion where the coal or natural gas is burned using high purity oxygen instead of air. This process results in a flue gas consisting mainly of water vapour and CO_2 . After condensation of H_2O , the CO_2 stream is ready for storage. Compared to post-combustion and pre-combustion captures, the energy penalty is still large although no heat has to be added to unload carbon dioxide from absorbents, huge amounts of oxygen have to be produced giving rise to the penalty value of ~ 10 percentage points. Since the combustion with pure oxygen is a highly exothermic reaction, high temperature resistant materials must be used in such power plants. To finally get rid of the captured CO_2 it is pressurized and transported to the storage site, e.g., geologic formations such as deep coal seams, depleted oil and empty gas reservoirs, the deep ocean, and aquifers. Many studies consider that CCS is technically and economically feasible only for large point sources, such as power and chemical plants ^[8]. It is estimated that these plants contribute half of the total CO_2 emissions to the atmosphere while the other half is due to domestic sources and transportation. Therefore, in the transition from a fossil fuel-based to a future H_2 economy, CG and SMR associated with CCS provide a carbon lean H_2 fuel supply for commercial H_2 -based technologies ^[9].

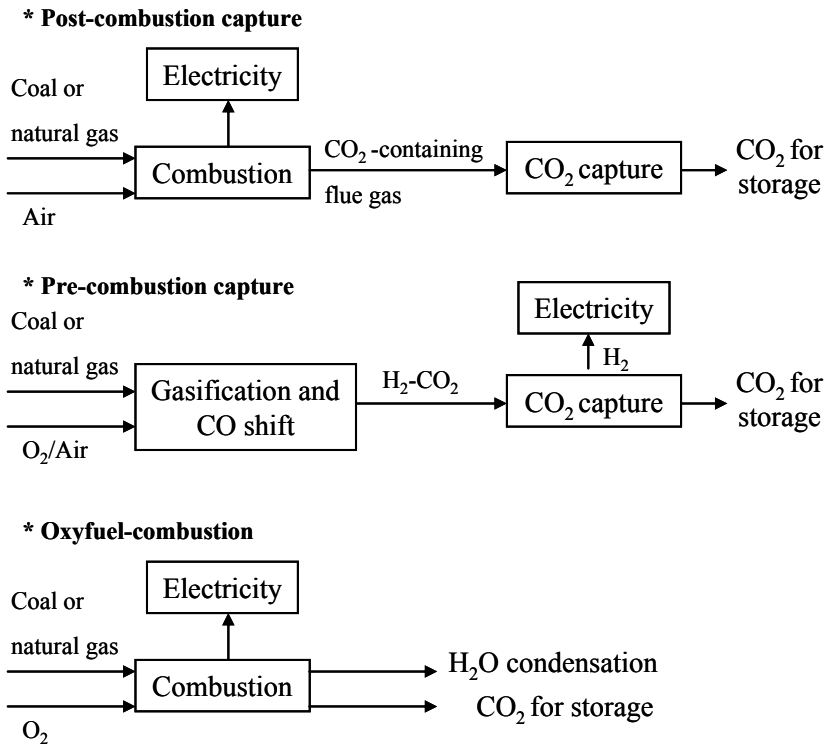


Figure 1-1: Three basic routes for CO₂ capture and storage. ^[4-6]

For the separation and purification of H₂ (Figure 1-1), membrane separation is considered to be an energy-efficient alternative to the conventional options, such as pressure swing adsorption (PSA) and cryogenic distillation ^[10, 11] which are also expensive and induce a larger efficiency penalty (up to 20%). Under normal conditions, CG and SMR are endothermic reactions (reactions (1-1 and 1-2) and WGS is an exothermic (reaction 1-3). H₂ generated from these reactions is removed by using H₂-selective membranes. Integrating a H₂-selective membrane within the reaction zone is referred to as a membrane reactor. The advantages of such an integrated system are:

- The inherent ability to combine the reactions and H₂ separation in a single unit reduces the size of the process equipment significantly.
- Continuous H₂ removal shifts the equilibrium towards the product side. As a consequence, an effective conversion of coal or CH₄, and CO shift occurs, thereby yielding higher H₂ production, and more importantly, at milder reaction conditions (~

500°C and 1 MPa ^[12]). This is referred to as a separation-enhanced reaction. This makes it possible to operate at optimum temperature and pressure and reduces the efficiency penalty. After separating H₂, CO₂ is kept at high pressure in the flue gas stream, which thus reduces the CO₂ compression energy needed for transportation and storage.

The principle of a membrane reactor, in which the steam-reforming reaction and the separation occur simultaneously, is illustrated in Figure 1-2. A single step or two-step reforming (SMR or/and WSG) takes place on the catalyst and H₂ permeates selectively through the membrane to the permeate side. Besides the non-recovered CH₄, CO, excess H₂O, and a small amount of H₂, CO₂ remains in the retentate side. This predominantly CO₂ containing stream could be ready for transport and eventually storage. In addition, a sweep gas stream, i.e., steam can be used at the permeate side for improving the H₂ permeation driving force. H₂-selective membranes show potential benefits in SMR and WGS, such as lowering the reaction temperature to ~ 500°C, enhancing the conversion of CH₄ to CO₂, and H₂ ^[12-15] ~ 85% instead of 75%, providing 99.99% H₂ ^[12] and a nearly pure CO₂ stream ready for storage. Without the H₂ separation step, the same value of CH₄ conversion can only be achieved at ~ 850°C.

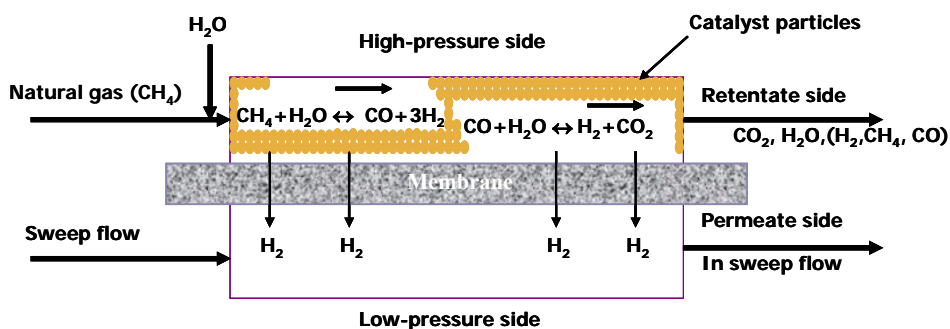


Figure 1-2: Schematic representation of a membrane reactor for MSR and WGS.

1.2 State-of-the-art inorganic membranes for hydrogen separation

Inorganic membranes can be classified by their composition and pore size d_p . One can distinguish non-porous (dense) membranes or porous membranes, i.e., microporous ($0.5 < d_p < 2$ nm), mesoporous ($2 < d_p < 50$ nm), and macroporous ($d_p > 50$ nm) using the International Union of Pure and Applied Chemistry (IUPAC) definition^[16].

Dense metallic membranes such as palladium and its alloys intrinsically have 100% selectivity to H_2 ^[17, 18]. Based on a *solution-diffusion mechanism*, H_2 molecules are dissociated into protons and electrons that are subsequently transported through the membrane, after which the protons and electrons are re-combined at the permeate side. However, a pure Pd membrane suffers from H_2 embrittlement due to the phase transition between the α - and β -hydride form in H_2 -containing environment and poisoning effects of sulphur (H_2S) and CO, which lead to membrane degradation. The chemical stability of the Pd membranes can be improved by alloying the Pd with other metals such as silver (Ag)^[19] or copper (Cu). Currently, Pd and Pd-alloy membranes are used only when ultra-pure H_2 is needed and only in the purification step because of their low-resistance towards H_2S and CO. Many research groups have investigated the preparation of robust thin Pd-based membranes with long-term stability under operating conditions, high flux, and selectivity.

Compared to dense membranes, microporous membranes have higher H_2 permeability. In fact, the flux is directly proportional to the pressure difference, whereas in dense Pd-based membranes it is proportional to the difference between the square roots of the feed and permeate pressures. Hence, microporous membranes become the more attractive option for H_2 separation. Several types of micro-porous membranes for H_2 separation can be distinguished based on the membrane materials, i.e., polymeric and inorganic membranes. In microporous membranes, the H_2 permeation can occur by different mechanisms: Knudsen diffusion, surface diffusion, capillary condensation, and micropore molecular sieving. In *Knudsen diffusion*^[20], the pore size is such that the diffusing species collide more frequently with the pore wall than with other diffusing molecules. With surface diffusion, molecules adsorb on the surface of the

pores and subsequently move from one site to another of lower concentration. *Capillary condensation* occurs when the pore size and the interactions of the gas molecules with the pore walls cause condensation in the pore that negatively influences the rate of diffusion through the membrane. *Micropore molecular sieving* ^[5] occurs when the pore size approaches the size of the diffusing molecules. The gas separation can be controlled by the much higher diffusion rates of the smallest molecule, but also by adsorption capacities for similarly sized molecules such as O₂ and N₂. The rate of diffusion is determined by an activation energy, thus the diffusion is referred to as activated diffusion. Given the high temperatures for SMR to occur, there is still a need to improve the thermal stability of inorganic membranes, while polymeric membranes ^[21] are successfully used for hydrogen separation at low temperatures. Amorphous microporous silica membranes prepared by the sol-gel technique exhibit very high H₂ fluxes due to their small thickness of >30 nm ^[22, 23]. H₂ transport through the membrane presumably occurs by hopping diffusion on a connected micropore system. De Vos et al. ^[24] used this diffusion mechanism to explain that the pore size of the microporous supported silica membranes can be estimated from the relation between the permeance and the kinetic diameter of the gases used. Microporous silica membranes prepared by Chemical Vapor Deposition (CVD) have yielded exceptionally high H₂ selectivities ^[23, 25], with the best H₂/CO₂ selectivity up to 1200 ^[26]. To make the silica membranes a viable option for application in steam reforming, material stability improvements are needed to avoid densification and structural changes under these hydrothermal conditions ^[27]. The molecular- sieve zeolite membranes ($d_p = 0.3\text{--}0.6$ nm) are a relatively new class of membranes ^[28-30] which have attracted considerable interest because of their substantially higher hydrothermal stability and potential to achieve both high selectivity and permeance for H₂. For such small pore sizes, the permeation through the membrane is expected to change from Knudsen-type diffusion to configurationally activated diffusion (activated diffusion based on molecular sieving) ^[31, 32]. Due to the inherent existence of the voids between zeolite grains and difficulty in reducing the membrane thickness without forming pinholes, zeolite membranes exhibit an incompatibility between H₂ selectivity and flux.

In recent years, there have been some preliminary studies on the state-of-the-art in silica membrane reactors. Giessler et al. ^[33] studied hydrophobic and hydrophilic silica membranes for WGS. The hydrophobic membranes presented very high hydrogen permeation fluxes at 250°C, which reinforces the idea that higher flow rates and high conversion can be obtained with such membrane reactors as compared to a conventional reactor. At higher temperature (280°C) another silica membrane ^[34] exhibited 95% CO conversion, which was achieved at 4×10^5 Pa.

From a general point of view, further technological breakthroughs in the processing of inorganic membranes are necessary before commercialization is feasible. There are quite a lot of different membranes that could be used to this end. While polymeric membranes are commercially used for H₂ separation at low temperatures (<250°C) with H₂/CO selectivity in the range 21-30, there is still a need to improve their thermal stability in high-temperature processes such as SMR. In comparison to their Pd and polymeric counterparts, ceramic membranes are not adversely affected by elevated operating temperatures and have higher chemical resistance, which make them good candidates for H₂ separation in reforming processes, provided they exhibit high (hydro)thermal stability.

1.3 Motivation and scope of the thesis

The objective of this thesis is to develop membranes to separate H₂ from CO₂ or CO under steam reforming or water-gas-shift conditions. The supported membrane concepts, synthesis methods, and attempts to provide an H₂-selective membrane will be discussed further. The research was carried out in the framework of the project “*Advanced Membrane Reactors for Carbon-Free Fossil Fuel Conversion*”, which appertained to the Global Climate & Energy Project (GCEP) ^[35] and was coordinated by Stanford University.

Considering the desired aspects for H₂ selective membranes such as high H₂ flux, robustness, reasonable cost, and high selectivity, microporous inorganic membranes are the most promising in steam-reforming processes at high temperatures. The state-of-the-art microporous silica membranes prepared by sol-gel and CVD methods ^{[22-25,}

^{36]} have good separation properties in H_2 separation but suffer from severe hydrothermal instability. Because in steam-reforming processes hydrothermal conditions ($\sim 500^\circ\text{C}$ and 1 MPa) are imposed, it is necessary to find alternative materials with higher stability. From the point of view of hydrothermal stability, materials such as Al_2O_3 , TiO_2 , and ZrO_2 have potential for this application. However, most of them are as mesoporous prepared ^[37-39], hence, the selectivity of the membrane is expected to be higher if the mesopore dimension can be tuned to the microporous range. According to the kinetic diameters of the gaseous species as shown in Figure 1-3, H_2 can be separated from a mixture of CO and CO_2 which is based on the difference in size rather than molecular weight.

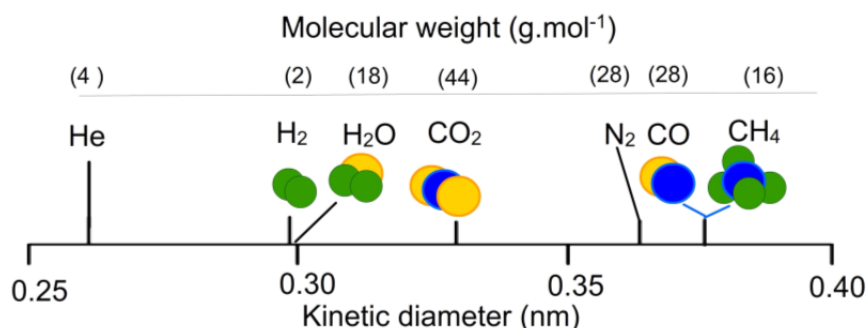


Figure 1-3: Properties of some small gaseous molecules.

It is very challenging and difficult to fabricate a thin porous membrane with pore sizes large enough for H_2 molecules to pass through but small enough to effectively prevent other molecules (CO_2 , CO, and H_2O) from entering the pores, based on the kinetic diameters which are very close to each other. According to literature data ^[40], the separation of H_2 from molecules like CO_2 , CO, and CH_4 relies on the competition between molecular diffusivity and/or the molecular sieving effect when the pore sizes are in the 0.5 nm range. This situation gives H_2 selectivity over other small gases, e.g., CO_2 and CO, which is expected higher than their Knudsen selectivity of 4.69 and 3.74, respectively. The Knudsen diffusion-governed selectivity (α_K) is determined by the molecular weight (M) of H_2 , CO_2 , and CO, which is given by:

$$\alpha_{K_{H_2/CO_2(or CO)}} = \sqrt{M_{CO_2(or CO)} / M_{H_2}} = \sqrt{M_{CO_2(or CO)} / 2} \quad (1-5)$$

Therefore, in order to be effective for H_2 selectivity over the other gases, the membrane pore size should be less than 1 nm^[40, 41]. With such small pores, the membrane should be thin (preferred to <100 nm) in order to have a high H_2 permeability. Such a thin membrane is too fragile to support itself and the mechanical strength of the membrane must be high enough to withstand the applied pressure difference. These considerations lead to the concept of an asymmetric porous membrane consisting of several layers^[40, 41]. In this thesis, the composite membrane system has the architecture of three layers at least as illustrated in Figure 1-4.

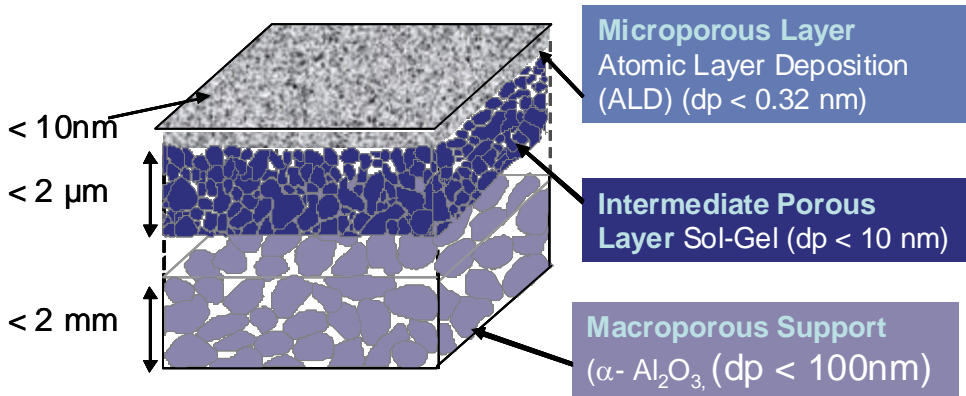


Figure 1-4: Architecture of the envisioned membranes.

The following steps describe how to reach the structural design of this type of membrane:

- Commercial macroporous α - Al_2O_3 with thickness of < 2 mm and pore size of 100 nm is used as a membrane support. This support provides the required mechanical strength (withstands many bars of pressure difference) and does not impose mass transfer resistance due to its large pore size.

- An intermediate layer (thickness $<2\ \mu\text{m}$) using the sol-gel method is coated on the support in order to reduce the pore size of the support to mesoporous sizes ($d_p < 10\ \text{nm}$). This process provides a homogeneous layer with a narrow pore size distribution and sufficient smoothness for the deposition of a microporous top layer. These are important in order to diminish support derived defects, minimize several processing steps of the deposition of the microporous layer and thus partially control the intrinsic separation selectivity and permeability of the membrane.

- A microporous layer preferably with thickness of $<10\ \text{nm}$ is deposited in order to modify the mesopores of the intermediate layer by growing a metal oxide layer (Al_2O_3 or TiO_2) either on the internal pore surface or at the entrances of the pores with Atomic Layer Deposition (ALD). The ALD process has been investigated because it allows thin metal-oxide films to be deposited onto complex porous substrates with a highly conformal film coverage ^[42-46]. In an ideal case, the ALD of Al_2O_3 or TiO_2 can be performed with monolayer precision to reduce the mesopore size to the desired dimension ($d_p < 1\ \text{nm}$) and, thereby improving the H_2 selectivity property of membranes. In general, it is quite difficult for the sol-gel method to satisfy the requirement of producing a membrane with a thickness of a few tens of nanometers. Thus ALD is a key deposition process for molecular level control of the film thickness and nanostructure of the top layer membrane. Moreover, the ALD technique has not been widely used to develop H_2 -selective membranes.

The two methods, e.g., the sol-gel and ALD process (see Figure 1-5), can be optimized independently and will be discussed in this thesis. As the proof of the pudding, the synthesized membranes are evaluated for H_2 separation performances in single and mixed gas permeation tests.

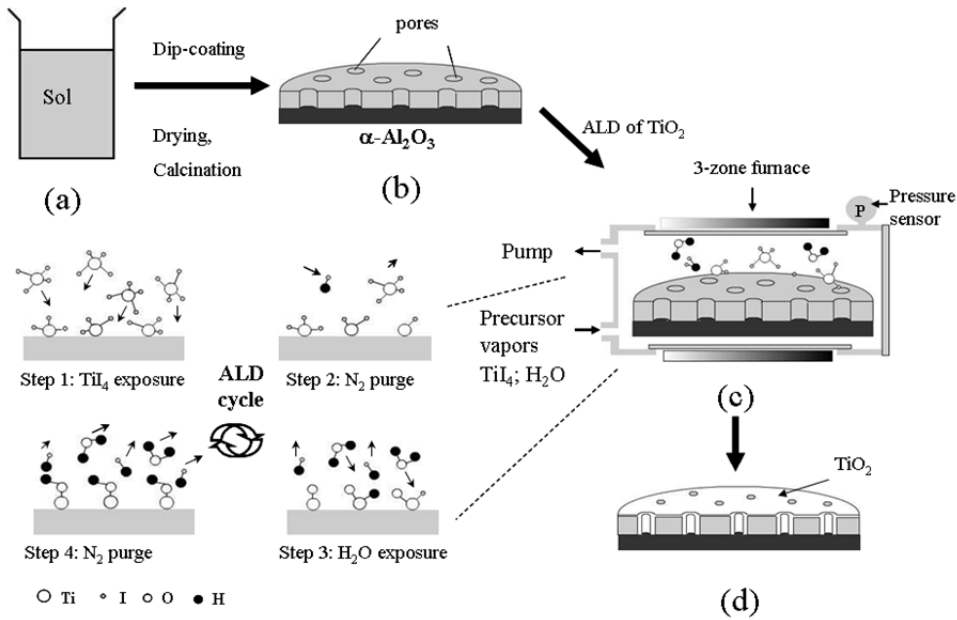


Figure 1-5: Schematic of the architecture of the membrane which includes (a) sol prepared with sol-gel technique, (b) sol-gel derived membrane, (c) Atomic layer deposition (ALD) of TiO_2 with TiI_4 and H_2O precursors, (d) TiO_2 modified sol-gel membrane.

1.4 Organization of the thesis

The thesis consists of 7 chapters as listed in Table of Contents. An introductory literature review is focused on H_2 production and membrane separation technology as discussed previously. This chapter 1 includes the problem definition in order to provide the basis and rationale to identify the research directions in this work.

Chapter 2 provides essential information on the preparation methods of the membranes, especially the sol-gel and ALD processes. The characterization techniques are also presented in this chapter.

In chapter 3, the synthesis procedures and characterization of alumina, silica, and hybrid alumina-silica thin films are described. Incorporation of alumina into the silica structure is proposed and its influence on microstructure and pore size is investigated by positron annihilation and N_2 physisorption experiments.

Chapter 4 is dedicated to research the results of ALD modification on the pore sizes of zirconia membranes. The influence of alumina deposition (cycle numbers) on the gas separation properties was studied with H_2/CO_2 mixtures.

In chapter 5, the combination of sol-gel of γ -alumina and plasma-enhanced ALD of titania for preparing an alumina-titania membrane is discussed with respect to H_2 selectivity and separation.

Chapter 6 deals with the deposition of titania from TiI_4/H_2O and $Ti(N(CH_3)_2)_4/H_2O$ processes in home-built ALD systems. The study on the gas permeation characteristics of the ALD modified membranes is presented. In addition, the in-situ growth-rate study of titania using ellipsometry is described.

Finally, in chapter 7, summary and future outlook are given with respect to the obtained results, advantages, and possible applications. All chapters have been written as separate chapters, which can, therefore, be read individually and as a consequence some information is duplicated.

References

- [1] Stott, P. A., Huntingford, C. H. R. I., Jones, C. D., and Kettleborough, J. A., "Observed climate change constrains the likelihood of extreme future global warming", *Tellus B*, Vol. 60, No. 1, 2008, pp. 76-81.
- [2] BP, "Statistical Review of World Energy," 2009.
- [3] World Coal Institute, "The coal resource: a comprehensive overview of coal," London, UK, 2005.
- [4] Yang, H. Q., Xu, Z. H., Fan, M. H., Gupta, R., Slimane, R. B., Bland, A. E., and Wright, I., "Progress in carbon dioxide separation and capture: A review", *Journal of Environmental Sciences*, Vol. 20, No. 1, 2008, pp. 14-27.
- [5] Ebner, A. D. and Ritter, J. A., "State-of-the-art Adsorption and Membrane Separation Processes for Carbon Dioxide Production from Carbon Dioxide Emitting Industries", *Separation Science and Technology*, Vol. 44, No. 6, 2009, pp. 1273-1421.

- [6] Davison, J. and Thambimuthu, K., "An overview of technologies and costs of carbon dioxide capture in power generation", *Proceedings of the Institution of Mechanical Engineers Part A-Journal of Power and Energy*, Vol. 223, No. A3, 2009, pp. 201-212.
- [7] Rackley, A. S., *Carbon capture and storage*, Elsevier ed., Butterworth-Heinemann 2009.
- [8] Muradov, N. Z. and Veziroglu, T. N., "From hydrocarbon to hydrogen-carbon to hydrogen economy", *International Journal of Hydrogen Energy*, Vol. 30, No. 3, 2005, pp. 225-237.
- [9] Goto, S., Tagawa, T., Assabumrungrat, S., and Praserttham, P., "Simulation of membrane microreactor for fuel cell with methane feed", *Catalysis Today*, Vol. 82, No. 1-4, 2003, pp. 223-232.
- [10] Sircar, S. and Golden, T. C., "Purification of hydrogen by pressure swing adsorption", *Separation Science and Technology*, Vol. 35, No. 5, 2000, pp. 667-687.
- [11] Huang, C. P. and Raissi, A., "Analyses of one-step liquid hydrogen production from methane and landfill gas", *Journal of Power Sources*, Vol. 173, No. 2, 2007, pp. 950-958.
- [12] Shirasaki, Y., Tsuneki, T., Ota, Y., Yasuda, I., Tachibana, S., Nakajima, H., and Kobayashi, K., "Development of membrane reformer system for highly efficient hydrogen production from natural gas", *International Journal of Hydrogen Energy*, Vol. 34, No. 10, 2009, pp. 4482-4487.
- [13] Jordal, K., Bredesen, R., Kvamsdal, H. M., and Bolland, O., "Integration of H₂-separating membrane technology in gas turbine processes for CO₂ capture", *Energy*, Vol. 29, No. 9-10, 2004, pp. 1269-1278.
- [14] Barelli, L., Bidini, G., Gallorini, F., and Servili, S., "Hydrogen production through sorption-enhanced steam methane reforming and membrane technology: A review", *Energy*, Vol. 33, No. 4, 2008, pp. 554-570.
- [15] Tong, J. H., Kashima, Y., Shirai, R., Suda, H., and Matsumura, Y., "Thin defect-free Pd membrane deposited on asymmetric porous stainless steel

substrate", *Industrial and Engineering Chemistry Research*, Vol. 44, No. 21, 2005, pp. 8025-8032.

[16] Everett, D. H., "Definitions, Terminology and Symbols in Colloid and Surface Chemistry; part I", *Pure and Applied Chemistry*, Vol. 579, No. 31, 1972, pp. 1-78.

[17] Paglieri, S. N. and Way, J. D., "Innovations in palladium membrane research", *Separation and Purification Methods*, Vol. 31, No. 1, 2002, pp. 1-169.

[18] Ma, Y. H., Mardilovich, I. P., and Engwall, E. E., "Thin composite palladium and palladium/alloy membranes for hydrogen separation", *Advanced Membrane Technology*, Vol. 984, 2003, pp. 346-360.

[19] Ma, Y. H., Mardilovich, I. P., and Engwall, E. E., "Thin composite palladium and palladium/alloy membranes for hydrogen separation", *Advanced Membrane Technology*, Vol. 984, 2003, pp. 346-360.

[20] Burggraaf, A. J., "Transport and separation properties of membranes with gases and vapours, in *Fundamentals of inorganic membrane science and technology*, edited by A. J. Burggraaf and L. Cot Membrane Science and Technology, Elsevier B.V., Amsterdam, 1996, pp. 331-434.

[21] Perry, J. D., Nagai, K., and Koros, W. J., "Polymer membranes for hydrogen separations", *MRS Bulletin*, Vol. 31, No. 10, 2006, pp. 745-749.

[22] Dong, J., Lin, Y. S., Kanezashi, M., and Tang, Z., "Microporous inorganic membranes for high temperature hydrogen purification", *Journal of Applied Physics*, Vol. 104, No. 12, 2008.

[23] Verweij, H., Lin, Y. S., and Dong, J. H., "Microporous silica and zeolite membranes for hydrogen purification", *MRS Bulletin*, Vol. 31, No. 10, 2006, pp. 756-764.

[24] de Vos, R. M. and Verweij, H., "Improved performance of silica membranes for gas separation", *Journal of Membrane Science*, Vol. 143, No. 1-2, 1998, pp. 37-51.

[25] Gopalakrishnan, S. and da Costa, J. C. D., "Hydrogen gas mixture separation by CVD silica membrane", *Journal of Membrane Science*, Vol. 323, No. 1, 2008, pp. 144-147.

[26] Araki, S., Mohri, N., Yoshimitsu, Y., and Miyake, Y., "Synthesis, characterization and gas permeation properties of a silica membrane prepared by high-pressure chemical vapor deposition", *Journal of Membrane Science*, Vol. 290, No. 1-2, 2007, pp. 138-145.

[27] Campaniello, J., Engelen, C. W. R., Haije, W. G., Pex, P. P. A. C., and Vente, J. F., "Long-term pervaporation performance of microporous methylated silica membranes", *Chemical Communications*, No. 7, 2004, pp. 834-835.

[28] Gu, X. H., Tang, Z., and Dong, J. H., "On-stream modification of MFI zeolite membranes for enhancing hydrogen separation at high temperature", *Microporous and Mesoporous Materials*, Vol. 111, No. 1-3, 2008, pp. 441-448.

[29] McLeary, E. E., Jansen, J. C., and Kapteijn, F., "Zeolite based films, membranes and membrane reactors: Progress and prospects", *Microporous and Mesoporous Materials*, Vol. 90, No. 1-3, 2006, pp. 198-220.

[30] Caro, J. and Noack, M., "Zeolite membranes - Recent developments and progress", *Microporous and Mesoporous Materials*, Vol. 115, No. 3, 2008, pp. 215-233.

[31] Kanezashi, M., O'Brien-Abraham, J., Lin, Y. S., and Suzuki, K., "Gas permeation through DDR-type zeolite membranes at high temperatures", *Aiche Journal*, Vol. 54, No. 6, 2008, pp. 1478-1486.

[32] Gu, X. H., Tang, Z., and Dong, J. H., "On-stream modification of MFI zeolite membranes for enhancing hydrogen separation at high temperature", *Microporous and Mesoporous Materials*, Vol. 111, No. 1-3, 2008, pp. 441-448.

[33] Giessler, S., Jordan, L., da Costa, J. C. D., and Lu, G. Q., "Performance of hydrophobic and hydrophilic silica membrane reactors for the water gas shift reaction", *Separation and Purification Technology*, Vol. 32, No. 1-3, 2003, pp. 255-264.

- [34] Brunetti, A., Barbieri, G., Drioli, E., Lee, K. H., Sea, B., and Lee, D. W., "WGS reaction in a membrane reactor using a porous stainless steel supported silica membrane", *Chemical Engineering and Processing*, Vol. 46, No. 2, 2007, pp. 119-126.
- [35] GCEP, <http://gcep.stanford.edu/> . 2011.
- [36] Tsuru, T., Morita, T., Shintani, H., Yoshioka, T., and Asaeda, M., "Membrane reactor performance of steam reforming of methane using hydrogen-permselective catalytic SiO₂ membranes", *Journal of Membrane Science*, Vol. 316, No. 1-2, 2008, pp. 53-62.
- [37] Uhlhorn, R. J. R., Keizer, K., and Burggraaf, A. J., "Gas and Surface-Diffusion in Modified Gamma-Alumina Systems", *Journal of Membrane Science*, Vol. 46, No. 2-3, 1989, pp. 225-241.
- [38] Wu, J. C. S. and Cheng, L. C., "An improved synthesis of ultrafiltration zirconia membranes via the sol-gel route using alkoxide precursor", *Journal of Membrane Science*, Vol. 167, No. 2, 2000, pp. 253-261.
- [39] Van Gestel, T., Sebold, D., Kruidhof, H., and Bouwmeester, H. J. M., "ZrO₂ and TiO₂ membranes for nanofiltration and pervaporation - Part 2. Development of ZrO₂ and TiO₂ topayers for pervaporation", *Journal of Membrane Science*, Vol. 318, No. 1-2, 2008, pp. 413-421.
- [40] Gu, Y. F., Hacılioglu, P., and Oyama, S. T., "Hydrothermally stable silica-alumina composite membranes for hydrogen separation", *Journal of Membrane Science*, Vol. 310, No. 1-2, 2008, pp. 28-37.
- [41] Zheng, Z., Hall, A. S., and Gulians, V. V., "Synthesis, characterization and modification of DDR membranes grown on alpha-alumina supports", *Journal of Materials Science*, Vol. 43, No. 7, 2008, pp. 2499-2502.
- [42] Elam, J. W., Routkevitch, D., Mardilovich, P. P., and George, S. M., "Conformal coating on ultrahigh-aspect-ratio nanopores of anodic alumina by atomic layer deposition", *Chemistry of Materials*, Vol. 15, No. 18, 2003, pp. 3507-3517.

- [43] Mahurin, S., Bao, L. L., Yan, W. F., Liang, C. D., and Dai, S., "Atomic layer deposition of TiO_2 on mesoporous silica", *Journal of Non-Crystalline Solids*, Vol. 352, No. 30-31, 2006, pp. 3280-3284.
- [44] Mccool, B. A. and DeSisto, W. J., "Self-limited pore size reduction of mesoporous silica membranes via pyridine-catalyzed silicon dioxide ALD", *Chemical Vapor Deposition*, Vol. 10, No. 4, 2004, pp. 190-194.
- [45] Elam, J. W., Routkevitch, D., Mardilovich, P. P., and George, S. M., "Conformal coating on ultrahigh-aspect-ratio nanopores of anodic alumina by atomic layer deposition", *Chemistry of Materials*, Vol. 15, No. 18, 2003, pp. 3507-3517.
- [46] Xiong, G., Elam, J. W., Feng, H., Han, C. Y., Wang, H. H., Iton, L. E., Curtiss, L. A., Pellin, M. J., Kung, M., Kung, H., and Stair, P. C., "Effect of atomic layer deposition coatings on the surface structure of anodic aluminum oxide membranes", *Journal of Physical Chemistry B*, Vol. 109, No. 29, 2005, pp. 14059-14063.

Chapter 2

Theoretical and Experimental Background

Abstract

Theoretical backgrounds of the sol-gel process related with the formation of microporous and mesoporous membranes are discussed. Attention is focused on the process parameters which result in stable sols and defect-free membranes.

An overview of the Atomic Layer Deposition (ALD) is presented. It is focused on the basic features of ALD such as ALD cycle, temperature window, precursor dose, and growth modes. Furthermore it has the aim to combine the information obtained from the literature which will be further adapted to our ALD processes investigated.

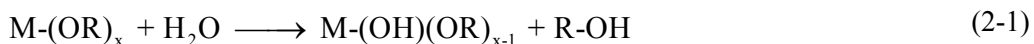
Nitrogen physisorption is generally used to characterize porosity of synthesized membrane films. Permeation and separation experiments on supported membranes are performed to determine the gas transport characteristics and separation performance of the membranes. An evaluation of pore size of the membrane is carried out using permoporometry of which the basic principle is based on capillary condensation of H₂O and its blocking effect on permeation of He. X-rays diffraction (XRD), Transmission Electron Microscopy (TEM), Scanning Electron Microscopy (SEM), and Atomic Force Microscopy (AFM) are used to characterize structural and morphological characteristics of the films and membranes.

2.1 Sol-gel chemistry

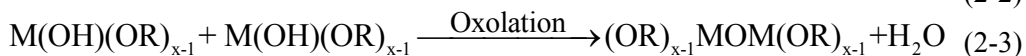
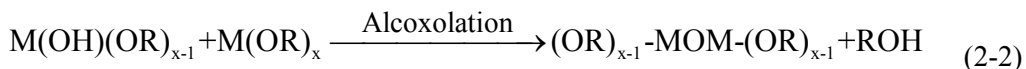
Sol-gel chemistry has triggered scientific interest in the field of thin films and membranes during recent decades and mainly due to its relatively simple procedure and its ability to easily change the chemical composition and properties of the prepared materials. A large number of papers concerning sol-gel processes exists including many reviews, notably that by Brinker et al. ^[1]. A major research effort in this field was focused on the silica systems, due to the moderate reactivity of the silicon precursors ^[2].

In general, there are two kinds of sol-gel syntheses according to the state of the sol, i.e., **colloidal and polymeric sols**. Colloidal sols are usually prepared in aqueous media (H₂O), while polymeric sols are synthesized in alcoholic media by the hydrolysis and condensation of metal alkoxide M-(OR)_x (M=Si, Ti, Zr, Al; OR=OC_nH_{2n+1}; x is the valence state of the metal) precursors. The overall hydrolysis-condensation reactions can be presented as follows:

Hydrolysis:



Condensation:



The hydrolysis reaction replaces alkoxy groups with hydroxyl groups. Subsequently, the condensation occurs through formation of an oxo-bridge (-O-) between two metal centers and the elimination of ROH (Alcoxolation) or H₂O (Oxolation).

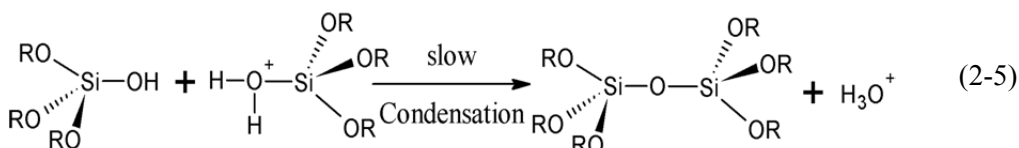
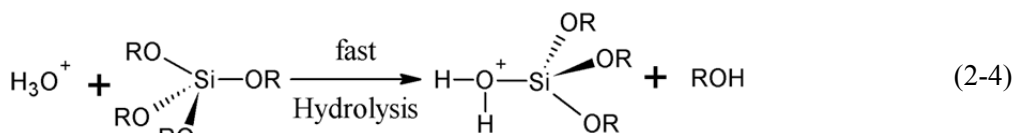
A colloidal sol is a suspension of colloids (particles with a dimension up to a micron) in water. Due to the small size of the particles, the effect of gravitational forces is negligible and the particles can aggregate or interact by Van der Waals attraction and surface charges. The sol can be stabilized when the particles are prevented from agglomeration by mutual repulsion forces among them. These repulsion forces come

from similar charges at the particle's surface, which are introduced by peptization with an inorganic acid such as HNO_3 , HCl , etc. The transition from a sol into a gel (gelation) begins when the sol starts being destabilized. It is a result of electrolytic effects such as changes of particle's surface charges and increase of the concentration of the particles through the evaporation of water or other solvent. During a certain time (gelation time) the particles' growth and the viscosity of the sol increase, which leads eventually to the formation of a tri-dimensional network. At the gel point the network becomes a semi-rigid mass of particles or clusters linked together by Van der Waals attractive forces (gel).

Colloidal sols are generally used for the production of crystalline, mesoporous materials, such as $\gamma\text{-Al}_2\text{O}_3$ in this thesis. Aluminium tri-secbutoxide (ATSB) is hydrolyzed with H_2O which yields a hydroxide, e.g., boehmite $[\text{Al}(\text{OOH})]$. This partially hydrolyzed alkoxide is now able to react with an other reactant, through the OH group to form a polyoxometalate or polyhydroxometalate. The viscosity of the solution will then increase and that indicates that the condensation process proceeds. The stable sol has a transparent light-blue colour after the HNO_3 peptization.

The second type of sol - **the polymeric one** leads to the formation of amorphous materials. Here, metal alkoxide precursors react in alcoholic media, where the polymeric particles remain separated because of their small size. Gelling in polymerised particle systems from metal alkoxide precursors occurs as a result of inter-particle polymerisation. The sol-gel chemistry of silica is one of the most widely studied topics in this area ^[1]. It is well known that silicon alkoxides $\text{Si}(\text{OR})_4$, such as tetraethylorthosilicate (TEOS/ $\text{Si}(\text{OCH}_2\text{CH}_3)_4$), are excellent precursors in the sol-gel process. At first this precursor undergoes hydrolysis, which can be catalyzed by an acid ^[3] or a base. As only acid catalysis is used in this thesis, the chemistry of TEOS under acid-catalysed conditions will be discussed. During acid-catalysed hydrolysis the alkoxy OR ($\text{R} = \text{CH}_2\text{CH}_3$) group is substituted by water according to a nucleophilic substitution reaction, $\text{S}_{\text{N}}2$, accompanied by inversion of the silicon tetrahedron (reaction 2-4). Condensation of the silanols is directed preferentially towards the ends of

siliceous oligomers which result in the formation of an oxo-bridge (Si-O-Si) as shown in the reaction (2-5) ^[4]:

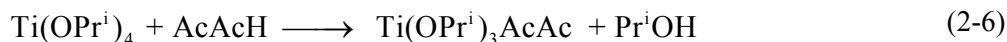


2.1.1 Factors influencing the sol-gel reactions

Both for the colloidal and polymeric sols, it is necessary to control hydrolysis and condensation reaction rates. Fast hydrolysis and condensation rates can result in a precipitated product instead of a stable sol. By controlling a number of factors such as the nature of the alkoxy groups, solvent, molar ratio of water/alkoxide, pH, aging temperature and time, and drying, it is possible to influence the rate of hydrolysis and condensation reactions.

- The hydrolysis rate can be influenced by the nature of the alkyl group of metal alkoxides. It is decreased in the order tertiary > secondary > primary group. This is attributed to steric hindrance effects and the decreased positive partial charge of the metal ion with increased alkyl chain length. Contrary to silicon alkoxides, the sol-gel chemistry of transition metal alkoxides is more complex, because transition metal precursors are highly reactive due to their small electronegativity and existence of various coordination numbers ^[5]. This in turn makes the metal ion very susceptible to nucleophilic attack, which makes it difficult to obtain a straightforward and controlled mechanism for hydrolysis-condensation reactions of these alkoxides. Dedicated chelating schemes have to be developed to prevent direct precipitation of the metal hydroxides. Substitution of the OR ligands by a chelating bidentate ligand such as acetylacetonate (AcAcH) ^[6] leads to the formation of a new molecular precursor which

exhibits a different molecular structure. Here AcAcH acts as a bidentate ligand on titanium isopropoxide ($\text{Ti}(\text{OPr}^i)_4$ with $\text{Pr}^i = \text{OCH}(\text{CH}_3)_2$):



- These complexing ligands are much more difficult to hydrolyse than alkoxy groups. They restrain the fast hydrolysis of the precursor and consequently slow down the condensation process.

- Selecting an appropriate solvent such as an aprotic solvent (tetrahydrofuran, dioxane) instead of a protic solvent (H_2O , alcohols) ^[7] can also slow down the hydrolysis rate, although the presence of H_2O is essential for the hydrolysis and subsequent condensation. Aprotic solvents render the OH^- ions more nucleophile, whereas protic solvents render the H_3O^+ ions more electrophile ^[4]. In general, the solvents most often used are parent alcohols, which have the same number of carbon atoms in the alkyl group as in the alkoxy group of the precursor. The precursor can be hydrolyzed with H_2O released in-situ by the esterification reaction ^[7], or the oxolation reaction (reaction 2-3).

- The molar ratio of water/alkoxide can control nucleation and growth of clusters in the sol. Wang et al. ^[8] prepared ultrafine titania particles (6nm) by carrying out hydrolysis of titanium isopropoxide with a high water/alcohol ratio of >50%.

- The pH is also an important parameter to prepare a sol. The peptization phenomenon with an inorganic acid such as HNO_3 , as previously mentioned to prepare a colloidal sol ^[5], is based on repulsive forces which prevent particle aggregation in the sol. When the pH value is decreased or increased far away from the isoelectric point (IEP) of metal oxides, high repulsive forces exist in the sol stage. Near the IEP a flocculation phenomenon occurs due to absence of repulsive forces between particles, which results in precipitate formation.

- The choice of solvent (acid- or base-catalyst) can influence the condensation reaction rate. For example, when hydrofluoric acid (HF) is used as a catalyst, F^- ions can replace hydroxyl ion in the hydrolysis product of reaction (2-4) and being more electronegative than the hydroxyl, they increase the attraction to other silanols. Thus,

the condensation rate increases with increasing concentration of HF. Moreover, higher condensation reaction rates result in higher porosity.

- Aging and drying can affect the final solid products. Aging time is the time between the gelation point and the start of drying of a gel. During the aging, polycondensation of the gel network continues along with syneresis (i.e., the shrinkage of the gel and the resulting expulsion of liquid from the pores), coarsening, and phase transformation. An aged gel can develop sufficient strength to resist cracking during drying.

2.1.2 Combination of sol-gel processing with evaporation-induced self-assembly (EISA)

Besides the conventional sol-gel processing as described above, the concept of surfactant assembly is introduced in the synthesis as evaporation-induced self-assembly (EISA)^[9]. EISA has been used to direct structure formation of porous metal oxides since the early 1990s when Mobil researchers reported the synthesis of mesoporous silicate molecular sieves, known as MCMs (Mobil Crystalline Materials or Mesoporous Crystalline Materials)^[9]. Considerable efforts have been aimed at expanding this type of MCMs by developing different pathways based on different metal oxides, surfactants, and reaction mechanisms. Most work was directed to the formation mechanism of long-range ordered micelle-silica hybrid phases. Work concerning other metal oxide based meso-structured materials is more restricted because of the synthetic difficulties related to both kinetic and coordination aspects as previously mentioned. Typically, the mesoporous silica materials synthesized under conditions of the EISA have high surface areas ($> 1000 \text{ m}^2.\text{g}^{-1}$), tunable and narrow pore size distributions (0.3-50nm), and possibly long-range ordered pore structures^[10, 11].

A general definition of self-assembly is the spontaneous organization of materials through non-covalent interactions (hydrogen bonding, Van der Waals forces, electrostatic forces, etc.) with no external intervention. The driving force of self-assembly is that amphiphilic surfactant molecules always try to minimize their surface

free energy. Amphiphilic surfactant molecules are composed of hydrophobic and hydrophilic parts. Depending on their head group charge, the surfactant can be classified into three categories as follows:

- Anionic surfactant: the hydrophilic part carries a negative charge, for example, carboxylate anionic surfactant ($C_nH_{2n+1}COONa$, $n = 11, 13, 15, 17$)^[10].
- Cationic surfactant: the hydrophilic part carries a positive charge, for example, cetyltrimethyl-ammonium-bromide (CTAB, $[C_{16}H_{33}N(CH_3)_3]Br$)^[9].
- Nonionic surfactant: the hydrophilic part is not charged, for example, triblock-copolymer Pluronic P123 ($EO_{20}PO_{70}EO_{20}$, EO = ethylene oxide, PO = propylene oxide)^[11].

In aqueous solution above the critical micelle concentration (CMC), surfactants assemble into micelles, spherical or cylindrical structures that maintain the hydrophilic parts of the surfactant in contact with water, while shielding the hydrophobic parts in the micelle interior. The concentration of surfactant molecules in solution is the key factor to determine the extent of micellization, the shape of the micelles, and the aggregation of micelles into the liquid. For example, cetyltrimethyl-ammonium-bromide surfactant in water can assemble into micelles, micelle rods, sheets of ordered micelles, as discussed in detail in reference^[9].

There is substantial debate in the literature about the mechanisms of self-assembly processes, which reflect the molecular interactions between inorganic material and the surfactant polar head groups. In MCMs, it was suggested that the presence of charged colloids has an inductive effect on the formation of micelle rods, around which the silicates polymerize to form a continuous solid material. The subsequent removal of surfactant by calcination at high temperatures yields the silicate framework with uniform pore dimensions in the range 2–10 nm.

In this thesis, the EISA process is applied in the sol-gel synthesizs of mesoporous titania and zirconia. The process can involve many different steps as illustrated in Figure 2-1. The first step consists of mixing the inorganic precursor sol and the micelle surfactant solution in the adequate proportions and chemical conditions. Since the pH

of the synthesized sol (usually below 2) is below the IEP of a metal oxide (titania (IEP ~ 6) and zirconia (IEP ~ 4 –6)), the metal oxide nanoparticles are positively charged. Once the sol is deposited on a support by dip-coating, the formation of a mesostructure film takes place via the EISA. The volatile solvents (e.g., $\text{C}_2\text{H}_5\text{OH}$, H_2O , and HCl) evaporates, which promotes surfactant micelle formation and then induces cooperative assembly of organic and inorganic species through electrostatic or hydrogen bonding interactions. These organic-inorganic interactions could be responsible for the thermal stability of the resulting mesoporous structure. In order to obtain ordered pore structures, it is necessary that the inorganic species condense around the micelles and the organic-inorganic interaction is not strong^[12]. Calcination is the last step to remove the surfactant and leads to the formation of mesoporous oxide film. During calcination at high temperatures ($>400^\circ\text{C}$), rearrangement of the individual nanoparticles can occur, which results in the formation of strong covalent bridges among the particles. The pore size of the mesoporous film can be effectively tuned in the range of 2–30 nm by using surfactants of different length and concentration^[13]. In addition, swelling of the micelles by addition of organic solvents, as well as control of parameters such as synthesis temperature and moisture content is crucial to further increase the pore size^[15, 16].

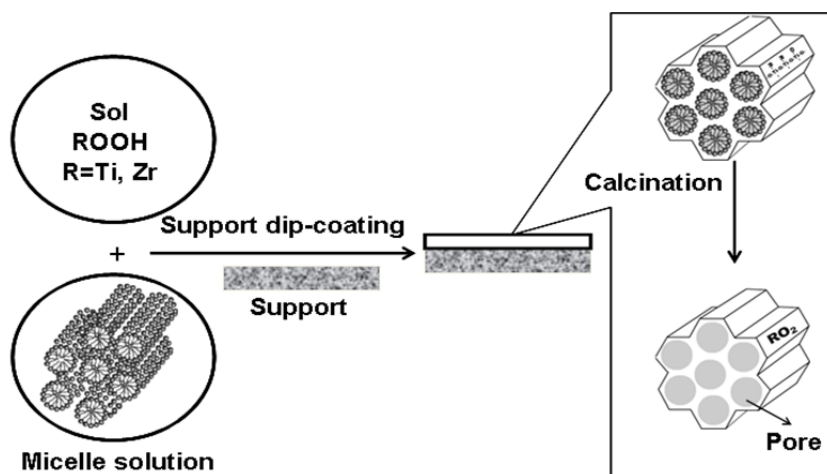


Figure 2-1: Schematic illustration of the sol-gel synthesis combined with the evaporation-induced self-assembly (EISA).

2.1.3 Sol-gel derived membrane preparation

Usually, a sol-gel preparation of a membrane involves first the formation of a sol and subsequently the coating of the sol on the surface of a porous support where a gel layer is formed by partial removal of the solvent. The solvents can be removed from the gel layer by either conventional drying in order to obtain a product known as a xerogel (in this thesis), or by drying with supercritical extraction in order to have an aerogel. Calcination of the gel at a temperature higher than the drying temperature causes further removal of the solvents and results in a porous ceramic layer. It can be a **microporous** (pore size $d_p < 2$ nm) or **mesoporous** ($2 < d_p < 50$ nm) membrane. Figure 2-2 shows all sequences of a conventional membrane preparation as described.

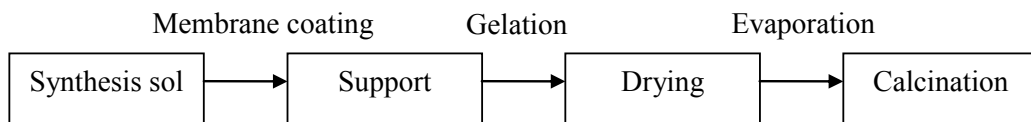


Figure 2-2: Sol-gel ceramic membrane preparation.

As stated in the previous section, it is necessary to prepare a stable sol before the porous membrane coating step. In the coating step a porous support is brought into contact by dipping it in the sol for a few seconds and is then slowly withdraw it from the sol reservoir. The movement entrains an initial “liquid” layer formed in the surface region by capillary suction of the sol in the pores of the support. When the upward moving flux of the entrained sol is balanced by evaporation, the dip-coating thickness is steady.

When the dipping time is short (few seconds), the thickness of the formed layer L (m) is mostly dependent on the dipping time t (s) and the viscosity of the sol η (N.m.s^{-2}) and defined as:

$$L = \frac{2\gamma C \cos\theta}{\eta} \sqrt{t} \quad (2-7)$$

where γ is the surface tension (N.m^{-1}), θ is the contact angle between the liquid and solid surface (rad), C is a constant (~ 0.8 for Newtonian liquid ^[14]).

For a long dipping time, the formed layer can reach a limiting thickness when all of the pores of the support are saturated with the dipping sol. This limit may lead to the longer evaporation time of solvent and water at the layer/support interface than that at the layer/air interface, which induces a gradient of concentration in the film thickness and a longer drying time. On the other hand, the rigid support imposes restriction on the relaxation of the gel network during the drying procedure, thereby developing shrinkage associated with large stresses. This may reduce the homogeneous structure and will result in micro-cracking of the membrane upon calcination.

In the initial stage of calcination (sintering), the formation of necks between primary particles takes place by surface diffusion and evaporation-condensation as part of the sintering mechanism ^[15]. The necks formed provide sufficient strength and a porous structure. A simple two-particle model is typically used to describe the sintering mechanism ^[15]. The model treated the primary particles as spheres with uniform size, and assumed the neck formation and growth by material transport. The dominant transport mechanism, however, can vary depending on particle size, neck radius, and temperature for a given system. In the intermediate stage, a significant shrinkage occurs, leading to the decrease of porosity. Based on the two-particle model, the shrinkage is caused by the neck growth with the approach of the centers of the particles. The dominant transport mechanisms are volume and grain boundary diffusion. The final stage of sintering is achieved when grain boundary migration occurs. The three-dimensional pore network collapses to isolated pores in grain boundaries. Then the porosity is further reduced. With respect to the change of porous structure, the heating and cooling processes during the calcination need to be controlled carefully in order to avoid the micro-cracking and delamination due to a large thermal expansion mismatch between support and layer or due to sintering shrinkage.

2.2 Atomic Layer Deposition (ALD)

2.2.1 ALD history

Historically speaking, Atomic Layer Deposition (ALD) was introduced as Atomic Layer Epitaxy (ALE) by Suntola and co-workers from Hensinki in the 1970s^[16, 17]. In the same period, the ALD technique was also developed by the group of Aleskovskii^[18] in the former Soviet Union. Partly because of its history, the ALD technique is referred to some other names, such as molecular layering (ML)^[18] and molecular layer epitaxy (MLE)^[19]. Suntola and co-workers^[16] developed ALD for the deposition of polycrystalline luminescent ZnS:Mn and amorphous large-area Al₂O₃ insulator films and thin-film electroluminescent (TFEL) displays, which were the first successful applications of ALD in industry. ALD is capable to produce uniform thin films with perfect conformality on every exposed surface of substrates with complex surface topographies. Its low deposition rate (see section 2.2.2) is no longer a limitation, since the film thickness required for other applications such as current-generation integrated circuits (ICs) are typically a few nanometers. Therefore, ALD has seen a break-through in recent years, but yet commercial applications on large scale surfaces are still limited. New materials, processes, and reactor designs for the ALD method have received increased attention in industry and university^[20-25].

With the advent of novel, synthetic nanostructured materials, ALD finds applications in microelectronics, photonics, microelectromechanical systems (MEMS), 3D optoelectronics, photovoltaics, catalysis, and fuel cells^[20]. There are developments in creating composite materials in the nanotechnology^[21], such as nanoporous membranes (anodic alumina^[22], γ -Al₂O₃^[23], silica^[23]) that have been coated using ALD. The ALD process appears to be a promising deposition technique for the modification of porous membranes. ALD of silica, titania and alumina to reduce the pore dimensions and, therefore, improve size selectivity properties of inorganic membranes has been successfully demonstrated^[22, 24-26].

2.2.2 Basic characteristics of ALD

ALD is a gas phase deposition technique where active vapor precursors are exposed alternately to a substrate (the precursor pulses) in order to deposit a monolayer or a fraction thereof on the surface at a time. The most important fact is that the chemisorption of the precursor with the surface groups of the substrate is a self-limiting surface reaction. Thus, the precursor pulses are followed by an inert gas purge or an evacuation of the reaction chamber in order to avoid gas-phase reactions between the two precursors. These sequential steps are referred to as one ALD cycle, which can be summarized in terms of the following process sequence as illustrated in Figure 2-3:

- First precursor exposure (precursor pulse)
- Inert gas purge
- Second precursor exposure (precursor pulse)
- Inert gas purge

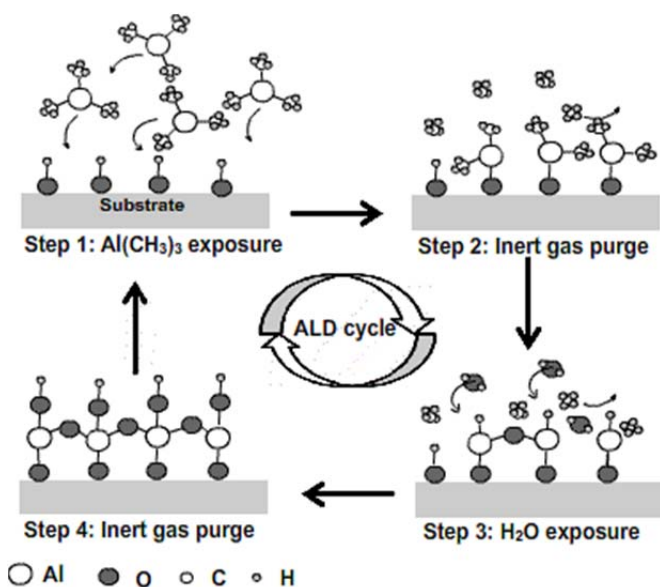


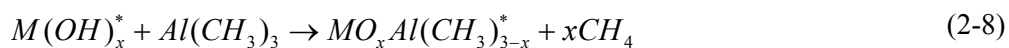
Figure 2-3: Schematic illustration of one ALD reaction cycle, where alumina deposition process using $\text{Al}(\text{CH}_3)_3$ and H_2O precursors is presented as an example.

Therefore, the number of cycles can be repeated as many times until the desired thickness of the deposited material is reached. The growth rate per cycle is usually obtained by dividing the resulting film thickness by the number of deposition cycles applied. The ALD process is especially suitable to deposit thin films in the range of 2-50 nm. Ideally, one ALD cycle should generate one monolayer of a film. However, the deposition can produce less than one monolayer per cycle due to steric hindrance between precursor molecules adsorbed at the surface, especially when these precursors have large ligands ^[27] and also possibly due to the limited number of reactive surface sites. For thin-film growth on dense substrates, one cycle is accomplished in a few seconds. In the processing of porous materials with large surface areas, longer reactant exposures, typically minutes or even hours, are required for one ALD cycle. The longer exposures are needed due to the increased diffusion times in these porous structures. As the ALD growth proceeds in a cyclical way and the cycle period depends on the reactor design, the deposition rate (deposited thickness per time) is low, i.e., up to few nm.min⁻¹. However, this low deposition rate is not anymore the major limitation of ALD, especially for the increased number of applications where only very thin films are needed. Moreover, batch sample reactors in ALD equipment designs can enable high throughput by coating multiple samples at the same time. Table 2-1 summarizes the beneficial features and limitations of ALD.

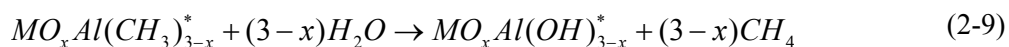
Table 2-1: Characteristic features of ALD.

Characteristics	Advantage	Limitation
Cycle growth	Best possibility of film thickness control	Low deposited thickness per time
Separated dosing precursors	Homogeneity No gas phase reaction , allowing the use of high reactive precursors	Limited selections for ALD precursors Need time for purging step
ALD temperature window (100 – 400°C)	Multilayer structures can be deposited at intermediate temperatures	Temperature-sensitive substrates such as polymer, organic molecules

The review paper by Puurunen ^[27] describes most aspects of the ALD cycle's sequence with trimethylaluminum (TMA/ $\text{Al}(\text{CH}_3)_3$) and water (H_2O) as a case study. These precursors are also used in this thesis (Chapter 4) for the Al_2O_3 deposition process. The process of Al_2O_3 film growth is schematically presented in Figure 2-3 by one ALD reaction cycle. Usually, the deposition of Al_2O_3 is carried out at the temperature range of 80-300 °C. In the first step, gas-phase TMA molecules are introduced into the reactor and then react only with the active sites (hydroxyl ligands) already present on the substrate surface. As a result of the condensation reaction, an Al ion having two methyl ligands forms a bond with oxygen on the substrate, giving off CH_4 as a volatile reaction product:



where M represents the substrate surface (a metal or a metal oxide) and the asterisks (*) indicate active surface species. Once all the active sites (hydroxyl groups) have reacted with TMA, the reaction stops, although more TMA reactant is available in the reactor. This characterises the *self-limiting surface* reaction. The purging gas introduced in the following step removes all excess TMA molecules, along with the volatile reaction product from the reactor. At this point, the first half cycle is finished with the substrate now having a methyl terminated surface. The second half cycle begins with the second pulse step, where water molecules are introduced into the reactor and replace methyl ligands on the surface with hydroxyl groups through the hydrolysis reaction:



where the asterisks (*) indicate active surface species. Finally, the next flow of purging gas is fed into the reactor to remove all residual gases and CH_4 , hence, completing one ALD cycle and leaving the surface hydroxyl groups ready for the next ALD cycle.

2.2.3 ALD temperature window

In an ideal ALD process, the ALD temperature window is the temperature range where the reaction deposition is self-limited, as illustrated in Figure 2-4. The ALD temperature window is relatively wide in the range of 100–400°C for the majority of processes ^[28] and also in this work. This makes the processes insensitive to small changes in temperature and precursor flows, and allows the processing of different materials to multilayer structures in a continuous process. Outside the ALD temperature window, the growth per cycle can change dramatically. At lower temperatures, the precursors may either react less efficiently with the surface due to an insufficient thermal energy which reduces the growth rate, or condense at the surface which results in a rapid increase in growth. If the temperature is higher than the ALD temperature window, the precursors can decompose into non-volatile products, which then etch to the surface, leading to an increasing growth rate per cycle of unwanted composition. Besides decomposition of the precursors, the deposited layer can chemically desorb from the surface, resulting in a decrease in growth rate per cycle.

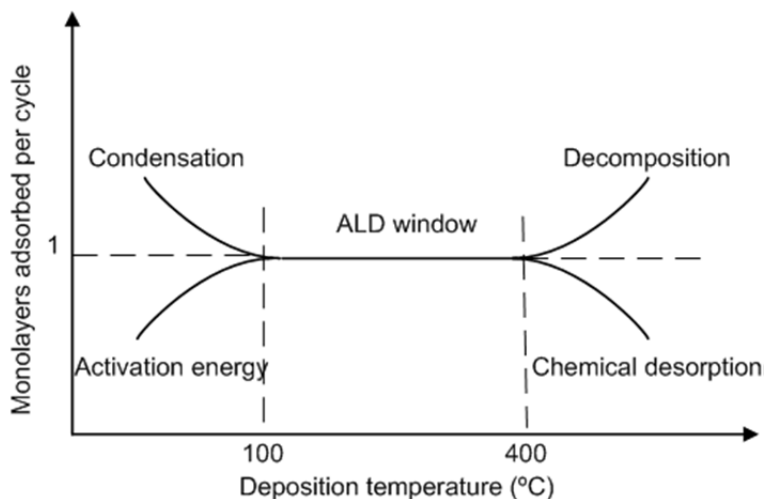


Figure 2-4: Schematic presentation of the dependence of the monolayers adsorbed per cycle on the deposition temperature, i.e., the ALD temperature window.

Often, but not always an ALD window is observed. Some ALD systems are not self-limiting because the surface species may decompose and allow additional adsorption.

This decomposition occurs even at the minimum temperatures required for the surface reactions. A non-ideal ALD behavior has been reported in the work of Elam et al.^[29] for TiN ALD using tetradimethylaminotitanium (TDMAT) and NH₃. According to their results, the growth rate of TiN did not saturate with increasing TDMAT exposure time and no “ALD window” was observed.

2.2.4 Precursor requirements for ALD

Typical metal precursors used in ALD are halides, alkoxides, organometallics, cyclopentadienyl-type, β -diketonates, alkylamides, and amidinates of metal compounds^[27]. The non-metal precursors used are: water, hydrogen peroxide, and ozone for oxygen; hydrides for chalcogens; ammonia, hydrazine, and amines for nitrogen. More details on the precursors used in this thesis will be referred to once needed. In general, precursors (gases, liquids, or solids) must have the following specific characteristics:

- Sufficient purity in order to prevent contamination by unwanted products.
- Volatile (i.e., liquid precursors must be vaporized and solid ones need to be sublimated).
- Reasonable vapor pressures in the range 13.33-133.3 Pa at a temperature at which precursors do not decompose during evaporation in order to ensure that the self-limiting reaction can take place in a reasonable time.
- Highly reactive towards the other precursor in a cycle, resulting in relatively fast kinetics and thus lowering deposition temperatures and cycle times.
- Ability to react with the active sites producing volatile reaction products, which can easily be removed in order to prepare for the subsequent step.
- Desirably nontoxic and environmentally friendly.
- Thermally stable at substrate temperatures (the ALD temperature window).

Plasma sources are also introduced into the ALD process^[30] to dissociate the precursors into desired radicals. A plasma generates highly reactive radical species that, for example, allow the deposition at lower temperatures than in thermally-

activated ALD. However, the plasma has a high energy which can create surface damage. In addition, both the plasma Debye length and the radical mean free path can exceed greatly the pore diameter, it also limits high penetration into the pores ^[31]. Typically, the plasma Debye length and the radical mean free path are in the range of several microns.

2.2.5 Growth rate and kinetics

As previously mentioned, the growth rate per cycle in units of Å.cycle⁻¹ or nm. cycle⁻¹ is usually less than a monolayer thickness. A change in growth per cycle does not always accurately indicate whether or not “true” ALD is occurring. The steric hindrance between precursor molecules adsorbed at the surface, the gradual loss of active surface sites with increasing substrate temperature ^[32], or substrate surface status can result in a deviation from an “ideal ALD growth rate”, i.e., one monolayer per cycle. There are two phenomena that account for this deviation, i.e., substrate enhanced and substrate inhibited growths ^[27]. In the first case, with substrate enhanced growth, the growth per cycle (GPC) value is under estimated and the film is thicker than expected. In the other and more common case, with the substrate inhibited growth, the GPC is over estimated. In most cases, the active sites are not homogeneously distributed on the surface and some areas have more reactive groups than others. During the very first cycles, ALD film growth will tend to start from the more reactive surface groups and form isolated islands. The islands will expand their size as the ALD proceeds further, then coalesce with each other and form a continuous film. As soon as a continuous film has been deposited the process will have a linear relation between the number of cycles used and the film thickness. Different active sites have been observed on substrates for ALD processes, for example, for silicon wafers, that the substrate surface can be ^[27, 33]:

- covered with a native silicon oxide (< 2nm) on the surface. The deposition is carried out without any preliminary surface pretreatment and the surface groups are silanol groups (Si-OH).

- or chemically oxidized to remove the native oxide and have a silicon oxide layer (< 2nm) with high quality. The surface pretreatment is introduced into the cleaning process of the substrate, which is based on sequential oxidative desorption and complexation with the solution of (H₂O₂-NH₄OH-H₂O) at room temperature. Finally, the active surface groups are Si-OH groups.

- chemically hydrided to remove the native oxide and have a passivated surface with terminating Si-H bonds (active surface groups) after the cleaning process. The surface pretreatment can be achieved by using the solution of (H₂O₂ + HCl + H₂O), followed by a deionized water, and then dilute HF /deionized water rinse /N₂ drying.

A distinguishing characteristic of ALD is the self-limiting surface chemisorption of each reactant during its respective half-cycle. This can be referred to as the limit of the so-called *monolayer capacity* of the surface, i.e., the maximum possible amount of adsorbate species per unit area on the substrate ^[27]. The monolayer capacity is a function of a number of kinetic and thermodynamic factors and is governed by the transport of gas-phase reactant from the precursor source to the substrate, the adsorption mechanism, the density of adsorption sites (active sites), and steric hindrance effects. The size and amount of ligands in the metal precursor can limit the maximum possible adsorption density. Therefore, film growth always depends on the reactant/surface combination being considered. Considering this, a quantity named *surface coverage* θ , i.e., the ratio of adsorbate species per unit area to the monolayer capacity of the surface, is used in ALD ^[34]. The surface coverage calculation is helpful for developing a simplified model of the film growth. The main model parameters are the gas pressure, the deposition temperature, and time.

Assuming that the adsorption of a gaseous molecule A on the surface adsorption site S takes place through this mechanism:



The rate of change of the surface coverage θ can be expressed by the Langmuir model:

$$\frac{d\theta}{dt} = k_{\text{ads}} P(1-\theta) - k_{\text{des}} \theta \quad (2-11)$$

where k_{ads} and k_{des} are the adsorption and desorption rate constants, respectively, and P is the partial pressure (Pa).

In the equilibrium adsorption the surface coverage θ can be expressed by the equation:

$$\theta_{\text{eq}} = \frac{1}{1 + (kP)^{-1}} \quad (2-12)$$

where $k = k_{\text{ads}}/k_{\text{des}}$ is the equilibrium constant of the adsorption.

In order to achieve ALD conditions with self-terminating reactions, the adsorption must be irreversible, so the desorption is ignored. In this case, k_{des} approaches zero and thus the limit of surface coverage θ is 1 for the saturation reaction. Solving by integrating from Eq. (2-11), the surface coverage θ ($0 \leq \theta \leq 1$) can be simply expressed by the rate constants as a function of time t (s):

$$\theta = 1 - \exp(-k_{\text{ads}} Pt) \quad (2-13)$$

The rate constant k_{ads} for the adsorption of the species on the surface is given by the Arrhenius equation:

$$k_{\text{ads}} = A \exp\left(\frac{-E_a}{RT}\right) \quad (2-14)$$

where A is the pre-exponential factor, E_a is the activation energy (J.mol^{-1}), R is the gas constant ($\text{J.mol}^{-1}\text{K}^{-1}$), and T is the absolute temperature (K).

Three basic growth modes such as the layer-by-layer growth (Frank-van der Werve growth) ^[35], the island growth (Volmer-Weber growth mechanism) ^[38, 41], and the layer-plus-island (random deposition growth) ^[35] have been proposed to predict the behavior of the growth on a flat substrate during the ALD as shown in Figure 2-5. The layer-by-layer growth involves a deposition of one monolayer at the time and results in a very smooth epitaxial film. It occurs when the atoms in the deposited film are more strongly bound to the substrate than to each other. The binding energy will

continuously decrease monotonically as each layer is added. The island growth mode occurs when the smallest stable clusters nucleate on the substrate and form islands. The binding energy of the atoms within the film is greater than the binding energy between the film and the substrate. The layer-plus-island growth is an intermediate combination of the aforementioned modes. This may occur when the monotonic decrease in binding energy is disturbed. For example, the release of strain energy due to film-substrate lattice mismatch may trigger island formation. More details of these growth modes are beyond the scope of the thesis, but it is appropriate to know that these growth modes are strongly dependent on initial substrate surface state and number of ALD cycles. In ALD of Al_2O_3 and TiO_2 , an island growth mode is experimentally observed for the TMA/water process^[27] and the $\text{TiI}_4/\text{H}_2\text{O}$ process^[36], which imposes a slow deposition rate in the period of island formation during the very first cycles. When the islands have coalesced to form a continuous layer, the layer-by-layer growth will occur. The growth modes are a thermodynamic approach to crystal growth, however, kinetic effects have to be considered. The individual atomic processes are responsible for adsorption and crystal growth on the surface. Therefore, atomistic simulation techniques such as classical molecular dynamics (MD), Monte Carlo (MC) methods, or Density Functional Theory (DFT) techniques have been developed^[37].

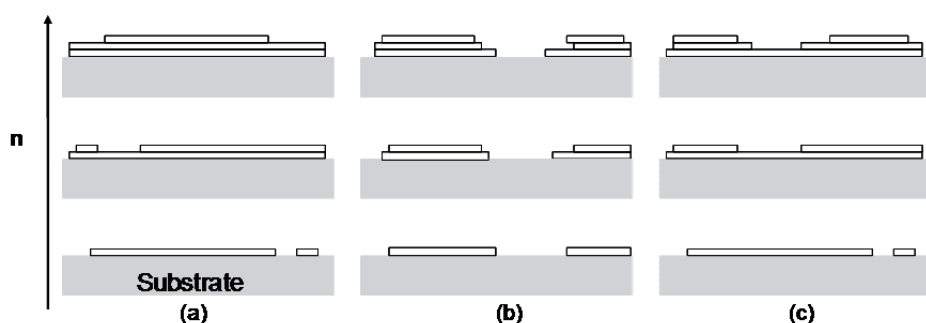


Figure 2-5: Cross-section illustration of the three growth modes with increasing the number n of ALD cycles including (a) layer-by-layer, (b) island, and (c) layer-plus-island growths.

2.2.6 Precursor dose

In the ALD reaction, each precursor is supplied from the gas phase to the surface of the substrate. Only a saturation dose is required in a self-limiting growth mechanism as illustrated in Figure 2-6. Hence, the pulse time t which is sufficient to adsorb an amount of the reactant to achieve the growth-rate saturation, i.e., 100% surface coverage ($\theta=1$), is required.

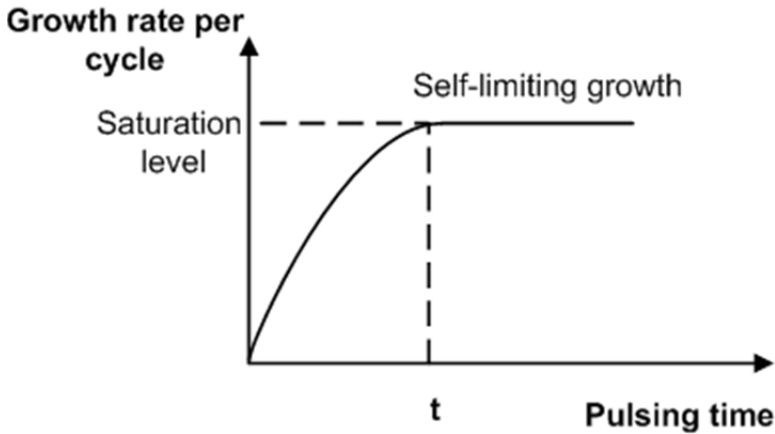


Figure 2-6: Behavior of growth rate vs. precursor pulse time (typical value of t in this work is 1-300 s).

The flux J of a gas impinging on the surface can be expressed by the Knudsen equation:

$$J = \frac{N_A P}{\sqrt{2\pi MRT}} \quad (2-15)$$

where N_A is Avogadro's number and M the molar mass of the gaseous molecule ($\text{g}\cdot\text{mol}^{-1}$).

The time t (s) required to supply a saturation dose D_s is then given by the equation^[38]:

$$t = \frac{D_s}{J} = \frac{\sqrt{2\pi MRT}}{N_A P} \quad (2-16)$$

where the saturation dose D_s (maximum number of molecules adsorbed on a square meter) can be estimated by the equation:

$$D_s = \left(\frac{\rho N_A}{M} \right)^{2/3} \quad (2-17)$$

where ρ is the density of precursor (g.m^{-3}).

Equation (2-16) yields the product of the precursor partial pressure and the pulse time (Pt), which is a useful quantity to determine the dose. Most commonly, the dose optimization is carried out by varying the pulse time t , but the precursor partial pressure may be varied as well. The transition of precursor from liquid to gas can be characterized by the Clausius-Clapeyron equation, where the vapor pressure of the precursor is a function of temperature,

$$\frac{d(\ln P)}{dT} = \Delta H_{\text{vap}} / R T^2 \quad (2-18)$$

where ΔH_{vap} is the enthalpy of vaporization (J.mol^{-1}), and T is the related precursor temperature (K). Thus, the vapor pressure increases when the temperature increases.

Because of steric hindrance effects, the practical pulse time is slightly longer than the calculated pulse time, especially for the used precursors for the mesoporous systems in this thesis. Longer exposure times are needed to allow the precursor molecules sufficient time to diffuse into the pores of these structures. Elam et al. [39] estimated the minimum precursor exposure time necessary to achieve the conformal coating in anodic alumina membranes with pore diameter d_p (m) and length L (m) from the following equation:

$$t = 2.3 \times 10^{-7} (133.3 \times P)^{-1} m^{1/2} \tau (L/d_p)^2 \quad (2-19)$$

where P is the precursor pressure (Pa), m is the mass of the reactant molecule (g.mol^{-1}) and τ is the density of ALD reactive sites in 10^{15} cm^{-2} . Based on this estimation, the exposure time used in this thesis is in the safety margin. Considering that the coating surface has the specific surface area S ($\text{m}^2.\text{g}^{-1}$), the dose D (mol) needed can be estimated by the equation:

$$D = \frac{D_s S m_s}{N_A} \quad (2-20)$$

where m_s is the mass of the coating layer (g). Therefore, the time t (s) can be rewritten as:

$$t = \frac{DRT}{PJ} \quad (2-21)$$

Another important parameter is the purge time. It depends on the configuration of ALD reactors, but must be long enough to completely remove any remaining reactant of the previous precursor pulse in order to avoid some kind of CVD. The purge time can be estimated by using the average gas residence time, t_{re} , as a lower limit. The average gas residence time t_{er} (s) is defined by:

$$t_{re} = \frac{P_0 V}{J} \quad (2-22)$$

where P_0 is the operating pressure (Pa), V the reactor volume (m^3), and J the gas flow rate ($Pa \cdot m^3 \cdot s^{-1}$). An additional consideration, especially with physisorbed precursors, i.e., H_2O , is the potential adsorption of the precursor on the reactor wall. Since the inert gas is used during the purge, it is necessary to consider the time needed for the diffusion/mixing of the reactant in the inert gas. In practice, a reasonable value of three times longer than the pulse time is often sufficient to achieve the complete purge^[39].

2.2.7 Features of ALD reactors

There are many commercial ALD systems on the market, developed by companies such as Aixtron®, ASM®, Picosun®, and Oxford-instruments®. The companies tend to manufacture their systems with flexibility that fulfill customer thin-film demands in various sectors of the electronics industry, i.e., dynamic random access memory (DRAM), microelectromechanical systems (MEMS), and transistor gate dielectrics. There are various types of ALD reactor configurations, but most of them are flow type systems and include the following components:

- Precursor sources with valving systems.
- Operation pressure control (high vacuum to atmospheric pressure).
- Inert gas supply systems (Ar or N_2).
- Temperature control (heating source, oven).

- Deposition reactor chambers.
- Electronic system control.
- Integrated characterization equipment such as spectroscopic ellipsometry, gas chromatographic mass spectrometry, and quartz crystal microbalance.

The control strategies for an ALD system are developed through experimentation and computational modeling. The ALD growth mechanism is complicated and many assumptions are often made to model all of the features of the ALD growth. Although the assumptions are reasonable and the modeling may be accurate in a reactor of one ALD system, it may not be applicable in reactors of different designs. Consequently, feedback from sample analysis provides useful data that can be used in computational modeling. In this thesis a significant part of research is carried out with ALD systems built in-house, as well as in commercial ALD systems. The operating principles and process control strategies of the ALD systems used will be described in the further chapters.

2.3 Characterization techniques used

2.3.1 Nitrogen physisorption technique

N₂ adsorption/desorption measurements are used for determining the characteristic porosities of unsupported membranes such as specific surface area, pore volume, and pore size distribution. The equipment used is an Autosorb-6B Surface Area and Pore Size Analyzer by Quantachrome instruments, nitrogen as adsorbed gas. Adsorption/desorption isotherms of N₂ (77 K) are carried out after pretreating all materials by evacuation below 1 kPa at 383 K for 16 hours. The adsorption isotherm of an outgassed sample is determined by measuring the amount of N₂ adsorbed at 77 K as a function of the relative pressures (i.e., the ratio of applied pressure and saturation pressure). The adsorption isotherm starts at low relative pressure. At a certain minimum pressure, the smallest pores will be filled with liquid nitrogen. As the pressure is increased further, larger pores are filled, and near the saturation pressure, all pores are filled. The pore filling mechanisms are dependent on the pore shape and are

influenced by the properties of N_2 and the adsorbent-adsorbate interactions. The total pore volume is determined by the quantity of gas adsorbed near the saturation pressure. Desorption isotherm occurs when the pressure is decreased from the saturation pressure downward. These isotherms can be grouped into the six types ^[40]. The type I isotherm is typical for microporous solids (pore size $d_p < 2\text{nm}$) and chemisorption isotherms. Type II is observed on finely divided non-porous solids. Type III and type V are typical for vapor adsorption (e.g. water vapor on hydrophobic materials). Type IV and V feature a hysteresis loop in which the desorption branch has more N_2 sorbed at a given pressure than does the adsorption branch. Finally, the rare type VI step-like isotherm is seen on special types of carbons. The isotherms obtained in this thesis are usually of type I and type IV as shown in Figure 2-7.

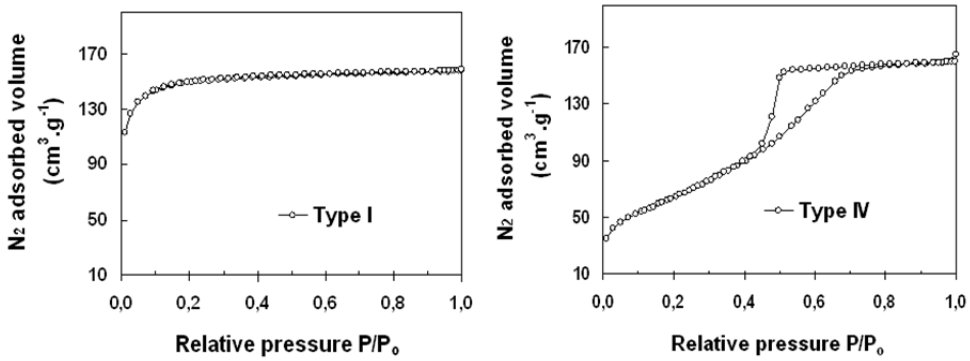


Figure 2-7: Examples of type I (microporous silica) and type IV (γ -alumina) of N_2 physisorption isotherms.

The specific surface area is determined from the adsorption isotherm according to the Brunauer, Emmett, and Teller (BET) method ^[41]:

$$\frac{P/P_0}{V_{\text{ads}}(1-P/P_0)} = \frac{1}{V_m C} + \frac{(C-1)}{V_m C} (P/P_0) \quad (2-23)$$

where P and P_0 are the applied and saturation pressures of N_2 (Pa), C is the BET constant (related to the energy of adsorption of the 1st layer), V_{ads} is the N_2 saturation

adsorption volume ($\text{cm}^3 \cdot \text{g}^{-1}$), and V_m is the volume of gas monolayer on the surface ($\text{cm}^3 \cdot \text{g}^{-1}$).

Equation (2-23) demonstrates that a plot of $[P/P_0/[V_{\text{ads}}(1-P/P_0)]]$ as a function of (P/P_0) should give a straight line in the relative pressure range of 0.05-0.3, which the intercept is $1/V_m C$ and the slope is $(C-1)/V_m C$. Hence, the values of C and V_m can be obtained.

The BET surface area is then obtained using the equation:

$$S_{\text{BET}} = \frac{V_m N_A \delta}{V} = V_m * 4.35 \quad (2-24)$$

where N_A is Avogadro's number, δ is the cross-sectional area occupied by a N_2 molecule on the surface (assumed to be 0.162 nm^2), and V is the molar volume of N_2 (i.e, 22.4 l at 77 K).

The specific surface area S can be determined by Equation (2-25):

$$S = \frac{S_{\text{BET}}}{\text{weight of sample}} \quad (2-25)$$

The total pore volume V_p is calculated from the N_2 volume ($\text{cm}^3 \cdot \text{g}^{-1}$) adsorbed at the relative pressure of 0.95. According to the Gurvitsch rule ^[40], under the assumption that N_2 is adsorbed in liquid form, the total pore volume V_p ($\text{cm}^3 \cdot \text{g}^{-1}$) can be estimated using Equation (2-26):

$$V_p = V_{\text{ads}} * 1.547 \times 10^{-3} \quad (2-26)$$

where the density of N_2 in the pores is assumed to be the density of liquid N_2 ($\sim 0.808 \text{ g} \cdot \text{cm}^{-3}$).

A number of modeling calculations such as the Density-Functional Theory (DFT) ^[42, 43], Barrett, Joyner, and Halenda (BJH) model ^[40], and the Horvath Kawazoe model (HK) ^[44] can be applied to different regions of the adsorption isotherms to evaluate the micropore and mesopore volume and pore size distributions. The microporous volume is usually determined by the t-plot method ^[45]. Mesopore size calculations are usually based on the Kelvin equation ^[46].

$$\ln(P/P_0) = \frac{-2\gamma V_l}{r_k RT} \quad (2-27)$$

where γ is the surface tension of liquid adsorbate (8.85 mJ.m⁻² for N₂), V_l is the molar volume of condensed adsorbate (34.7*10⁻⁶ cm³ for N₂), r_k is the Kelvin radius of the pore (m), R is the gas constant (8.314 J.mol⁻¹.K⁻¹), and T is the liquid nitrogen temperature (77K).

Using the constants for nitrogen in equation (2-27), the Kelvin radius of the pore can be reduced to:

$$r_k = \frac{4.15}{\log(P/P_0)} \quad (2-28)$$

The relation between the real pore radius (r_p) and the Kelvin radius (r_k) is $r_p = r_k + t$ where t is the thickness of the N₂ monolayer formed on the inner surface of the pores, which is approximately 0.5 nm.

2.3.2 Gas permeation

Gas permeation tests are carried out in the temperature range of room temperature to 448 K by passing gas or gas mixtures through a membrane. Equipment is a home-built gas permeation set-up. A schematic diagram of the gas permeation equipment is presented in Figure 2-8. The system consists of a membrane cell, pressure controllers, oven, temperature controller, mass flow meters, and gas chromatography (Varian Micro-GC4900) with a flame ionization detector (FID), and a thermal conductivity detector (TCD). A total pressure on the feed side (F) is varied in the range of 1 – 4 x10⁵ Pa and the permeate side (P) is kept constant at atmospheric pressure. The pressure difference over the membrane is adjusted by a pressure controller. The permeate flow is measured with a soap meter and the gas compositions are analyzed by a gas chromatography. The permeance, Per (mol m⁻²s⁻¹Pa⁻¹), of the gas permeating through the membrane is defined as:

$$Per = \frac{J}{\Delta P A} \quad (2-29)$$

where J is the gas flow through the membrane (mol.s^{-1}), $\Delta P = P_f - P_p$ is the pressure difference (Pa), P_f and P_p being the pressures in the feed side and permeate side, respectively, and A is the exposed area of the membrane (m^2).

The separation factor $\alpha_{\text{H}_2/\text{CO}_2}$ is expressed as a function of the molar fractions by the following equation:

$$\alpha_{\text{H}_2/\text{CO}_2} = \frac{y_{\text{p,H}_2}}{x_{\text{r,H}_2}} \frac{x_{\text{r,CO}_2}}{y_{\text{p,CO}_2}} \quad (2-30)$$

where $y_{\text{p,H}_2}$ and $y_{\text{p,CO}_2}$ are the molar fractions of H_2 and CO_2 at the permeate side and $x_{\text{r,H}_2}$ and $x_{\text{r,CO}_2}$ are the molar fractions of H_2 and CO_2 at the retentate side (R).

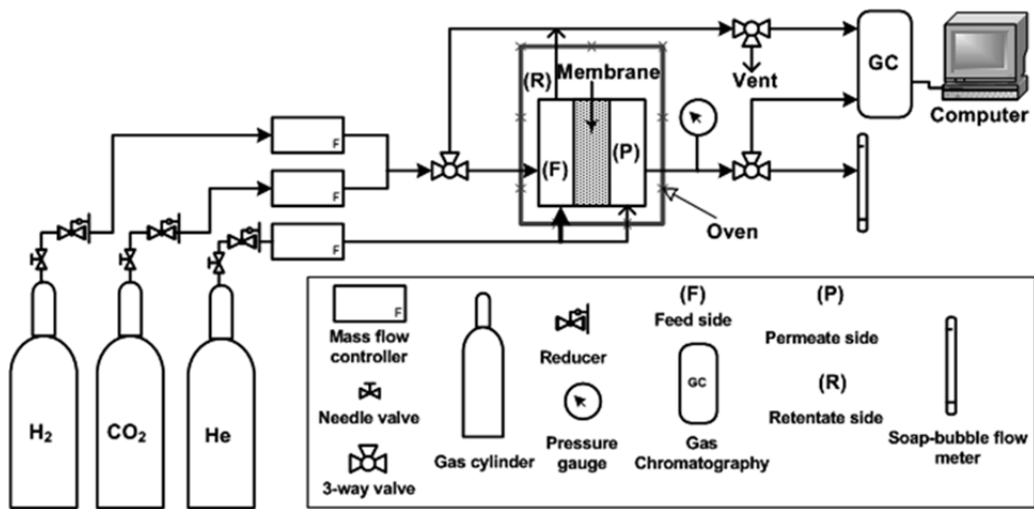


Figure 2-8: Gas permeation equipment.

2.3.3 Permporometry

Permporometry is a method employed to determine the pore size distribution of a mesoporous layer supported on a macroporous support and to check whether defects in the layer are present. Equipment is a home-built permporometry equipment in the Energy Research Centre of the Netherlands (ECN). A schematic diagram of the permporometry equipment is presented in Figure 2-9. The system consists of a

membrane cell, pressure controller, temperature controller, cold traps, and mass flow meters.

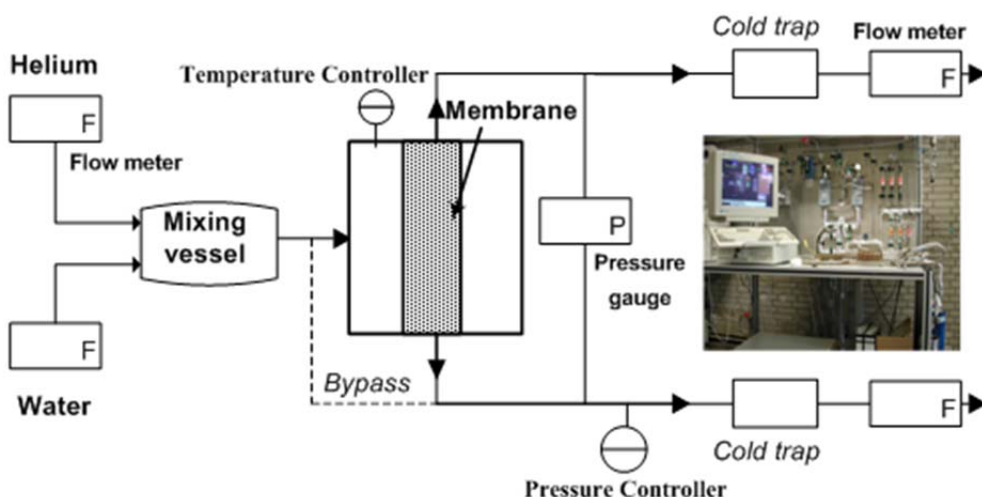


Figure 2-9: Permporometry equipment.

In short, a condensable vapor (H_2O) and a noncondensable gas (He) are passed through the membrane. During the measurement the pores are stepwise blocked with increasing partial vapor pressure of water by the condensation of H_2O vapor as illustrated in Figure 2-10. The pore sizes in which capillary condensation of H_2O can still occur are expressed as a function of the relative H_2O pressure by the Kelvin equation^[46]. For each relative pressure, P_{rel} , all pores with radius smaller than the threshold value r_K , the Kelvin radius of the pore, are blocked by the condensed vapor. At a relative pressure of 1 all pores of the membrane are filled and He transport through the membrane is not possible provided there are no large defects in the membrane present. When the vapor pressure is reduced, pores with larger size than r_K are emptied and become available for He transport. During the experiment the pressure at the permeate side of the membrane is kept equal to 10^5 Pa and the temperature at 343 K. The Kelvin radius of the pore, does not correspond exactly to the actual pore radius. In order to obtain the real pore

radius, r_K must be corrected by including the thickness of the H_2O monolayer, which forms on the surface of the pores before capillary condensation occurs ^[46].

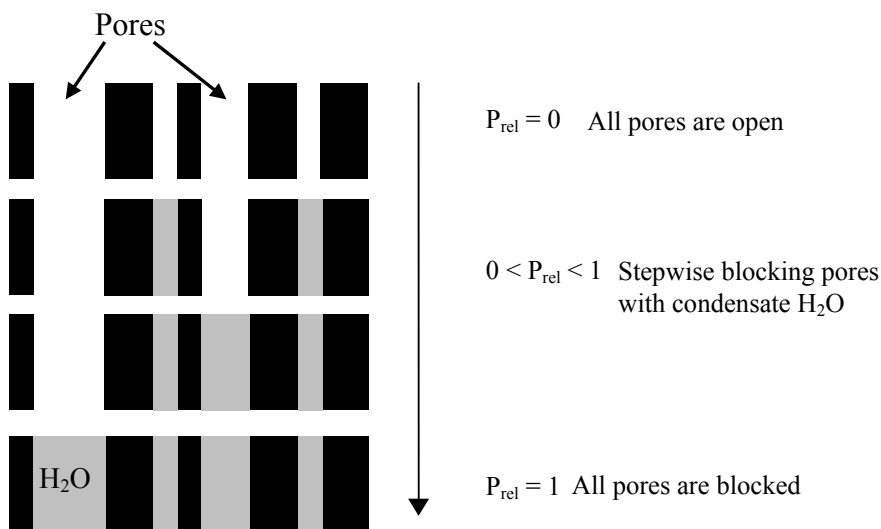


Figure 2-10: Blockage of the pores as a function of the relative H_2O pressure.

2.3.4 X-ray diffraction (XRD)

The theory of XRD, the experimental methods and the main applications can be obtained from the work by Cullity ^[47], for example. This section briefly discusses the fundamental principles of XRD. X-rays have a relatively short wavelength, i.e., high energy electromagnetic radiation. After they are generated from a source and focused into a fine beam, the X-rays can be directed to a solid sample. When there is constructive interference of scattered X-rays from the atomic planes in a crystal as shown in Figure 2-11, a diffraction peak is observed. The condition for constructive interference from planes with the d_{hkl} spacing is given by Bragg's equation:

$$\lambda = 2d_{hkl} \sin \theta \quad (2-31)$$

where λ is the wavelength (m), d_{hkl} is the separation distance between planes (m), and θ is the diffraction angle (degree).

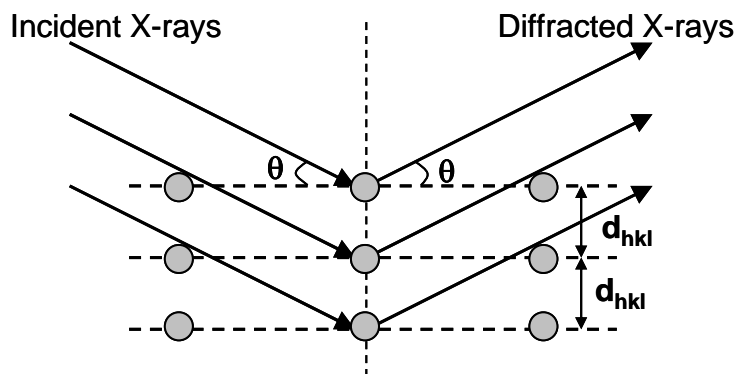


Figure 2-11: Schematic presentation of the principle of the Θ - 2Θ scan.

The XRD analysis is performed using a Bruker D8 Advance diffractometer (Cu $K\alpha$ radiation, $\lambda = 1.54178 \text{ \AA}$) of a conventional X-ray source powered at 40 kV and 50 mA. The diffraction patterns are obtained by scanning the samples from 10° - 80° (2θ) with a counting time of 5s per step with a step of 0.02° in a continuous scan mode. The patterns are plotted and compared with data from the Joint Committee Powder Diffraction Standards (JCPDS) for analysis. The XRD patterns are also taken from 1° - 10° (2θ) to check the presence of long-range ordering and the symmetry of the pore structure. Two main characteristics of a self-supported membrane, i.e., the grain size (using the Scherrer equation) and the phase composition of the synthesized materials can therefore be deduced from the knowledge of the scattering intensity and angle. Moreover, for mesoporous materials with a regular pore diameter as illustrated in Figure 2-12, the sum of a pore diameter and a pore wall thickness can be estimated based on the d_{hkl} spacing calculated from the Bragg equation. The difficulty here is that these reflections occur at very low angle, close to the direct beam.

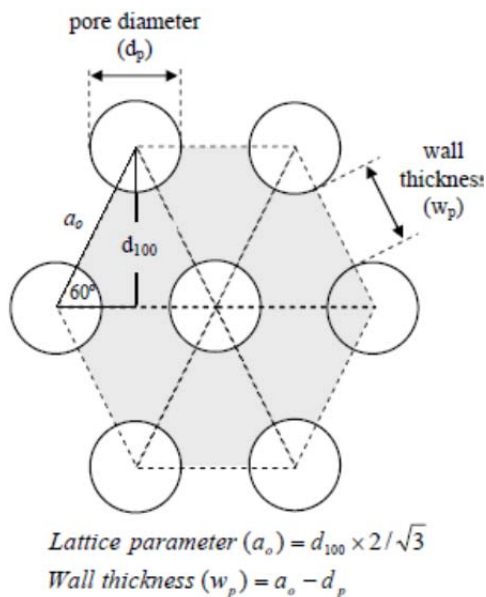


Figure 2-12: Model of lattice parameter and wall thickness of the hexagonal pore arrangement.

2.3.5 Imaging techniques in structural membrane characterization

Transmission Electron Microscopy (TEM), Scanning Electron Microscopy (SEM), and Atomic Force Microscopy (AFM) have been widely used for the observation of morphology and microstructure of membranes. In this work, the characterizations of supported membranes are performed by using TEM (Philips CM30T electron microscope with a LaB₆ filament as electron source operated at 300 kV), SEM (JEOL-6330F), and AFM (NTMDT Ntegra microscopy). These techniques mostly provide visual information about particle size and shape, surface roughness, surface, layer thickness, and in certain cases a pore size. TEM involves in observing electrons from an incident electron beam that are transmitted through different sample zones which correspond to different chemical compositions. As the name implies, in TEM a sample has to be thin enough to transmit electrons, which requires a specialized preparation in order to avoid destroying the real porous structure of the sample. On the other hand, SEM uses secondary electrons that are emitted when a sample is irradiated with a beam

of electrons. In this case, to proceed the membrane characterization a sample pretreatment is required in order to provide the sample with a conducting surface. Usually, a very thin conducting gold layer (~ 1 nm) is sputtered on the surface of the sample. Figure 2-13 shows an example of γ - Al_2O_3 membrane prepared by a sol-gel synthesis, which consists of a top γ - Al_2O_3 layer on top of a support with larger, coarser particles of α - Al_2O_3 . Because the resolution is not high enough to visualize the pores in the membrane, the SEM image can only give qualitative information about the membrane morphology, any defect (cracks, pinholes) on the surface, and an estimation of the γ - Al_2O_3 thickness (~ 1.5 μm). The TEM image shows a clear vision of particles between γ - Al_2O_3 and α - Al_2O_3 layers. AFM is based on a sharp tip with a diameter smaller than 10 nm, which is scanning across a surface of a sample with a constant force. The movement of the tip is induced by London –van der Waals forces between the particles of the surface and the tip which is recorded. This results in a profile of the scanning surface. Examples of AFM images can be found in Chapter 6.

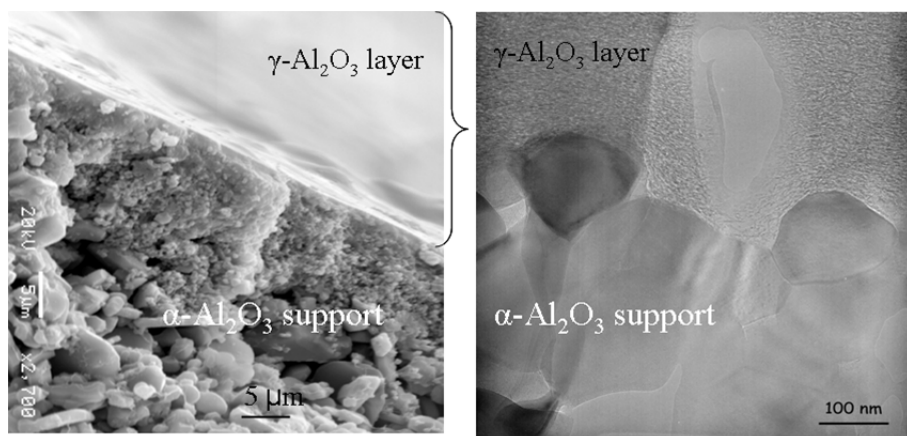


Figure 2-13: Cross-sectional SEM and TEM images of a sol-gel derived γ - Al_2O_3 membrane on α -alumina support.

References

- [1] Brinker, C. J., Hurd, A. J., Schunk, P. R., Frye, G. C., and Ashley, C. S., "Review of sol-gel thin-film formation", *Journal of Non-Crystalline Solids*, Vol. 147, 1992, pp. 424-436.
- [2] Brinker, C. J. and Scherer, G. W., *Sol-Gel Science: The Physics and Chemistry of Sol-Gel Processing*, Academic Press ed., Boston, 1990.
- [3] Wu, J. C. S. and Cheng, L. C., "An improved synthesis of ultrafiltration zirconia membranes via the sol-gel route using alkoxide precursor", *Journal of Membrane Science*, Vol. 167, No. 2, 2000, pp. 253-261.
- [4] Brinker, C. J. and Scherer, G. W., *Sol-Gel Science: The Physics and Chemistry of Sol-Gel Processing*, Academic Press ed., Boston, 1990.
- [5] Yoldas, B. E., "Alumina gels that form porous transparent Al_2O_3 ", *Journal of Materials Science*, Vol. 10, No. 11, 1975, pp. 1856-1860.
- [6] Grosso, D., Cagnol, F., Soler-Illia, G. J. D. A., Crepaldi, E. L., Amenitsch, H., Brunet-Bruneau, A., Bourgeois, A., and Sanchez, C., "Fundamentals of mesostructuring through evaporation-induced self-assembly", *Advanced Functional Materials*, Vol. 14, No. 4, 2004, pp. 309-322.
- [7] Kessler, V. G., "Geometrical molecular structure design concept in approach to homo- and heterometallic precursors of advanced materials in sol-gel technology", *Journal of Sol-Gel Science and Technology*, Vol. 32, No. 1-3, 2004, pp. 11-17.
- [8] Wang, C. C. and Ying, J. Y., "Sol-gel synthesis and hydrothermal processing of anatase and rutile titania nanocrystals", *Chemistry of Materials*, Vol. 11, No. 11, 1999, pp. 3113-3120.
- [9] Brinker, C. J., Lu, Y. F., Sellinger, A., and Fan, H. Y., "Evaporation-induced self-assembly: Nanostructures made easy", *Advanced Materials*, Vol. 11, No. 7, 1999, pp. 579-585.

- [10] Chen, F. X., Huang, L. M., Li, Q. Z., and Li, Q. Z., "Synthesis of MCM-48 using mixed cationic-anionic surfactants as templates", *Chemistry of Materials*, Vol. 9, No. 12, 1997, pp. 2685-2686.
- [11] Richman, E. K., Brezesinski, T., and Tolbert, S. H., "Vertically oriented hexagonal mesoporous films formed through nanometre-scale epitaxy", *Nature Materials*, Vol. 7, No. 9, 2008, pp. 712-717.
- [12] Hudson, M. J. and Knowles, J. A., "Preparation and characterisation of mesoporous, high-surface-area zirconium(IV) oxide", *Journal of Materials Chemistry*, Vol. 6, No. 1, 1996, pp. 89-95.
- [13] Zhao, D. Y., Feng, J. L., Huo, Q. S., Melosh, N., Fredrickson, G. H., Chmelka, B. F., and Stucky, G. D., "Triblock copolymer syntheses of mesoporous silica with periodic 50 to 300 angstrom pores", *Science*, Vol. 279, No. 5350, 1998, pp. 548-552.
- [14] Spiers, R. P., Subbaraman, C. V., and Wilkinson, W. L., "Free coating of a Newtonian liquid onto a vertical surface", *Chemical Engineering Science*, Vol. 29, No. 2, 1974, pp. 389-396.
- [15] Svoboda, J. and Riedel, H., "New Solutions Describing the Formation of Interparticle Necks in Solid-State Sintering", *Acta Metallurgica et Materialia*, Vol. 43, No. 1, 1995, pp. 1-10.
- [16] Suntola, T., Pakkala, J., and Lindfors, G. S., Method for performing growth of compound thin films. FI 790680[4413022], 1-13. 1983. US.
- [17] Suntola, T., "Atomic Layer Epitaxy", *Thin Solid Films*, Vol. 216, No. 1, 1992, pp. 84-89.
- [18] Shevjakov, A. M., Kuznetsova, G. N., and Aleskovskii, V. B., "Chemistry of high temperature materials, Proceedings of the second USSR conference on high-temperature chemistry of oxides", Leningrad, Nauka, 1967, pp. 149-155.
- [19] Nishizawa, J., Abe, H., and Kurabayashi, T., "Molecular Layer Epitaxy", *Journal of the Electrochemical Society*, Vol. 132, No. 5, 1985, pp. 1197-1200.

[20] Ritala, M. and Niinistö, J., "Atomic layer deposition, **in** *Chemical Vapour Deposition: Precursors, Processes and Applications*, edited by C. A. Jones and L. M. Hitchman Royal Society of Chemistry, UK, 2009, pp. 158-206.

[21] Knez, M., Niesch, K., and Niinisto, L., "Synthesis and surface engineering of complex nanostructures by atomic layer deposition", *Advanced Materials*, Vol. 19, No. 21, 2007, pp. 3425-3438.

[22] Elam, J. W., Routkevitch, D., Mardilovich, P. P., and George, S. M., "Conformal coating on ultrahigh-aspect-ratio nanopores of anodic alumina by atomic layer deposition", *Chemistry of Materials*, Vol. 15, No. 18, 2003, pp. 3507-3517.

[23] Herrera, J. E., Kwak, J. H., Hu, J. Z., Wang, Y., and Peden, C. H. F., "Synthesis of nanodispersed oxides of vanadium, titanium, molybdenum, and tungsten on mesoporous silica using atomic layer deposition", *Topics in Catalysis*, Vol. 39, No. 3-4, 2006, pp. 245-255.

[24] Xiong, G., Elam, J. W., Feng, H., Han, C. Y., Wang, H. H., Iton, L. E., Curtiss, L. A., Pellin, M. J., Kung, M., Kung, H., and Stair, P. C., "Effect of atomic layer deposition coatings on the surface structure of anodic aluminum oxide membranes", *Journal of Physical Chemistry B*, Vol. 109, No. 29, 2005, pp. 14059-14063.

[25] Mahurin, S., Bao, L. L., Yan, W. F., Liang, C. D., and Dai, S., "Atomic layer deposition of TiO₂ on mesoporous silica", *Journal of Non-Crystalline Solids*, Vol. 352, No. 30-31, 2006, pp. 3280-3284.

[26] Mccool, B. A. and DeSisto, W. J., "Self-limited pore size reduction of mesoporous silica membranes via pyridine-catalyzed silicon dioxide ALD", *Chemical Vapor Deposition*, Vol. 10, No. 4, 2004, pp. 190-194.

[27] Puurunen, R. L., "Surface chemistry of atomic layer deposition: A case study for the trimethylaluminum/water process", *Journal of Applied Physics*, Vol. 97, No. 12, 2005, pp. 959-972.

[28] Niinisto, L., Ritala, M., and Leskela, M., "Synthesis of oxide thin films and overlayers by atomic layer epitaxy for advanced applications", *Materials Science*

and *Engineering B-Solid State Materials for Advanced Technology*, Vol. 41, No. 1, 1996, pp. 23-29.

[29] Elam, J. W., Schuisky, M., Ferguson, J. D., and George, S. M., "Surface chemistry and film growth during TiN atomic layer deposition using TDMAT and NH₃", *Thin Solid Films*, Vol. 436, No. 2, 2003, pp. 145-156.

[30] Potts, S. E., Keuning, W., Langereis, E., Dingemans, G., van de Sanden, M. C. M., and Kessels, W. M. M., "Low temperature plasma-enhanced atomic layer deposition of metal oxide thin films", *Journal of the Electrochemical Society*, Vol. 157, No. 7, 2010, pp. 66-74.

[31] Jiang, Y. B., Liu, N. G., Gerung, H., Cecchi, J. L., and Brinker, C. J., "Nanometer-thick conformal pore sealing of self-assembled mesoporous silica by plasma-assisted atomic layer deposition", *Journal of the American Chemical Society*, Vol. 128, No. 34, 2006, pp. 11018-11019.

[32] Ott, A. W., Klaus, J. W., Johnson, J. M., and George, S. M., "Al₂O₃ thin film growth on Si (100) using binary reaction sequence chemistry", *Thin Solid Films*, Vol. 517, No. 20, 1997, pp. 5950.

[33] George, S. M., "Atomic Layer Deposition: an overview", *Chemical Reviews*, Vol. 110, No. 1, 2010, pp. 111-131.

[34] Everett, D. H., "Definitions, Terminology and Symbols in Colloid and Surface Chemistry; part I", *Pure and Applied Chemistry*, Vol. 579, No. 31, 1972, pp. 1-78.

[35] Puurunen, R. L. and Vandervorst, W., "Island growth as a growth mode in atomic layer deposition: A phenomenological model", *Journal of Applied Physics*, Vol. 96, No. 12, 2004, pp. 7686-7695.

[36] Kukli, K., Aidla, A., Aarik, J., Schuisky, M., Harsta, A., Ritala, M., and Leskela, M., "Real-time monitoring in atomic layer deposition of TiO₂ from TiI₄ and H₂O-H₂O₂", *Langmuir*, Vol. 16, No. 21, 2000, pp. 8122-8128.

[37] Mazaleyrat, G., Esteve, A., Jeloica, L., and Djafari-Rouhani, M., "A methodology for the kinetic Monte Carlo simulation of alumina atomic layer

deposition onto silicon", *Computational Materials Science*, Vol. 33, No. 1-3, 2005, pp. 74-82.

[38] Gordon, R. G., Hausmann, D., Kim, E., and Shepard, J., "A kinetic model for step coverage by atomic layer deposition in narrow holes or trenches", *Chemical Vapor Deposition*, Vol. 9, No. 2, 2003, pp. 73-78.

[39] Elam, J. W., Routkevitch, D., Mardilovich, P. P., and George, S. M., "Conformal coating on ultrahigh-aspect-ratio nanopores of anodic alumina by atomic layer deposition", *Chemistry of Materials*, Vol. 15, No. 18, 2003, pp. 3507-3517.

[40] Sing, K. S. W., Everett, D. H., Haul, R. A. W., Moscou, L., Pierotti, R. A., Rouquerol, J., and Siemieniewska, T., "Reporting physisorption data for gas solid systems with special reference to the determination of surface-area and porosity (Recommendations 1984)", *Pure and Applied Chemistry*, Vol. 57, No. 4, 1985, pp. 603-619.

[41] Brunauer, S., Emmett, P. H., and Teller, E., "Adsorption of gases in multimolecular layers", *Journal of the American Chemical Society*, Vol. 60, 1938, pp. 309-319.

[42] Evans, R., "The nature of the liquid-vapour interface and other topics in the statistical mechanics of non-uniform, classical fluids", *Advances in Physics*, Vol. 28, No. 2, 1979, pp. 143-200.

[43] Lastoskie, C., Gubbins, K. E., and Quirke, N., "Pore-size heterogeneity and the carbon slit pore - a density-functional theory model", *Langmuir*, Vol. 9, No. 10, 1993, pp. 2693-2702.

[44] Horvath, G. and Kawazoe, K., "Method for the Calculation of Effective Pore-Size Distribution in Molecular-Sieve Carbon", *Journal of Chemical Engineering of Japan*, Vol. 16, No. 6, 1983, pp. 470-475.

[45] Deboer, J. H., Linsen, B. G., Vanderpl, T., and Zonderva, G. J., "Studies on pore systems in catalysts VII. Description of pore dimensions of carbon blacks by t-method", *Journal of Catalysis*, Vol. 4, No. 6, 1965, pp. 649-653.

[46] Cuperus, F. P., Bargeman, D., and Smolders, C. A., "Permporometry - the determination of the size distribution of active pores in UF Membranes", *Journal of Membrane Science*, Vol. 71, No. 1-2, 1992, pp. 57-67.

[47] Cullity, B. D., *Elements of X-Ray Diffraction*, Addison-Wesley 1956, pp. -531.

Chapter 3

Structural characterization and porosity analysis in self-supported porous alumina-silica thin films

Abstract

In this study, alumina, silica and alumina-silica binary (36 % mol silica) thin films are synthesized using the sol-gel technique. These form the basis for future gas separation membranes. The characterization of the synthesized oxides was performed using nitrogen physisorption, X-ray diffraction (XRD), Doppler-broadening measurements on the 511 keV annihilation photon peak, together with $3\gamma/2\gamma$ analysis, and Fourier transform infrared spectroscopy (FTIR) of adsorbed CO. It is found that silica is microporous, γ -alumina is mesoporous, and the binary material shows fingerprints of both the meso- and microporous nature of its constituents as well as of the respective crystal structures. These results open the possibility to also investigate thin supported porous films (a few microns thick), and especially the setting and drying aspects on porous supports for membrane production, using the positron annihilation technique.

3.1 Introduction

The field of nanoporous inorganic materials (pore sizes between 1-100 nm) is experiencing explosive growth in a widening field of important applications, such as catalysis in chemical engineering and fuel production ^[1], purification and separations ^[2], and clean energy production and carbon capture ^[3, 4]. Mature synthesis technologies, such as the sol-gel technique, have been developed to produce materials with flexibility and tailor-made porosity and pore size ^[5]. Sol-gel based thin films and membranes have been extensively studied in previous decades, but still trigger the interest of material scientists active in this field. In particular, the improvement of inorganic porous membranes to operate in hostile chemical environments and under crucial pressure and temperature conditions, as opposed to the limited polymeric membrane operating window, is an issue that many scientific publications ^[6-8] and review papers ^[9, 10] deal with. Among sol-gel derived membranes developed to date, amorphous microporous silica membranes are the most notable of inorganic membranes with the capability of separating H₂ from mixed gas streams. However, microporous silica materials are not hydrothermally stable, due to the degradation of the silica microstructure in the presence of water vapor or liquid which results in hydrolysis of siloxane bridges (Si-O-Si) both at low ^[11] and high temperatures ^[12], and the rupture of the whole membrane layer. Therefore, improving the hydrothermal stability of microporous SiO₂ membranes has received much attention. One of the options for instance is doping the starting silica sol with a metal oxide such as Al₂O₃, TiO₂, ZrO₂, or NiO ^[12-15]. For example, the alumina-doped silica membrane exhibited separation properties similar to the pure silica membranes and the hydrothermal stability was improved after doping with 3% alumina ^[12]. Upon exposure to 50 mol% steam/air at 600°C for 30h, the alumina-doped silica had 64% reduction in the surface area and a loss of 86% micropore volume, compared to 85% and 94%, respectively, for the pure silica.

The effectiveness of the alumina-silica binary is also the subject of our research. In an attempt to obtain binary alumina-silica membranes with tailor-made porosity features,

different mixed Al-Si compositions were prepared by controlling the molar Al/Si ratio range of 0 -100 mol % Si. In the present study, the alumina-silica binary with 36 mol % Si is selected, because it starts showing the evident fingerprints of both the meso- and microporous nature of its constituents. More important than the porous properties of the alumina-silica binary system is its homogeneity in the preparation. The porous structure of this composite self-supported film is investigated and compared to those of pure γ -alumina and silica. The quantitative information from the N_2 physisorption technique, the X-ray diffraction (XRD), the positron annihilation Doppler broadening (PADB) technique, and Fourier transform infrared (FTIR) spectroscopy of adsorbed CO are complementary to each other and together help in assessing the micro-structural properties of the alumina-silica self-supported film. The interesting point of the study is to highlight the advantage of positron in PADB technique to probe nanostructure of porous thin films for membrane applications.

3.2 Experimental details

3.2.1 Thin film synthesis

All samples were prepared using the sol-gel technique, using either a boehmite sol or a silica sol or a mixture of both. The boehmite sol was synthesized by the colloidal route [8]. Aluminium tri-sec-butoxide (ASB, 99% purity, Sigma-Aldrich) was added to water at 80°C under vigorously stirring. Two liters of water were used per mol of alkoxide. The solution was kept at 90°C and, about half to one hour after addition of the alkoxide, 0.07 mol HNO_3 (Sigma-Aldrich) per mol alkoxide was added to peptize the sol. The sol was kept boiling in an open reactor for about two hours to evaporate most of the butanol and was subsequently kept at 90°C during about 16h under reflux conditions. The final boehmite sol had an opaque-blue color and the $AlOOH$ concentration was 0.92 M.

The polymeric silica sol was prepared by acid-catalyzed hydrolysis and condensation of tetraethyl-orthosilicate (TEOS, purity 99.9 % Sigma-Aldrich) in ethanol (purity >99.9 Merck). Molar ratios of TEOS/Water/ HNO_3 /Ethanol were: 1.0/6.4/0.085/3.8.

The sol was prepared by careful drop-wise addition of water and acid to the TEOS ethanol solution followed by 2h refluxing at 80°C under stirring ^[16].

A small amount of boehmite or silica sol was poured into different Petri dishes. Mixed alumina/ silica samples were prepared by mixing a boehmite and polymeric silica sol beforehand in the targeted proportions of Al₂O₃/SiO₂. The sample used for this study contains 36 mol % of SiO₂. After drying for 3-5 days under ambient conditions, the samples were calcined at 600°C for 3h with a heating rate of 60°C/h. In order to have a sufficient mechanical strength, the self-supported thin films with approximately dimensions of 10 mm × 10 mm × 1 mm were prepared for the characterizations.

3.2.2 Characterization

A conventional pore-size analysis method, i.e., N₂ physisorption was used to assess the total surface area and the pore size distribution. These measurements were carried out in an Autosorb 1-B physisorption set-up (Quantachrome Instruments). The samples were degassed at 150 ° C under vacuum ($P < 10^{-3}$ Pa) for 16 h. From the change in pressure due to the adsorption (desorption) and known gas volume at 77K (liquid N₂ normal boiling point), the quantity of adsorbed (desorbed) N₂ can be calculated when the dead volume is calibrated by a non-adsorbing gas like He. The specific surface area can thus be deduced from the N₂ isotherm data in the relative pressure P/P_0 range of 0.05 - 0.30, using the Brunauer, Emmett, and Teller (BET) equation ^[17]. For the calculation of the pore size distribution the Density Functional Theory (DFT) ^[18, 19] and the Horvath Kawazoe model (HK) ^[20] were applied for the mesopores (diameter of 2-50nm) and micropores (diameter <2nm), respectively. The total pore volume V_p is calculated from the N₂ volume (cm³·g⁻¹) adsorbed at the relative pressure of 0.975. According to the Gurvitsch rule, under the assumption that N₂ is adsorbed in liquid form, the total pore volume V_p (cm³·g⁻¹) is estimated as follows:

$$V_p = V_{ads} \times 1.547 \times 10^{-3} \quad (3-1)$$

where V_{ads} is the N₂ saturation adsorption volume (cm³·g⁻¹). The density of N₂ in the pores is assumed to be that of liquid N₂ (i.e., 0.808 g·cm⁻³). The total pore volume V_p

is also used to calculate the porosity. The porosity is defined as the ratio of the total pore volume to the total volume of a sample V ($\text{cm}^3 \text{g}^{-1}$). The total volume V of the sample is directly related to the density of the sample ρ (g cm^{-3}) as follows:

$$V = V_p + 1/\rho \quad (3-2)$$

The wide-angle XRD measurements were performed with a Bruker D8 Advance diffractometer using the Cu $K\alpha$ radiation ($\lambda = 1.54178 \text{ \AA}$) of a conventional X-ray source powered at 40 kV and 50 mA. The diffraction patterns were obtained by scanning the samples from $10^\circ - 80^\circ$ (2θ), with a counting time of 5s per step with a step of 0.02° in a continuous scan mode to identify the metal oxide phases present.

Positron annihilation spectroscopy is based on the fact that positrons, the positive anti-particle of electrons, annihilate with electrons in the subjected material, resulting in two γ rays according to the energy-matter equation $E = mc^2$ which is 511 keV for an electron. Positrons can form positronium (Ps), a hydrogen-like bound state with an electron, when positrons are injected into a pore. Ps gradually dissipates its energy by means of inelastic collisions with the pore wall. Even epithermal Ps ($E > kT$) is not able to re-enter the solid and remains confined to the pore volume. However, connected pores forming clusters allow Ps motion on a larger length-scale. Therefore, both thermal and epithermal Ps can escape from the sample by finding a route through an open pore to the sample surface and Ps emission into the vacuum may be observed. Ps initially forms in two states, para, p-Ps ($\uparrow\downarrow$ electron-positron spin configuration) and ortho o-Ps ($\uparrow\uparrow$), whose annihilation characteristics are different. p-Ps annihilates into two photons (2γ), with a lifetime in vacuum of 0.125 ns. o-Ps annihilates into three photons (3γ) by self-annihilation or annihilates with an electron from the pore wall into two photons (2γ) by the so-called “pickoff” annihilation. The probability of the latter depends on the collision frequency with pore walls which can shorten the o-Ps lifetime (its initial lifetime in vacuum is 142 ns). The rate of “pickoff” annihilation is related to the size of the pore because of its dependence on the electron density in the annihilation site. It influences the ratio of the $3\gamma/2\gamma$ annihilation peak intensity and can, therefore, be used to derive porosity properties. In this study, the PADB experiments

were performed at the Reactor Institute Delft using the Delft Variable Energy Positron beam. All experiments were carried out at room temperature under a vacuum of 10^{-6} Pa. In this setup positrons emitted from a ^{22}Na source are moderated to thermal energies, subsequently accelerated, and then injected into the samples with a kinetic energy E tuned between 100 eV and 25 keV. The annihilation spectrum recorded at each positron implantation energy E is analyzed for two parameters, i.e., the $3\gamma/2\gamma$ annihilation ratio (given by the R parameter) and the Doppler broadening of the annihilation radiation (given by the S parameter). The R parameter is the ratio between the number of 3γ counts (T) in the low-energy region ($E_\gamma < 511$ keV) and the total number of counts (P) in the annihilation spectrum around 511 keV. The S-parameter is defined as the ratio between the number of counts in a chosen, fixed central region, to the number of counts in the entire 511 keV annihilation peak.

The mean implantation depth $\langle z \rangle$ (nm) of the positrons into the sample is given by:

$$\langle z \rangle = \frac{A}{\rho} E^{1.62} \quad (3-3)$$

where A is a material independent parameter ($40 \mu\text{g}\cdot\text{cm}^{-2} \text{keV}^{-1.62}$), ρ is the density of the sample ($\text{g}\cdot\text{cm}^{-3}$), and E is the positron implantation energy (keV). For example, in alumina ($\rho \sim 3.9 \text{ g}\cdot\text{cm}^{-3}$) positrons with an energy of 25 keV have a mean implantation depth of about $2 \mu\text{m}$.

For in-situ FTIR measurements, pellets of the samples were prepared and placed inside an IR cell which allowed in-situ high-temperature treatments, CO dosage, and IR measurements at liquid nitrogen temperature to be made. CO is a weakly basic probe molecule which is particularly suitable to probe the presence of Brønsted acid sites. When interacting with acid hydroxyl groups, the $\text{OH}\cdots\text{CO}$ acid/base adducts leads the perturbations of the vibrational frequencies (or wavenumbers) of OH and CO stretching modes. The positions of the OH and CO vibrational bands and their behaviors (wavenumber shifts) upon CO adsorption can be directly related to the acidic strength of bridging hydroxyl groups of Brønsted acid sites and Lewis acid sites^[21-25]. The IR spectra were recorded with a Bruker Equinox 55 spectrometer at 2 cm^{-1}

resolution. The spectra are presented in absorbance scale after normalization with respect to the pellet weights.

3.3 Results and discussion

The porous characteristics for γ -alumina, silica, and the alumina-silica (36 mol % Si) binary obtained by the N_2 adsorption-desorption measurements are summarized in Table 3-1. As shown in Figure 3-1, the pure γ - Al_2O_3 sample has an isotherm of type IV according to the IUPAC classification ^[26] with N_2 hysteresis loop between the relative pressures P/P_0 of 0.4–0.75, which is characteristic for mesoporous material. A similar isotherm type with a smaller hysteresis loop is also observed for the binary sample. However, the binary sample has a higher volume of N_2 adsorption at low $P/P_0 < 0.4$, which reflects a important amount of micropores along with mesopores in the structure. Therefore, it has a higher BET surface area than that of γ - Al_2O_3 . The BET surface area of the binary sample is about $380 \text{ m}^2\text{g}^{-1}$, while the BET surface area of γ - Al_2O_3 is $280 \text{ m}^2\text{g}^{-1}$. The porosities are estimated to be 40% and 48%, respectively. On the other hand, the isotherm observed for the SiO_2 sample is very different in that the absence of a hysteresis loop, which is assigned to a type I ^[20] and characteristic for microporous material. The SiO_2 sample yields a highest surface area of $480 \text{ m}^2\text{g}^{-1}$ and a porosity of $\sim 34 \%$. No trend about the relationship between the surface area and pore volume can be deduced from these results, but there is concern that sintering effects can occur at the high calcination temperature of 600°C and may result in a denser structure of SiO_2 .

Table 3-1: Structural characteristics for γ -alumina, silica, and the alumina-silica (36 % Si) binary samples. (* according to the IUPAC classification^[26] and all standard deviations were obtained with triplicated measures).

Samples	Isotherm type (*)	BET area (m^2g^{-1})	Pore volume V_p (cm^3g^{-1})	Porosity (%)	Mean pore diameter D (nm)
Al_2O_3	IV	280 ± 17	0.236 ± 0.03	48 ± 1.44	5.5 ± 0.4
SiO_2	I	480 ± 29	0.230 ± 0.03	35 ± 1.05	2 ± 0.5
$\text{Al}_2\text{O}_3/\text{SiO}_2$	IV	380 ± 23	0.229 ± 0.02	40 ± 0.8	0.5 ± 0.1 and 3 ± 0.5

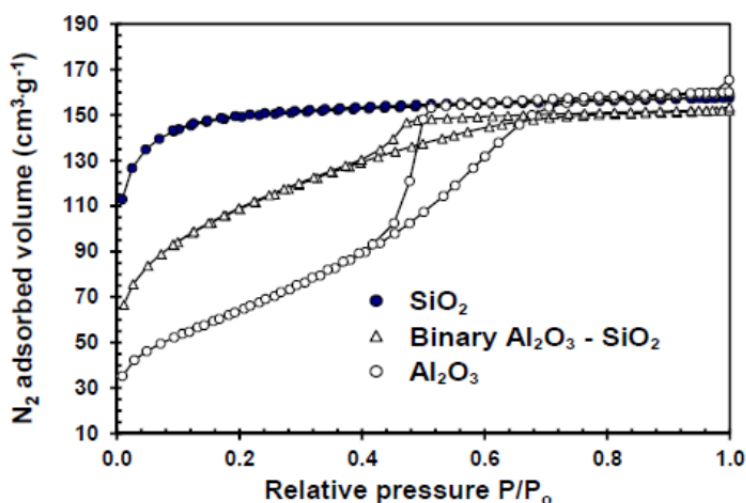


Figure 3-1: Nitrogen physisorption isotherms of γ -alumina, silica, and the alumina-silica binary.

The porosity features of all samples are better understood by analyzing the pore-size distributions. Pure γ - Al_2O_3 is characterized by a broad pore size distribution with a mean pore size of 5.5 nm as shown in Figure 3-2. In the binary sample, a bimodal pore size distribution with maxima around 3 nm and 0.5 nm can be seen from the combined results obtained from the DFT model (Figure 3-2) and those from the HK model (Figure 3-3). The two models do not give the same pore size distribution because the

DFT method based on the Kelvin equation (is reliable in the mesopore region) and the HK method is strictly only valid for micropores (< 2 nm). The DFT and HK results on the SiO_2 sample, however, both yield a pore size distribution in the small pore range of 0.5-2 nm.

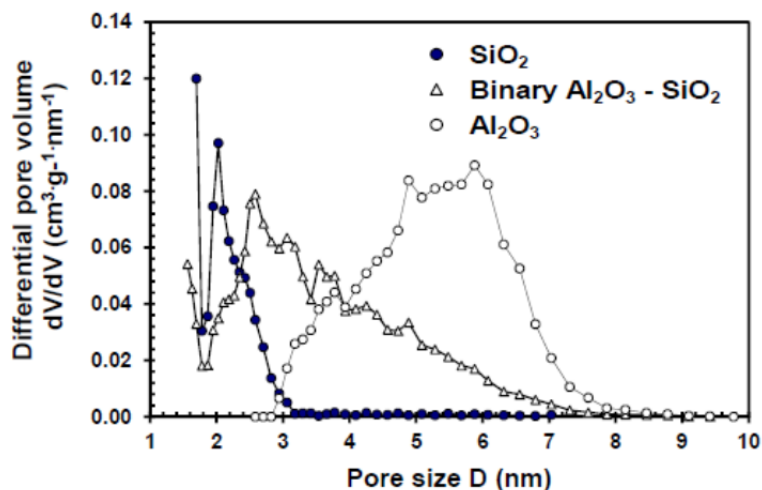


Figure 3-2: Mesoporous size distribution obtained by Density Functional Theory (DFT) for γ -alumina, silica, and the alumina-silica binary.

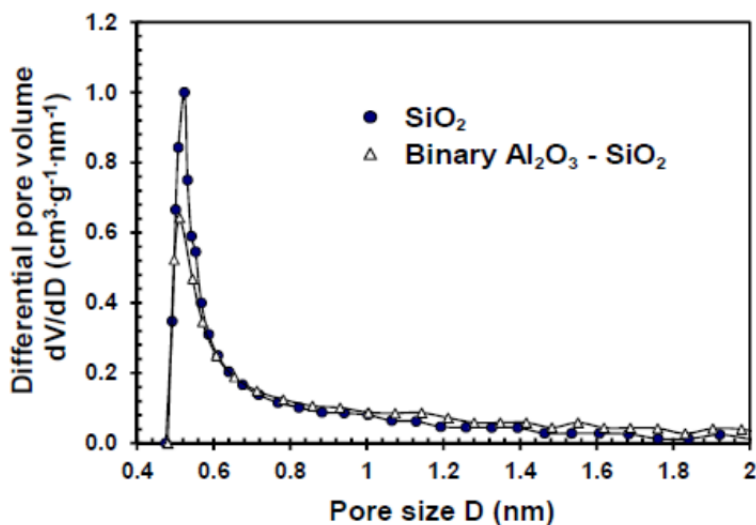


Figure 3-3: Microporous size distribution of silica and the alumina-silica binary obtained by the Horvath Kawazoe (HK) model.

The wide-angle XRD patterns for the γ -alumina, silica, and the alumina-silica binary samples are presented in Figure 3-4. The observed peaks corresponding to the gamma phase appear obviously in the XRD pattern of γ -alumina sample. The XRD pattern of silica contains only a broad peak characteristic of amorphous silica, which can be discerned around 24° . The binary sample presents two broad peaks with low intensities, at approximately 47° and 67° , which are close to the position of the strongest peaks in the γ -alumina system. There is also an increase in the background signals at the right angle hinting at the presence of silica. The alumina-silica sample, however, is rather amorphous which hampers a clear-cut identification of other possible phases' presence. Thus, the XRD results need to be substantiated with results obtained from other complementary techniques. The PADB and FTIR will then provide the conclusive information.

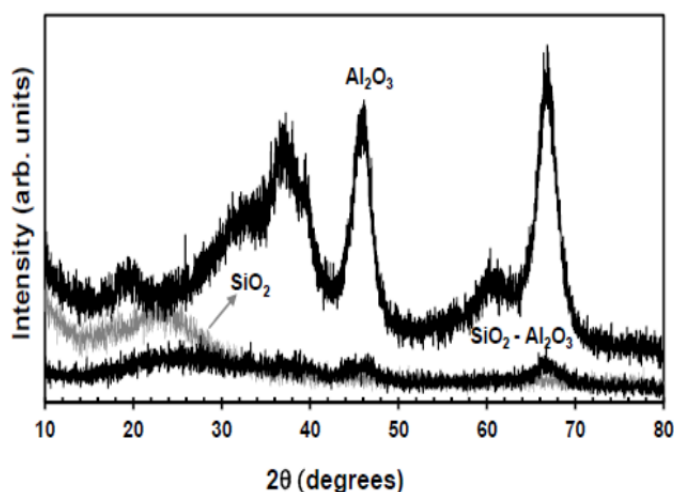


Figure 3-4: Wide-angle XRD patterns of γ -alumina, silica, and the alumina-silica binary.

The surface and up to two microns in-depth of the as-prepared thin films are investigated by PADB. From the R-parameter data a clear distinction can be made between the pure γ - Al_2O_3 and the other two samples. The trend of the curve in the pure γ - Al_2O_3 (Figure 3-5) shows that o-Ps annihilation decay via R ($3\gamma/2\gamma$ annihilation ratio) is observed up to the maximum positron implantation energy. The 3γ decay

originates from the o-Ps self-annihilation, which is reflected in the R-parameter, i.e., an increase in the 3γ annihilation contributes to the increase of R. The binary sample only shows a relevant amount of 3γ decay events up to a depth of approximately 80 nm (see upper axis of Figure 3-5). This increase at such low incident positron energies is attributed to the back-scattering of non-thermalized or fast positrons that pick up electrons at the surface and escape back to vacuum as fast Ps (p-Ps and o-Ps). For the pure silica sample the o-Ps signal extends to a somewhat larger depth of about 200 nm. This is attributed to additional back-diffusion of thermalized positrons to the surface followed by the emission of thermal Ps. The Doppler broadening of positron-annihilation measurements are presented by the S-parameter versus mean positron implantation energy (mean positron implantation depth, upper axis as shown in Figure 3-5).

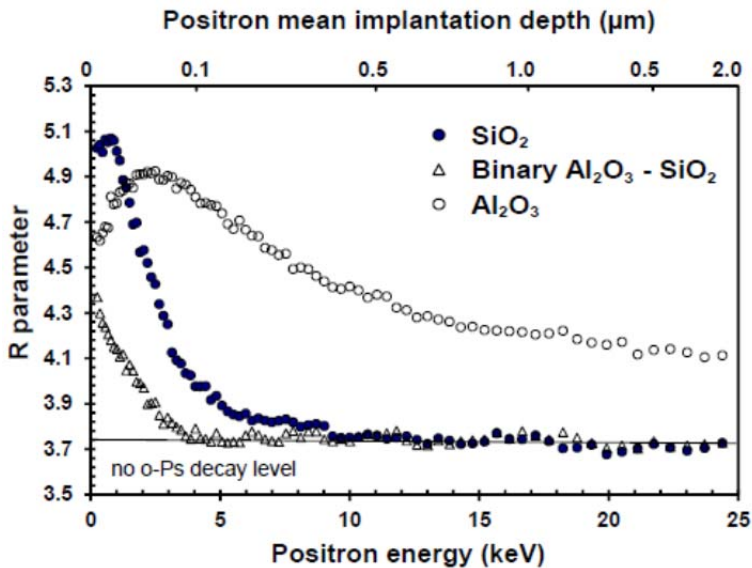


Figure 3-5: The R parameter as a function of positron implantation energy (bottom x-axis) and corresponding mean implantation depth (top x-axis).

As for the R parameter, with increasing positron implantation energy, the S parameter firstly characterizes the surface, then the sub-surface, and finally the bulk up to a depth of about 2 μm . As shown in Figure 3-6, no significant difference between pure $\gamma\text{-Al}_2\text{O}_3$

and SiO_2 is observed when going from the surface to the interior of the film. The trends of the S parameter indicate positron annihilation in a homogeneous layer. In contrast, the binary sample shows lower S values. These lower S values can be attributed to the reaction of Ps with Brønsted acid sites of the binary material. Huang et al.^[27] reported that the Brønsted acid sites are responsible for the change in the annihilation characteristics of Ps by means of its oxidation with Brønsted protons. This reflects the value of S parameter, i.e., the decrease in the value of S parameter with increasing Brønsted acid sites. By incorporating the silicon atoms into alumina network, the formation of the bridged hydroxyl groups (Brønsted acid sites) Si-OH-Al can be present^[24, 25, 27]. Therefore, the lower S values are observed, which is also indicative of the homogeneous distribution of silica-like domains in a γ -alumina matrix. A minimum of the S parameter is observed at an energy of about 3.5 keV, indicating the presence of a sub-surface region or interface capable of effectively trapping positrons and thus preventing back diffusion of thermal positrons towards the surface. The above mentioned energy is in accordance with the onset of the 3γ decay events depicted in Figure 3-5. A possible reason for this asymmetry may be explained by the evaporation mechanism that occurs during the drying of the film. The one face is open to the ambient enabling quick drying by evaporation, and then leads to the denser packing of the particles. On the other hand the side in contact with the Petri dish lacks this quick evaporation pathway. The apparent difference in R- and S-dependence can be accounted for by constructing a branching scheme for the different positron annihilation channels. This has been shown for positron studies of internal pore surfaces in sol-gel-derived silicate films^[28]. The general information emerging from the positron data is that in the pure $\gamma\text{-Al}_2\text{O}_3$ pores are present that are large enough to accommodate Ps formation and the subsequent decay from the o-Ps state. The silica sample shows no sign of o-Ps decay via 3γ annihilation, putting an upper limit to the pore size. The high value of S (within the experimental uncertainty equal to that of alumina) is attributed to the intrinsic decay of p-Ps. With the settings of the momentum windows for determining the S parameter p-Ps decay is expected to yield an S of approximately 0.75. The fraction of positrons annihilating from this state accounts for

the observed value of S and thus hints at the formation of Ps. In the binary sample no o-Ps is observed. In addition, the low S value indicates that annihilation channels other than p-Ps decay are involved. This interpretation leads to the conclusion that in the alumina-silica binary sample Ps may preferentially interact with Brønsted protonic sites and annihilates as a free positron.

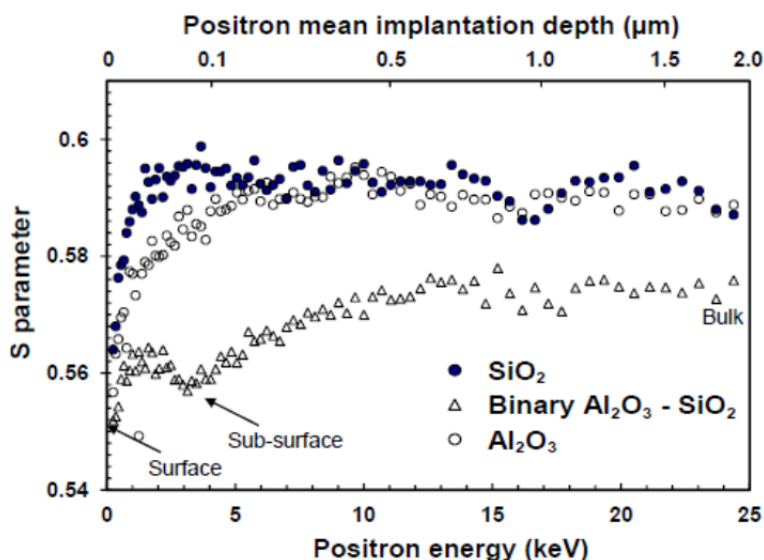


Figure 3-6: The S parameter as a function of positron implantation energy (bottom x-axis) and corresponding mean implantation depth (top x-axis).

The presence of Brønsted acid sites in the binary sample, which are absent in pure alumina or silica as already reported in the literature ^[21-25], is probed by FTIR spectroscopy under CO adsorption. Figure 3-7 shows the selected in-situ FTIR spectra 1–6 of CO adsorption on the silica-alumina binary sample at 77K for different equilibrium pressures. Spectrum 6 represents the highest CO adsorption of the sample. In the CO stretching region one broad and weak band appears initially at 2163 cm^{-1} , then increases its intensity and slightly shifts its position to 2156 cm^{-1} when the CO pressure is increased. This can be assigned to CO adsorbing on the OH of Brønsted acid sites. It should be noted that weak Lewis sites formed by dehydration of Brønsted acid sites also contributed in this band ^[25]. The other band growing with less prominent is observed at $\sim 2345\text{ cm}^{-1}$. According to the literature, this band may be

assigned to the formation of CO_2 on Lewis sites [29, 30]. In the OH stretching region, sharp bands are present at 3747 cm^{-1} , which are attributed to the silanol (SiOH) groups. Such OH groups with very weak acidity barely interact with a weakly basic CO. The absence of bridging OH stretching bands may be due to the fact that the silanol density is much higher than that of the bridging hydroxyl together with the low signal-to-noise ratio in this region. The FTIR result again points to silica islands in a γ -alumina matrix where the Brønsted sites are on the oxide interface.

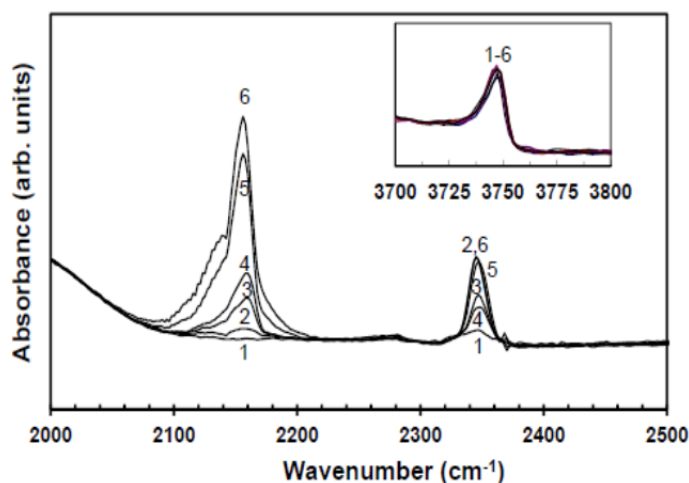


Figure 3-7: In-situ FTIR spectra (1-6) of CO adsorption on the alumina-silica binary sample, at 77K with different equilibrium pressures of 15Pa, 520Pa, 540 Pa, 560Pa, 1400 Pa, and 3500 Pa, respectively.

3.4 Conclusions

The investigation of the sol-gel derived porous membranes deposited as self-supported films, has generated a great deal of insight into the meso and microporous nature of their constituents, i.e., silica is microporous, γ -alumina is mesoporous, and the binary shows fingerprints of both the meso- and microporous structure. This is confirmed by all characterisation techniques used. The formation of bridging hydroxyl groups reflected from the positron annihilation and FTIR results reveal that the binary sample consists of more or less homogenous γ -alumina and silica regions with a chemical interaction between these phases. The fact that there are still silica rich regions can be

reflected in the inability of other authors to obtain good results on hydrothermally stable membranes upon mixing silica with another metal oxide. Interestingly, the positron annihilation technique, however complex, is very useful to evaluate the structural differences of such porous materials in a wide range of pore sizes and in the presence of specific acidic groups. The use of variable positron implantation energies (in the range of 100 eV–25 keV corresponding to a probe depth up to two microns) has been shown an ideal means for also characterizing porous supported membranes, of which the thickness (the amount of material) is even less than the self-supported films investigated in this work. This technique could be valuable for the assessment of drying mechanisms during membrane preparation, e.g., evaporation rate and capillary suction effects of thin film depositions (a few μm thick) on porous supports in future investigations.

Acknowledgements

The authors wish to thank Stanford University for supporting this work through the Global Climate Energy Project (GCEP) and the sponsors of GCEP. We gratefully acknowledge Prof. F. Kapteijn and his co-workers (Delft University of Technology) for providing access to the Autosorb 1-B, Quantachrome Instrument and FTIR spectroscopy.

References

- [1] Song, C. S., "Fuel processing for low-temperature and high-temperature fuel cells - Challenges, and opportunities for sustainable development in the 21st century", *Catalysis Today*, Vol. 77, No. 1-2, 2002, pp. 17-49.
- [2] Ockwig, N. W. and Nenoff, T. M., "Membranes for hydrogen separation", *Chemical Reviews*, Vol. 107, No. 10, 2007, pp. 4078-4110.
- [3] Benard, P. and Chahine, R., "Storage of hydrogen by physisorption on carbon and nanostructured materials", *Scripta Materialia*, Vol. 56, No. 10, 2007, pp. 803-808.

- [4] Han, S. S., Mendoza-Cortes, J. L., and Goddard, W. A., "Recent advances on simulation and theory of hydrogen storage in metal-organic frameworks and covalent organic frameworks", *Chemical Society Reviews*, Vol. 38, No. 5, 2009, pp. 1460-1476.
- [5] Guizard, C. G., Julbe, A. C., and Ayral, A., "Design of nanosized structures in sol-gel derived porous solids. Applications in catalyst and inorganic membrane preparation", *Journal of Materials Chemistry*, Vol. 9, No. 1, 1999, pp. 55-65.
- [6] Campaniello, J., Engelen, C. W. R., Haije, W. G., Pex, P. P. A. C., and Vente, J. F., "Long-term pervaporation performance of microporous methylated silica membranes", *Chemical Communications*, No. 7, 2004, pp. 834-835.
- [7] Verweij, H., Lin, Y. S., and Dong, J. H., "Microporous silica and zeolite membranes for hydrogen purification", *MRS Bulletin*, Vol. 31, No. 10, 2006, pp. 756-764.
- [8] Bonekamp, B. C., van Horssen, A., Correia, L. A., Vente, J. F., and Haije, W. G., "Macroporous support coatings for molecular separation membranes having a minimum defect density", *Journal of Membrane Science*, Vol. 278, No. 1-2, 2006, pp. 349-356.
- [9] Ockwig, N. W. and Nenoff, T. M., "Membranes for hydrogen separation", *Chem.Rev.*, Vol. 107, No. 10, 2007, pp. 4078-4110.
- [10] Bernardo, P., Drioli, E., and Golemme, G., "Membrane Gas Separation: A Review/State of the Art", *Ind.Eng.Chem.Res.*, Vol. 48, No. 10, 2009, pp. 4638-4663.
- [11] Campaniello, J., Engelen, C. W. R., Haije, W. G., Pex, P. P. A. C., and Vente, J. F., "Long-term pervaporation performance of microporous methylated silica membranes", *Chem.Comm.*, No. 7, 2004, pp. 834-835.
- [12] Fotou, G. P., Lin, Y. S., and Pratsinis, S. E., "Hydrothermal Stability of Pure and Modified Microporous Silica Membranes", *Journal of Materials Science*, Vol. 30, No. 11, 1995, pp. 2803-2808.

- [13] Gu, Y. F. and Oyama, S. T., "Permeation properties and hydrothermal stability of silica-titania membranes supported on porous alumina substrates", *Journal of Membrane Science*, Vol. 345, No. 1-2, 2009, pp. 267-275.
- [14] Yoshida, K., Hirano, Y., Fujii, H., Tsuru, T., and Asaeda, M., "Hydrothermal stability and performance of silica-zirconia membranes for hydrogen separation in hydrothermal conditions", *Journal of Chemical Engineering of Japan*, Vol. 34, No. 4, 2001, pp. 523-530.
- [15] Kanezashi, M. and Asaeda, M., "Hydrogen permeation characteristics and stability of Ni-doped silica membranes in steam at high temperature", *Journal of Membrane Science*, Vol. 271, No. 1-2, 2006, pp. 86-93.
- [16] de Vos, R. M. and Verweij, H., "Improved performance of silica membranes for gas separation", *Journal of Membrane Science*, Vol. 143, No. 1-2, 1998, pp. 37-51.
- [17] Brunauer, S., Emmett, P. H., and Teller, E., "Adsorption of gases in multimolecular layers", *Journal of the American Chemical Society*, Vol. 60, 1938, pp. 309-319.
- [18] Evans, R., "The nature of the liquid-vapour interface and other topics in the statistical mechanics of non-uniform, classical fluids", *Advances in Physics*, Vol. 28, No. 2, 1979, pp. 143-200.
- [19] Lastoskie, C., Gubbins, K. E., and Quirke, N., "Pore-Size Heterogeneity and the Carbon Slit Pore - A Density-Functional Theory Model", *Langmuir*, Vol. 9, No. 10, 1993, pp. 2693-2702.
- [20] Horvath, G. and Kawazoe, K., "Method for the Calculation of Effective Pore-Size Distribution in Molecular-Sieve Carbon", *Journal of Chemical Engineering of Japan*, Vol. 16, No. 6, 1983, pp. 470-475.
- [21] Daniell, W., Schubert, U., Glockler, R., Meyer, A., Noweck, K., and Knozinger, H., "Enhanced surface acidity in mixed alumina-silicas: a low-temperature FTIR study", *Applied Catalysis A-General*, Vol. 196, No. 2, 2000, pp. 247-260.
- [22] Crepeau, G., Montouillout, V., Vimont, A., Maréchal, L., Cseri, T., and Mauge, F., "Nature, structure and strength of the acidic sites of amorphous silica

alumina: An IR and NMR study", *Journal of Physical Chemistry B*, Vol. 110, No. 31, 2006, pp. 15172-15185.

[23] Trombetta, M., Busca, G., Rossini, S., Piccoli, V., Cornaro, U., Guercio, A., Catani, R., and Willey, R. J., "FT-IR studies on light olefin skeletal isomerization catalysis III. Surface acidity and activity of amorphous and crystalline catalysts belonging to the SiO₂-Al₂O₃ system", *Journal of Catalysis*, Vol. 179, No. 2, 1998, pp. 581-596.

[24] Gruver, V. and Fripiat, J. J., "Lewis-Acid Sites and Surface Aluminum in Aluminas and Mordenites - An Infrared Study of Co Chemisorption", *Journal of Physical Chemistry*, Vol. 98, No. 34, 1994, pp. 8549-8554.

[25] Lavalley, J. C., "Infrared spectrometric studies of the surface basicity of metal oxides and zeolites using adsorbed probe molecules", *Catalysis Today*, Vol. 27, No. 3-4, 1996, pp. 377-401.

[26] Sing, K. S. W., Everett, D. H., Haul, R. A. W., Moscou, L., Pierotti, R. A., Rouquerol, J., and Siemieniewska, T., "Reporting Physisorption Data for Gas Solid Systems with Special Reference to the Determination of Surface-Area and Porosity (Recommendations 1984)", *Pure Appl.Chem.*, Vol. 57, No. 4, 1985, pp. 603-619.

[27] Huang, W. F., Huang, D. C., and Tseng, P. K., "Surface-Acidity by Positron-Annihilation Lineshapes", *Catalysis Letters*, Vol. 26, No. 3-4, 1994, pp. 269-275.

[28] Galindo, R. E., van Veen, A., Schut, H., Falub, C. V., Balkenende, A. R., de With, G., and De Hosson, J. T. M., "Nano-porosity in silica reinforced methyltrimethoxysilane coatings studied by positron beam analysis", *Composites Science and Technology*, Vol. 63, No. 8, 2003, pp. 1133-1139.

[29] Rakic, V. M., Hercigonja, R. V., and Dondur, V. T., "CO interaction with zeolites studied by TPD and FTIR: transition-metal ion-exchanged FAU-type zeolites", *Microporous and Mesoporous Materials*, Vol. 27, No. 1, 1999, pp. 27-39.

[30] Montanari, T., Marie, O., Daturi, M., and Busca, G., "Cobalt on and in zeolites and silica-alumina: Spectroscopic characterization and reactivity", *Catalysis Today*, Vol. 110, No. 3-4, 2005, pp. 339-344.

Chapter 4

Hydrogen separation properties of a sol-gel derived zirconia membrane with pore sizes tuned using atomic layer deposition of alumina

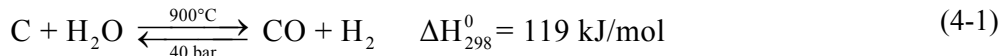
Abstract

In this study the H₂ separation properties of a composite alumina-zirconia membrane, prepared via the sol-gel route in combination with atomic layer deposition (ALD) of alumina, are evaluated. The gas permeation properties of this modified zirconia exhibit results similar to microporous silica membranes. Gas permeation tests show a preferential permeation of H₂ and a separation factor of H₂ over CO₂ of about 3.8. For future H₂/CO₂ separation in the subsequent water-gas shift reactor the membrane, however, still needs to out-perform the membrane described in this paper. The results of this work, however, already show the potential of these techniques to develop non-silica microporous membranes for H₂ separation.

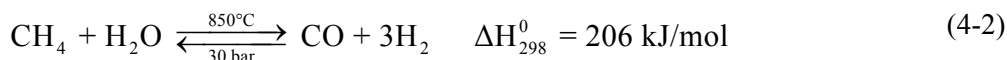
4.1 Introduction

An increasing interest in H₂ fuel systems is mainly related to environmental issues in pollutant emissions from fossil fuel burning. Both are responsible for the greenhouse effect on a worldwide scale and the (mega)-cities' air quality on a smaller scale. H₂ is considered as a sustainable energy carrier that eventually will be produced from renewable energy sources. At present the production of H₂ from fossil-based resources is still dominant ^[1, 2]. In this context, the concept of H₂ production coupled with CO₂ capture and storage (CCS) has been advocated by a number of research groups worldwide ^[3, 4]. This can help to establish an H₂ supply infrastructure and commercialize fuel cells in automobile and stationary applications. Conventionally, coal or methane is reformed to a syngas, mainly consisting of carbon monoxide (CO) and H₂ (Eq.1 and 2), which is further converted to carbon dioxide (CO₂) and H₂ mixture, as shown in Eq.3 ^[2, 5].

(a) Coal gasification (CG)

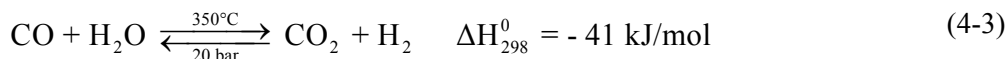


(b) Steam-methane reforming (SMR)



In the second step, CO in the syngas is converted into CO₂ and H₂ via the water-gas-shift (WGS) reaction:

(c) Water-gas-shift (WGS)



In order to capture CO₂ from the gas mixture and to use H₂ as a clean fuel, it needs to be separated from CO and CO₂. This can be achieved in-situ by combining the reforming process with H₂ separation in a membrane reactor ^[6]. One of the advantages of a membrane reactor is the separation of H₂ (or CO₂) from the equilibrium mixture which increases the conversion of coal (or methane) and enables a lower reaction temperature (less energy consumption). It is important to note at this point that the

reactor size can be remarkably reduced for small scale H₂ sites. Therefore, various membranes are under development for the H₂ separation at elevated temperatures, including palladium alloys, porous-silica-, zeolite-, and carbon-based membranes [6]. Silica and related siliceous materials exhibit interesting properties such as high H₂ permeability, good selectivity, and low cost. However, the problem is that for the application in a steam-containing environment silica-based materials are not stable [7]. The use of more stable oxides would be desirable. Zirconia has received particular attention because the hydrothermal stability of zirconia-based material is demonstrated by its use in solid oxide fuel cells operated at high temperature (700-1000 °C) and in a severe oxidizing and reducing environment [8]. A mesoporous zirconia membrane can be prepared via a sol-gel process in combination with a surfactant-based self-assembly method [9]. While this route can yield a membrane with a narrow pore size distribution and a low tortuosity, the permeation selectivity of the membrane for gas mixtures is still insufficient due to its large pore size inherent to the use of surfactant and templating agents.

Different strategies, such as the chemical modification by sulfuric acid [10] or the use of atomic layer deposition (ALD) as in this study, were developed in order to decrease the pore size of the sol-gel derived zirconia membrane and thus to improve separation selectivity. ALD of metal oxides proceeds through a pair of sequential exposures to active vapor precursors on a substrate. The process results in successive reactions of adsorption and hydrolysis of metal precursors. The precursor exposures are separated by inert gas purging in order to avoid gas-phase reactions between the two precursors. In such a cyclic manner, it allows to deposit layer-by-layer of a metal oxide thin film on a substrate. This easy thickness control has been shown to reduce the pore size of anodic alumina and silica membranes by increasing number of deposition cycles [11-14]. Moreover, the scalability of ALD offers an important prospect for industrial applications [15, 16].

In this study, the composite alumina-zirconia membranes, particularly targeting at H₂/CO₂ separation, have been prepared. The approach consists of two steps: production of a mesoporous zirconia membrane using the sol-gel and then grafting alumina on

mesoporous zirconia with ALD. The impact of ALD of alumina on the reduction of the pore size of zirconia-based thin films and the performance of a membrane made out of it, are investigated. The permeability and selectivity of supported membranes towards CO₂ and H₂ are presented.

4.2 Experimental details

4.2.1 Preparations of zirconia thin-films and membranes

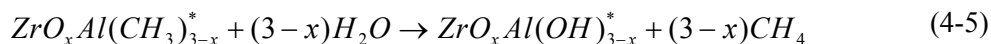
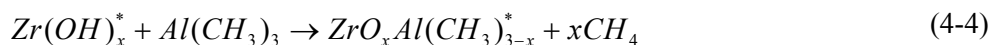
The mesoporous zirconia membrane layers were synthesized using the sol-gel method combined with the surfactant-based self-assembly technique ^[17]. In the present synthesis procedure adopted for thin films, cetyl-trimethylammonium bromide (CTAB, Aldrich, 99%) surfactant and tetrahydrofuran (THF, Aldrich, 99.8%) were added to ethanol (C₂H₅OH, Aldrich, 99.5%) and deionized water (resistivity: 18 MΩ.cm). After 15 min of stirring, zirconium oxychloride (ZrOCl₂.8H₂O, Aldrich, 99.9%) was added to the solution which has a pH of about 1. After 30 min, glacial acetic acid (CH₃COOH, Aldrich, 99.7%) was added and the mixture was stirred for 1 h. The molar ratio of the final sol was H₂O:C₂H₅OH: CTAB: THF: ZrOCl₂.8H₂O:CH₃COOH= 5.6:27.7:0.5:0.62:1.0:4.24. The sol was aged for two hours at 80 °C in order to obtain a stable sol solution. Zirconia thin films (unsupported membranes) were prepared by pouring the sol in a clean Petri dish. In order to obtain zirconia supported membranes, commercial α-alumina supports (the thickness is 2 mm with a diameter of 25 mm and an average pore size of 150 nm, Pervatech©) were immersed into the prepared sol for a few seconds (< 5 s), and were then removed from the sol and dried in air at room temperature. With the ramping rate set at 1°C/min, the samples were heated at 60 °C for 12 h, then to 120 °C for 12 h, and finally at 500 °C for calcination in air for 3 h.

4.2.2 Alumina deposition using TMA and H₂O precursors

ALD of Al₂O₃ was developed to tailor the pore-opening of the as-synthesized mesoporous zirconia using a viscous-flow ALD reactor. The reactor has been used in an earlier study to coat particles ^[18]. Typically, the pre-treatment of the samples was

carried out at high temperature (500 °C) in order to remove any organic and especially water vapour contamination throughout the porous structure. The unsupported zirconia film (around 0.2 g) was loaded as a free standing film in the reactor that was subsequently purged with dry nitrogen at an operating temperature of 160 °C for 12 h. The supported ones were placed in the reactor with the gas flow laterally across the zirconia mesoporous layer. The liquid $\text{Al}(\text{CH}_3)_3$ (TMA) was held in a 250 ml steel bubbler (Akzo Nobel semiconductor grade, 99.9%) at 20 °C. During the TMA exposure, the TMA was delivered into the reactor as a vapour by passing N_2 gas (TriGas, 99.9%) at the controlled flow rate (0.1 l min^{-1}) through the bubbler. Deionised water (resistivity: $18 \text{ M}\Omega\cdot\text{cm}$) was held in a 250 ml steel bubbler at 20 °C. Water vapour was introduced into the reactor by passing N_2 gas at the controlled flow rate (0.1 l min^{-1}) through the bubbler. One ALD cycle is carried out in the following order of steps: TMA exposure, N_2 purging, H_2O exposure, and N_2 purging. The duration of each cycle was between 20 and 45 min. These times were not rigorously optimized, but were calculated to be able to remove even a five-fold higher dose of reactants and CH_4 product during the N_2 purge step. The surface reactions were performed at a temperature of 160 °C and a total pressure of 100 kPa. Two experiments with 15 and 30 ALD cycles were performed with the unsupported samples and 5 ALD cycles for the supported sample, which are further discussed in this paper.

The surface reactions (4) and (5) which define the cycle for ALD of Al_2O_3 are:



where the asterisks (*) indicate surface species. The repetition number of these two step reactions determines the thickness of the resulting Al_2O_3 layer.

4.2.3 Characterization

Nitrogen adsorption-desorption measurements were performed with unsupported membranes only in an Autosorb 1-B physisorption set-up (Quantachrome Instruments). The morphology and structure of the unsupported membranes were investigated by

Transmission Electron Microscopy (TEM, Philips CM30T electron microscope with a LaB₆ filament as electron source operated at 300 kV) equipped with an energy-dispersive X-ray system, and X-ray diffraction (Bruker D8 Advance XRD with Co K α -radiation) analysis on powders. The layer thickness of the supported membrane was determined on a fractured surface by Scanning Electron Microscopy (SEM, JEOL 6330F microscope). Permporometry is used to determine the pore size distribution of a mesoporous layer supported on a macroporous support and to check whether defects in the layer are present.

4.2.4 Gas permeation tests

Single-gas permeation tests were carried out by passing He, H₂, CO₂, N₂, or SF₆ through the selective-layer (mesoporous zirconia or zirconia modified with ALD of alumina) of the supported membrane. The permeate flow of a gas was measured with a soap meter. In this test, a total pressure on the feed side was kept in the range of 2–5 $\times 10^5$ Pa and the permeate side was kept constant at atmospheric pressure. The permeation temperature is limited at 100 °C due to the presence of low-temperature O-ring seals in the equipment. Error estimates were in most cases within 5 % of the calculated permeance and so error bars were not included in plots as they were difficult to visualize from the data points. The permeance Per (mol.m⁻²s⁻¹Pa⁻¹) of the gas permeating through the membrane is defined as:

$$\text{Per} = \frac{J}{\Delta P A} \quad (4-6)$$

where J is the gas flow through the membrane (mol.s⁻¹), $\Delta P = P_f - P_p$ is the pressure difference (Pa), P_f and P_p are the pressures in the feed side and permeate side, respectively, and A is the exposed area of the membrane (m²).

The permselectivity for gas A over gas B is calculated by the ratio of their permeances and the ideal Knudsen separation factor $\alpha_{K(A/B)}$ is defined as follows:

$$\alpha_{K(A/B)} = \sqrt{\frac{M_B}{M_A}} \quad (4-7)$$

where M_A and M_B are the molecular weights of the separated gases A and B.

In addition, the membranes were further tested with a H_2/CO_2 mixture (50:50/v:v) at 10^5 Pa pressure difference across the membrane. The gas compositions were analyzed by gas chromatography (Varian Micro-GC4900) with a flame ionization detector (FID) and a thermal conductivity detector (TCD). The separation factor α_{H_2/CO_2} is expressed as a function of the molar fractions by the following equation:

$$\alpha_{H_2/CO_2} = \frac{y_{p,H_2}}{x_{r,H_2}} \frac{x_{r,CO_2}}{y_{p,CO_2}} \quad (4-8)$$

where y_{p,H_2} and y_{p,CO_2} are the molar fractions of H_2 and CO_2 at the permeate side and x_{r,H_2} and x_{r,CO_2} are the molar fractions of H_2 and CO_2 at the retentate side.

4.3 Results and Discussion

4.3.1 The effects of alumina deposition on the pore size of unsupported zirconia membranes

Figure 4-1 shows the N_2 isotherms at 77 K of the starting unsupported zirconia and after ALD of alumina using 15 and 30 cycles. It is evident that the three samples exhibit the classical shape of type IV isotherm according to the IUPAC classification [20]. They are characteristic for mesoporous materials. Each isotherm exhibits a hysteresis of type H1 between the adsorption and desorption branches due to the capillary condensation of nitrogen inside the template-induced mesopores and in the large mesopores formed among randomly packed powder particles at a high relative pressure ($P/P_0 > 0.8$). With an increasing number of alumina deposition cycles (Figure 4-2), the H1 hysteresis loop becomes smaller in magnitude, as well as the volume of absorbed nitrogen. The Brunauer-Emmett-Teller (BET) surface areas also decrease from 52.1 to 36 $m^2 \cdot g^{-1}$ with the decrease of pore volumes from 0.18 to 0.08 $cm^3 \cdot g^{-1}$ as listed in

Table 4-1. The starting BET area is rather low, which is probably due to the collapse of the pore structure during sintering. The observed pores are mainly interparticle in origin. From the BET-constant C using the BET equation ^[21], which is indicative of the strength of the interaction of N_2 molecule with polar surface groups (e.g., OH, CH_3 -O), it does not show a clear difference between the non-modified and the modified ALD samples. It does not provide additional structural information because they have similar hydroxy groups on the surface. The pore size distributions (Figure 4-2) are calculated using the non-local density functional theory (NLDFT) method ^[22]. The zirconia has a mesopore size distribution centred at 11 nm which shifts to lower diameters as increasing ALD cycle number. After 30 ALD cycles, the mean pore size is reduced from 11 to 8 nm. The reduction indicates that the deposited alumina can cover the pore entrance and/or part of the pore walls. Theoretically, if the pores in the zirconia are larger than the diameters of the precursor molecules, i.e., TMA and H_2O , the precursors can diffuse into the pores and form a layer of Al-OH. As expected, the pore size decreases with increasing number of ALD cycles. It is noteworthy that alumina growth on dense substrates (Si wafers) is relatively linear in the number of deposition cycles as reported in many references ^[23, 24]. The typical alumina growth rate is around 0.1 nm per cycle. The growth rate of the deposited layer in the pores is likely diminished due to the effect of the steric hindrance of the TMA moiety on entering the pore, and the presence of less hydroxyl groups on the pore wall surface after each ALD cycle ^[24]. Another hampering factor can be that the removal of residual reactants and byproducts is inhibited when the pores become smaller. Therefore, further deposition cycles result in much longer deposition time.

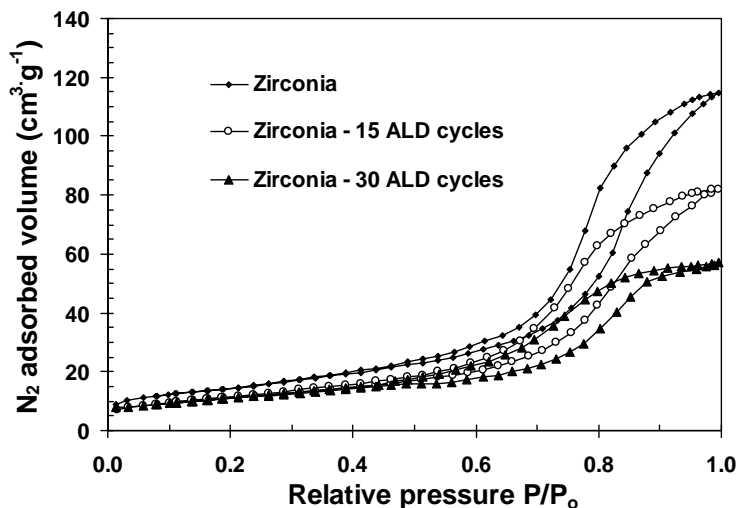


Figure 4-1: N_2 adsorption-desorption isotherms at 77 K for unsupported mesoporous zirconia before and after modification with 15 and 30 ALD cycles of alumina (adsorption branch is a lower curve).

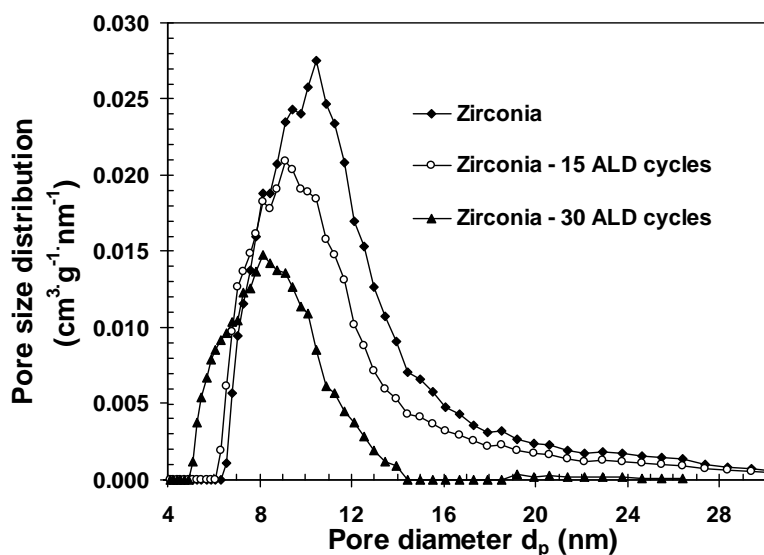


Figure 4-2: Pore size distributions by using the non-local density functional theory (NLDFT) corresponding to the isotherms in Figure 4-1.

Table 4-1: BET surface area, pore size and pore volumes as obtained from nitrogen physisorption data and alumina content estimation based on the alumina growth rate of 0.1 nm/cycle (all standard deviations were obtained from triplicate measurements).

Sample	Zirconia	deposited 15 ALD cycles	deposited 30 ALD cycles
BET surface ($\text{m}^2 \cdot \text{g}^{-1}$)	52.1 ± 2.1	40.6 ± 2.1	36.3 ± 1.5
BET-constant C	103.4 ± 3.1	99.23 ± 3.1	92.6 ± 3.1
Pore volume ($\text{cm}^3 \cdot \text{g}^{-1}$)	0.18 ± 0.01	0.14 ± 0.01	0.08 ± 0.01
Pore size (nm)	11.0 ± 0.5	9.0 ± 0.5	8.0 ± 0.5
Alumina weight (%)	0	22.4 ± 10.2	36.6 ± 20.1

Figure 4-3a and b show the wide-angle XRD patterns of the unsupported zirconia sample and after 30 ALD cycles. The zirconia pattern (Figure 4-3a) has the fingerprints of the crystalline monoclinic and tetragonal phases ^[25]. Figure 4-3c shows the low-angle XRD pattern of the same sample. A small single peak is observed at $2\theta = 1.8^\circ$ corresponding to the (010) reflection. This peak is arising from a lattice of aligned cylinders as reported for mesoporous crystalline material (MCM-41) ^[26, 27]. Because the zirconium specie is not as well condensed as siliceous one ^[26, 27] and the organic-Zr interaction is stronger than the organic-Si, disorder or structural rearrangement occurs during calcination at temperatures above 350°C ^[28]. Upon the complete template removal at the selected temperature (500°C), the mesoporous structure is still remained in the zirconia sample, but undergoes transformation to a disordered structure. After the ALD of alumina, the XRD pattern (Figure 4-3b) is very similar to the pattern of the originally zirconia sample. Thus, the deposited alumina on the sample is too amorphous to produce well defined reflection peaks in XRD.

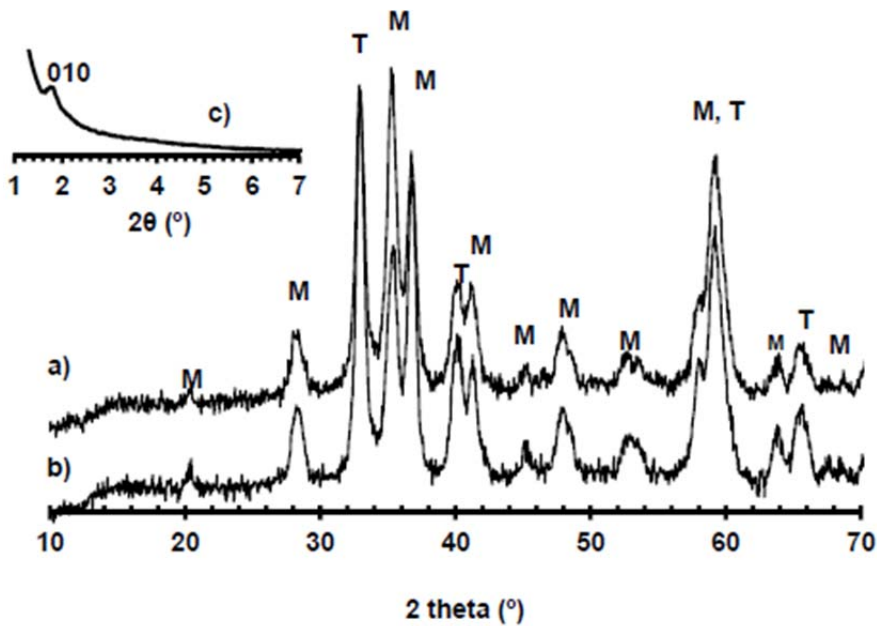


Figure 4-3: Wide-angle XRD powder patterns of mesoporous zirconia (a) and after modification with 30 ALD cycles of alumina (b), revealing monoclinic (M) and tetragonal (T) phases, and low-angle XRD powder pattern of mesoporous zirconia (c).

TEM images (Figure 4-4) reveal that the initial mesoporous zirconia film is composed of aggregated and sintered nano-particles in the range of 10–20 nm. The only visible periodicity is in the rows of atoms of which the interplanar distance was calculated to be 0.29 nm. This d-spacing value corresponds to the (101) reflection of the tetragonal zirconia phase ^[25]. This unfortunately does not give a clue as to the presence, orientation, and ordering of the expected cylindrical mesopores. The structural morphology is not changed after 30 cycles of alumina ALD. From visual inspection in high resolution, a thin amorphous layer of alumina is more and less defined on the edge formed between aggregated nano-particles. EDX analysis indicates qualitatively the presence of Al but also an artefact due to background noise.

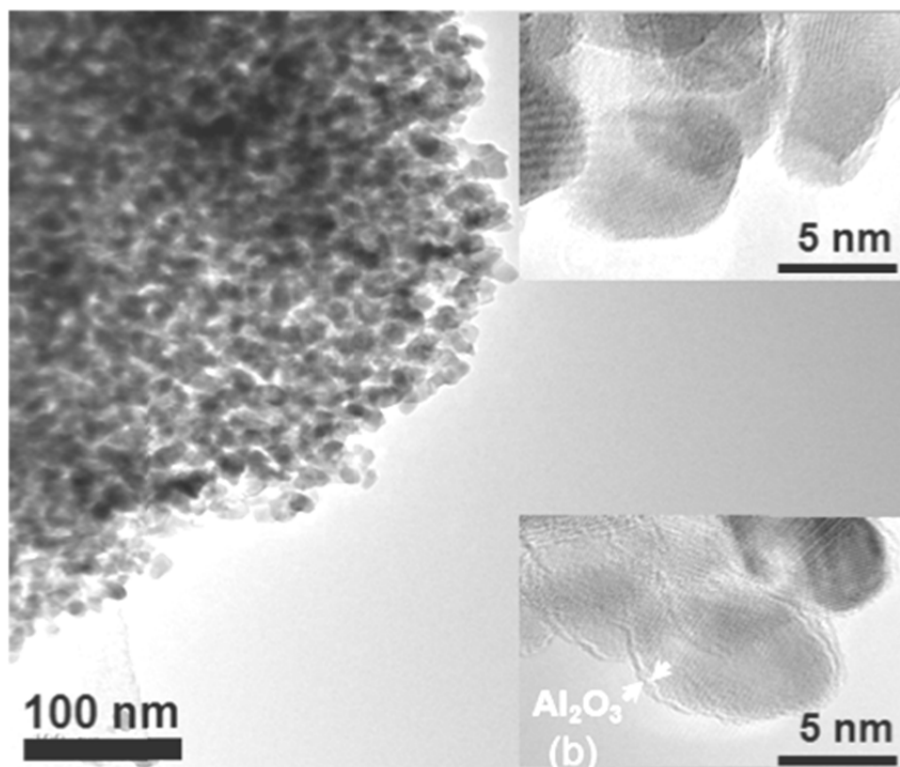


Figure 4-4: TEM images for mesoporous zirconia and HR-TEM images of mesoporous zirconia before (a) and after 30 ALD cycles of alumina (b).

4.3.2 Membrane permeation and separation experiments

Figure 4-5 shows the single gas permeances of different probe molecules at 25 °C and pressure difference of 10^5 Pa for a pure supported zirconia membrane and after 5 ALD cycles of alumina (modified membrane). The zirconia membrane has higher permeance values but its permselectivities are lower than the ideal Knudsen separation factor values. This indicates the presence of defects where viscous flow contributes to the gas transport. The modified membrane has lower permeance values and higher permselectivities values. Its permselectivities are mainly in the Knudsen regime. It is also noted that the H_2/SF_6 permselectivity (9.7) is higher than the ideal Knudsen separation factor (8.54). Taking into account the kinetic diameters of H_2 (0.3 nm) and SF_6 (0.55 nm), the result reveals that the modified membrane separates also on

molecular size, i.e., in the micropores regime. Table 4-2 presents the H₂ and CO₂ single gas and H₂/CO₂ mixed gas (50:50/v:v) permeances of these membranes at 25 °C and 100 °C. The H₂/CO₂ permselectivity is higher in the modified membrane, 4.22 and 4.45 as compared to 2.42 and 2.50 in the zirconia one. However, the permeances of the modified membrane are around half an order of magnitude smaller than for the pure zirconia. For the binary gas permeation with the H₂/CO₂ mixture (50:50/v:v), it is also observed that the separation factor α_{H_2/CO_2} increases to 3.8 with increasing temperature in the modified membrane, while no change in the zirconia one is observed. The separation factor is not high enough for the desirable 90% H₂ selectivity in practical applications. However, the observed separation factor of the modified membrane is comparable to that of a supported microporous silica membrane under similar conditions as reported in the literature ^[29], even in the presence of defects as observed in SEM (Figure 4-6). The results indicate that the ALD modification has a substantially beneficial impact on the transport of gases. In the modified membrane, the H₂ permeance slightly increases with temperature while hardly any difference is observed for the CO₂ permeance. This behavior is ascribed to an activated surface diffusion process and is in accordance with the Arrhenius-type relationship described in the literature ^[30, 31]. Since CO₂ has the higher absorption interaction and activation energy, at temperatures below 100 °C, CO₂ adsorption onto the pore walls is higher than for H₂. This explains that the H₂ permeance increases a bit when going from 25 °C to 100 °C while that of CO₂ does not. Therefore, the H₂/CO₂ separation factor of the modified membrane can be expected to be significantly higher at higher temperatures, as well as by further reducing pore size through ALD cycles. Unfortunately, further deposition cycles, i.e., the 15 ALD cycles resulted in a strong decrease of the gas permeation down to the limit of the test set-up.

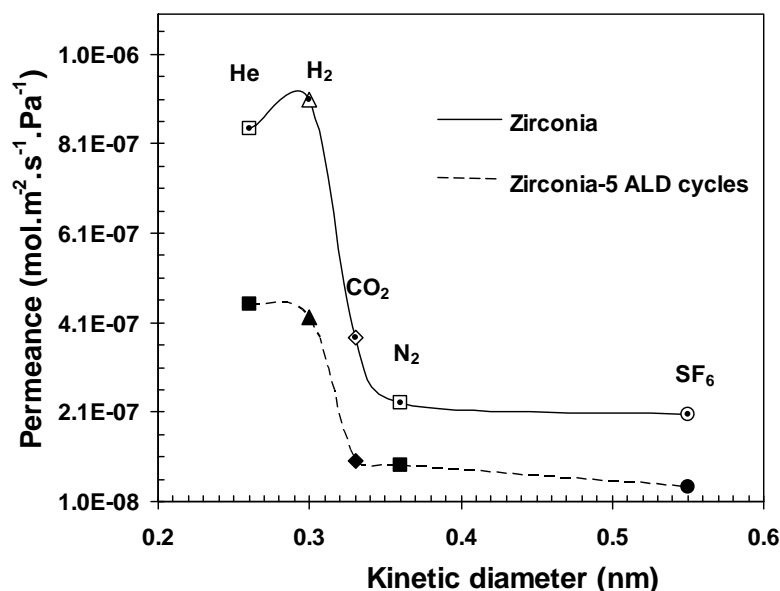


Figure 4-5: Permeance of single gases ($T = 25^{\circ}\text{C}$) through zirconia membranes and after alumina ALD (5 ALD cycles).

Table 4-2: Permeation and separation properties of the zirconia and alumina-deposited zirconia (5 ALD cycles) membranes at 25°C and 100°C and 10^5 Pa of the mean pressure (Error estimates were in most cases within 5 % of the calculated permeance).

Sample	Zirconia		Zirconia - 5 ALD cycles	
Temperature ($^{\circ}\text{C}$)	25	100	25	100
H ₂ permeance ($\cdot 10^{-7} \text{ mol m}^{-2} \text{ Pa}^{-1} \text{ s}^{-1}$)	9.09	9.30	4.22	4.46
CO ₂ permeance ($\cdot 10^{-7} \text{ mol m}^{-2} \text{ Pa}^{-1} \text{ s}^{-1}$)	3.75	3.73	1.0	0.98
Permselectivity	2.4	2.5	4.2	4.4
Separation factor H ₂ /CO ₂ (50/50)	1.5	1.5	2.6	3.8

4.3.3 Membrane surface characterization

SEM photographs (Figure 4-6) of zirconia after 5 ALD cycles of alumina show a top view of the surface (Figure 4-6a) and a cross section (Figure 4-6b). During the dip-coating process, only one dipping step has been applied. This is probably the reason that the zirconia layer has pinholes and cracks formed during the calcination that are too large to be covered with 5 cycles of alumina ALD (see Figure 4-6a). Since the difference in thermal expansion coefficient between zirconia and $\alpha\text{-Al}_2\text{O}_3$ is small, cracks are expected only due to shrinkage during CTAB removal at high temperatures. Using this short dip-coating time (few seconds), it is expected that one would obtain a very thin membrane that has a high permeance, at the risk of not having a defect-free membrane. As can be observed in Figure 4-6b, the zirconia/alumina layer has a thickness of around $1\mu\text{m}$ and is well adhered to the $\alpha\text{-alumina}$ substrate.

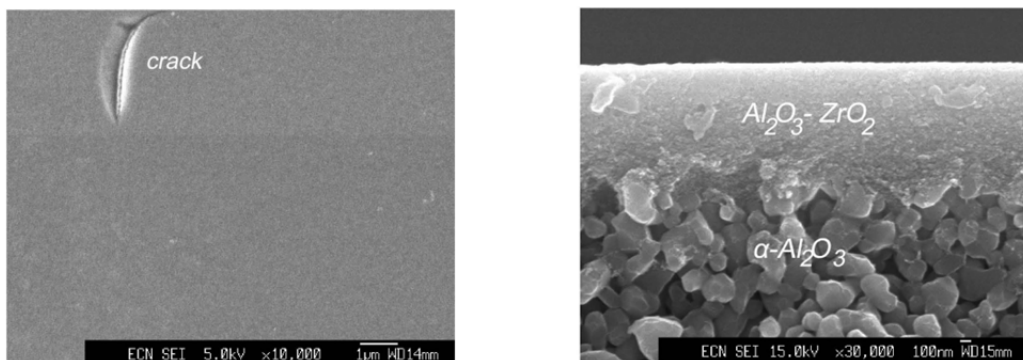


Figure 4-6: SEM pictures of an upper top-surface with drying crack (a) and a cross section (b) of alumina-coated zirconia supported $\alpha\text{-Al}_2\text{O}_3$ substrate.

4.3.4 Pore size analysis on supported membranes

In order to estimate the Kelvin pore size distribution of the porous top layer of the supported membranes after 5 ALD cycles, permporometry was carried out at 60°C . This is one of the few analytical techniques that can measure active pore sizes in-situ on a supported membrane ^[19]. Figure 4-7 shows the permeance of He through the membrane during the adsorption and desorption of H_2O . The Kelvin pore diameter is directly calculated using the Kelvin equation with the relative pressures and properties

of H₂O. The He permeance is reduced from 2.2×10^{-7} to 1.7×10^{-7} mol·m⁻²·Pa⁻¹·s⁻¹ at a relative pressure of 0.63, which corresponds with a Kelvin diameter of ~ 4 nm, and then remains constant until a relative pressure of 0.99. This result indicates a distribution of pores with diameters smaller than 4 nm and the presence of defects. The defects (cracks, pinholes larger than 4nm) cannot be blocked by the condensation of H₂O vapor at the relative humidity values used. A typical permeance for water-blocked defect-free membranes would be around 10^{-8} mol·m⁻²·Pa⁻¹·s⁻¹.

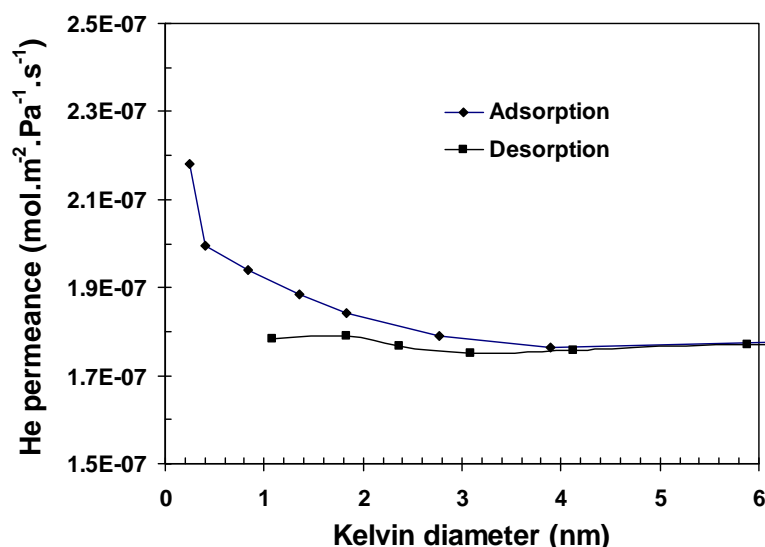


Figure 4-7: Permporometry adsorption and desorption curves for a zirconia membrane modified with 5 ALD cycles with H₂O used as adsorbate (T=60 °C).

4.4 Conclusions

The background of this research is the H₂ production from fossil fuels that plays a major role in an affordable H₂ infrastructure without CO₂ emissions. High H₂ separation can be realized when the membrane can be operated in a steam environment and at high temperatures and has a pore size small enough to achieve substantial differences in molecular diffusivity between H₂ and CO, CH₄, or CO₂. ALD is a flexible and reproducible method to reduce the pore size of zirconia membranes. By finely tuning the ALD parameters, the pore size of zirconia was successfully reduced.

The reduction of the size of the accessible zirconia pores via alumina ALD is confirmed with nitrogen physisorption and gas permeation measurements on unsupported and supported zirconia membranes, respectively. A supported zirconia membrane modified with ALD shows an increase of the H₂ selectivity, but also a strong decrease of permeance. Due to the defects in the zirconia layer, the separation factor for H₂ is still quite modest, 3.8, but already comparable to that of microporous silica membranes under the same conditions used. If optimized, the chosen strategy appears promising in the development of H₂-selective microporous membranes. Further research is focused on making defect-free zirconia thin layers with the right orientation of the cylinders and improving the H₂ selectivity at higher temperatures and in relevant gas mixtures.

Acknowledgements

The authors wish to thank Stanford University for supporting the research through the Global Climate Energy Project (GCEP) and the sponsors of GCEP. We gratefully acknowledge Dr. J. R. van Ommen and M. de Niet for providing access to ALD experiments, Prof. F. Kapteijn (Delft University of Technology) and his co-workers for providing access to equipment for membrane characterization and Dr. U. Lafont (Delft University of Technology) for TEM analysis.

References

- [1] BP, "Statistical review of world energy," 2009.
- [2] World Coal Institute, "The coal resource: a comprehensive overview of coal," London, UK, 2005.
- [3] Yang, H. Q., Xu, Z. H., Fan, M. H., Gupta, R., Slimane, R. B., Bland, A. E., and Wright, I., "Progress in carbon dioxide separation and capture: A review", *Journal of Environmental Sciences*, Vol. 20, No. 1, 2008, pp. 14-27.

- [4] Muradov, N. Z. and Veziroglu, T. N., "'Green' path from fossil-based to hydrogen economy: An overview of carbon-neutral technologies", *International Journal of Hydrogen Energy*, Vol. 33, No. 23, 2008, pp. 6804-6839.
- [5] Barelli, L., Bidini, G., Gallorini, F., and Servili, S., "Hydrogen production through sorption-enhanced steam methane reforming and membrane technology: A review", *Energy*, Vol. 33, No. 4, 2008, pp. 554-570.
- [6] Ockwig, N. W. and Nenoff, T. M., "Membranes for hydrogen separation", *Chemical Reviews*, Vol. 107, No. 10, 2007, pp. 4078-4110.
- [7] Campaniello, J., Engelen, C. W. R., Haije, W. G., Pex, P. P. A. C., and Vente, J. F., "Long-term pervaporation performance of microporous methylated silica membranes", *Chemical Communications*, No. 7, 2004, pp. 834-835.
- [8] Steele, B. C. H., "Material science and engineering: The enabling technology for the commercialisation of fuel cell systems", *Journal of Materials Science*, Vol. 36, No. 5, 2001, pp. 1053-1068.
- [9] Hudson, M. J. and Knowles, J. A., "Preparation and characterisation of mesoporous, high-surface-area zirconium(IV) oxide", *Journal of Materials Chemistry*, Vol. 6, No. 1, 1996, pp. 89-95.
- [10] Kusakabe, K., Fumio, S., Eda, T., Oda, M., and Sotowa, K. I., "Hydrogen production in zirconia membrane reactors for use in PEM fuel cells", *International Journal of Hydrogen Energy*, Vol. 30, No. 9, 2005, pp. 989-994.
- [11] Elam, J. W., Routkevitch, D., Mardilovich, P. P., and George, S. M., "Conformal coating on ultrahigh-aspect-ratio nanopores of anodic alumina by atomic layer deposition", *Chemistry of Materials*, Vol. 15, No. 18, 2003, pp. 3507-3517.
- [12] Xiong, G., Elam, J. W., Feng, H., Han, C. Y., Wang, H. H., Iton, L. E., Curtiss, L. A., Pellin, M. J., Kung, M., Kung, H., and Stair, P. C., "Effect of atomic layer deposition coatings on the surface structure of anodic aluminum oxide membranes", *Journal of Physical Chemistry B*, Vol. 109, No. 29, 2005, pp. 14059-14063.

- [13] Mahurin, S., Bao, L. L., Yan, W. F., Liang, C. D., and Dai, S., "Atomic layer deposition of TiO_2 on mesoporous silica", *Journal of Non-Crystalline Solids*, Vol. 352, No. 30-31, 2006, pp. 3280-3284.
- [14] Mccool, B. A. and DeSisto, W. J., "Self-limited pore size reduction of mesoporous silica membranes via pyridine-catalyzed silicon dioxide ALD", *Chemical Vapor Deposition*, Vol. 10, No. 4, 2004, pp. 190-194.
- [15] Cassir, M., Ringuede, A., and Niinisto, L., "Input of atomic layer deposition for solid oxide fuel cell applications", *Journal of Materials Chemistry*, Vol. 20, No. 41, 2010, pp. 8987-8993.
- [16] van Ommen, J. R., Yurteri, C. U., Ellis, N., and Kelder, E. M., "Scalable gas-phase processes to create nanostructured particles", *Particuology*, Vol. 8, No. 6, 2010, pp. 572-577.
- [17] Blin, J. L., Flamant, R., and Su, B. L., "Synthesis of nanostructured mesoporous zirconia using CTMABr- $\text{ZrOCl}_2 \cdot 8\text{H}_2\text{O}$ systems: a kinetic study of synthesis mechanism", *International Journal of Inorganic Materials*, Vol. 3, No. 7, 2001, pp. 959-972.
- [18] Beetstra, R., Lafont, U., Nijenhuis, J., Kelder, E. M., and van Ommen, J. R., "Atmospheric pressure process for coating particles using atomic layer deposition", *Chemical Vapor Deposition*, Vol. 15, No. 7-9, 2009, pp. 227-233.
- [19] Cuperus, F. P., Bargeman, D., and Smolders, C. A., "Permporometry - the determination of the size distribution of active pores in UF Membranes", *Journal of Membrane Science*, Vol. 71, No. 1-2, 1992, pp. 57-67.
- [20] Sing, K. S. W., Everett, D. H., Haul, R. A. W., Moscou, L., Pierotti, R. A., Rouquerol, J., and Siemieniewska, T., "Reporting physisorption data for gas solid systems with special reference to the determination of surface-area and porosity (Recommendations 1984)", *Pure and Applied Chemistry*, Vol. 57, No. 4, 1985, pp. 603-619.
- [21] Brunauer, S., Emmett, P. H., and Teller, E., "Adsorption of gases in multimolecular layers", *Journal of the American Chemical Society*, Vol. 60, 1938, pp. 309-319.

[22] Lastoskie, C., Gubbins, K. E., and Quirke, N., "Pore-size heterogeneity and the carbon slit pore - a density-functional theory model", *Langmuir*, Vol. 9, No. 10, 1993, pp. 2693-2702.

[23] Elam, J. W., Groner, M. D., and George, S. M., "Viscous flow reactor with quartz crystal microbalance for thin film growth by atomic layer deposition", *Review of Scientific Instruments*, Vol. 73, No. 8, 2002, pp. 2981-2987.

[24] Puurunen, R. L., "Surface chemistry of atomic layer deposition: A case study for the trimethylaluminum/water process", *Journal of Applied Physics*, Vol. 97, No. 12, 2005, pp. 959-972.

[25] JCPDS Database, "International Center for Diffraction Data, PA, PDF 79-1767 and 74-0815," 2001.

[26] Kresge, C. T., Leonowicz, M. E., Roth, W. J., Vartuli, J. C., and Beck, J. S., "Ordered mesoporous molecular-sieves synthesized by a liquid-crystal template mechanism", *Nature*, Vol. 359, No. 6397, 1992, pp. 710-712.

[27] Sayari, A. and Hamoudi, S., "Periodic mesoporous silica-based organic - Inorganic nanocomposite materials", *Chemistry of Materials*, Vol. 13, No. 10, 2001, pp. 3151-3168.

[28] Hudson, M. J. and Knowles, J. A., "Preparation and characterisation of mesoporous, high-surface-area zirconium(IV) oxide", *Journal of Materials Chemistry*, Vol. 6, No. 1, 1996, pp. 89-95.

[29] de Vos, R. M. and Verweij, H., "Improved performance of silica membranes for gas separation", *Journal of Membrane Science*, Vol. 143, No. 1-2, 1998, pp. 37-51.

Chapter 5

Plasma-enhanced atomic layer deposition of titania on alumina for its potential use as a hydrogen-selective membrane

Abstract

As a clean energy carrier, hydrogen has attracted global attention in recent years, because it could address issues that are related to reducing global climate change. It has to be stipulated that to date's processes for hydrogen production using fossil fuels need to be coupled with CO₂ separation and storage. Thermally and hydrothermally stable microporous membranes with intrinsic high H₂/CO₂ selectivity are highly demanded in steam-reforming and water gas-shift processes for H₂ gas separation. In this study a composite alumina-titania membrane was synthesized by the combination of atomic layer deposition (ALD) and sol-gel processes. By adjusting the number of ALD cycles (280 cycles), a thin TiO₂ layer corresponding to a thickness of ~ 10 nm was deposited on the surface of γ -Al₂O₃ membranes. The gas permeation was tested to assess the membranes' gas separation performance. The membranes exhibited a good balance between H₂ permeance and separation properties. At 450K, the H₂ permeance is approximately $12.5 \times 10^{-8} \text{ mol.m}^{-2}.\text{s}^{-1}.\text{Pa}^{-1}$ and the separation factor is 5.8 for a H₂/CO₂ mixture. The results clearly demonstrate that the studied deposition method ALD is a promising route to prepare ceramic microporous membranes for hydrogen separation.

5.1 Introduction

Atomic layer deposition (ALD) is a variant of chemical vapor deposition (CVD) to deposit a thin film with precise thickness control at the sub-monolayer level ^[1]. The technique is a self-limiting layer-by-layer thin film deposition method, which is based on sequential and saturating surface reactions of the alternately applied precursors ^[1, 2]. Usually, the ALD of metal oxides is comprised of sequential steps of adsorption and hydrolysis/oxidation of metal precursors such as metal halide and metalorganic precursors. Plasma sources are also introduced into the ALD process of metal oxides process ^[2] to dissociate the reactants into desired radicals, instead of using H₂O to hydrolyse the metal precursors. A plasma generates highly reactive radical species that for example allow the deposition at lower temperatures than in purely thermally-driven ALD. Besides the ALD of metal oxides, the ALD of metal nitrides and metals on dense substrates have been studied widely for many applications ^[3]. The ability of ALD to deposit monolayers on high aspect ratio structures, such as porous supports with nanoscale pore diameters and lengths, is also one of the prominent characteristics of ALD. Control of the internal pore diameter and uniformity of ALD-deposited layers inside the pores have been explored in anodic aluminum oxide (AAO) membranes. ALD of Al₂O₃ and ZnO to reduce the pore diameter of AAO membranes has been successfully demonstrated by Elam et al. ^[4]. However, these studies did not include gas separation properties of these membranes, yet instead of evaluating the time-dependence of the ALD reactant exposures to achieve conformal films growth in the pores. Because of the high potential for reproducibility and flexibility, the use of ALD may be suitable also for developing other membranes for gas separation.

Microporous inorganic membranes have attracted considerable interest in the past two decades for applications in gas separation ^[3]. The processing of microporous silica membranes is developed by several researchers using sol-gel ^[5-9] and CVD ^[10-12] methods. Sol-gel derived silica membranes exhibit high permeance up to 10⁻⁶ mol.m⁻².s⁻¹.Pa⁻¹^[9] and good selectivity (~ 50) for H₂/CO₂ as opposed to CVD silica ones which reveal an associated low permeance (~ 10⁻⁸ mol.m⁻².s⁻¹.Pa⁻¹) and an

enhanced selectivity up to 1200 ^[13]. The main disadvantage of these silica membranes is their hydrothermal instability ^[5]. This is a major problem for gas separation in a steam environment, such as the steam-methane reforming process ^[6]. From the viewpoint of hydrothermal stability, zeolites are more interesting because they are not susceptible to densification at high temperatures or degradation in steam. However, they have inadequate combination of H₂ permeance and selectivity due to the presence of inter-crystallite pores in their structure ^[7]. While much efforts have been focused on the improvement of the stability of silica ^[6-8], or the reduction of the intercrystallite pores in zeolites ^[8], it is eventually desirable to develop microporous non-silica based membranes for their potential in H₂ separation. In nanofiltration applications, titania is generally recognized for its chemical and hydrothermal stabilities for use in a membrane pervaporation process ^[8].

This chapter introduces the use of Plasma-Enhanced (PE)-ALD of TiO₂ to reduce the pore opening of alumina-based mesoporous membranes for the selective transport of hydrogen. The approach attempted to combine the sol-gel of alumina and ALD of titania for preparing membranes with the same properties as silica membranes. The effect of a deposited TiO₂ layer on the gas permeation of the membranes was investigated. Comparison between H₂ permeance and selectivity of the as-synthesized membrane and recent inorganic microporous membranes reported in the literature is made as well. The pore size was characterized before and after PE-ALD with the permoporometry technique. The resulting materials were examined using scanning electron microscopy (SEM) and energy-dispersive X-ray (EDX) spectroscopy.

5.2 Experimental details

5.2.1 γ -Al₂O₃ membrane preparation

The γ -Al₂O₃ membranes were prepared by depositing γ -Al₂O₃ layers on a commercial α -Al₂O₃ supports (Pervatech, The Netherlands) using the dip-coating process. The supports are of 2 mm thickness and have a diameter of 25 mm and an average pore size of about 100 nm in the top layer. The supports were dip-coated with a sol of boehmite

(γ -AlOOH) for a few seconds (~ 2 s), dried in air at room temperature (\sim two days), and then calcined at 873 K in air for three hours (heating rate $1 \text{ K} \cdot \text{min}^{-1}$). The boehmite sol was synthesized via the colloidal route^[5]. The coating step was repeated twice so as to reduce defects (pinholes, cracks).

5.2.2 Plasma-enhanced ALD of TiO_2

The titania deposition on the γ - Al_2O_3 membranes was performed using a PE-ALD reactor (Oxford Instruments FlexAL). The temperature of the γ - Al_2O_3 membranes inside the reactor chamber was kept at 573 K during the deposition. Trimethoxy(pentamethylcyclopentadienyl) titanium – $\text{TiCp}^*(\text{OMe})_3$ ($\text{Cp}^* = \text{C}_5\text{Me}_5$, $\text{Me} = \text{CH}_3$) was evaporated at 343 K with an Ar flow (100 standard cubic centimeters per minute (sccm)) as carrier gas and was injected into the reactor chamber using fast switching ALD valves. The typical operating pressures varied from 1 to 13.3 Pa during the precursor pulses while the pressure in the evacuated state was 10^{-4} Pa. For the plasma process, the oxidation step took place with a 400 W O_2 plasma at a pressure of 1 Pa. The O_2 flow was kept at 50 sccm during the deposition cycle. A typical cycle time of 13s was obtained by employing a $\text{TiCp}^*(\text{OMe})_3$ pulse of 2 s, an Ar purge of 3 s, a plasma step of 5 s, and an Ar purge of 3 s. It should be noted that this cycle time was optimized using planar substrates. Although some details about the reaction mechanism of ALD of TiO_2 from $\text{TiCp}^*(\text{OMe})_3$ and O_3 have recently been reported^[18], the surface chemistry for the PE-ALD process from this titanium precursor and O_2 plasma has not been unravelled yet. However, it has been observed that during the O_2 step (a fraction of) the ligands remaining on the surface after precursor adsorption are combusted into CO_2 and H_2O species, which were measured by mass spectrometry. More extensive results on the surface chemistry will be presented in future work. Furthermore, it is noted that the TiO_2 is believed to be amorphous before annealing, although films with an anatase crystal structure have been reported at deposition temperatures ≥ 573 K after reaching a certain film thickness and also being manifested by a increase in the growth rate per cycle^[2]. The TiO_2 films deposited on the surface of

γ -Al₂O₃ membranes were only ~ 10 nm thick, which is obtained by repeating 280 ALD cycles. After the deposition, the membranes were annealed at 773 K in air for one hour.

5.2.3 Characterization

Surface characterization of the membranes was performed using a Scanning Electron Microscope (SEM, JEOL 6330F microscope) and energy dispersive X-ray (EDX) spectroscopy (NORAN instrument). The samples were prepared by cutting a 2 mm thick cross-section from the coated membrane using a diamond-wafering saw.

The membrane quality and pore size were analyzed using permoporometry technique. The details of the technique were described in Chapter 2.

Single-gas permeation tests were carried out in a gas permeation equipment. The permeate flow of H₂ or CO₂ was measured with a soap meter. In this test, a total pressure on the feed side was kept in the range of 2 – 4 x10⁵ Pa and the permeate side was kept constant at atmospheric pressure. The permeation temperature is limited to 448K due to the use of low temperature O-ring seals in the equipment. Error estimates were in most cases within ca. 5% of the calculated permeance and so error bars were not included in the plots, as they were difficult to visualize from the data points. In addition, the membranes were further tested with a H₂/CO₂ mixture (50:50/v:v) at 10⁵ Pa pressure difference and He as a sweep gas. The gas compositions were analyzed by gas chromatography (Varian Micro-GC4900) with a flame ionization detector (FID) and a thermal conductivity detector (TCD).

5.3 Results and discussion

5.3.1 Membrane surface characterization

Figure 5-1 shows SEM images of γ -Al₂O₃ membranes modified by PE-ALD. The top surface of the modified γ -Al₂O₃ membranes appears smooth and no pinholes are observed. The TiO₂ layer deposited by PE-ALD is not clearly visible as shown in the cross-section SEM image (Figure 5-1b). Apparently the γ -Al₂O₃ layer (~2 μ m thick) is not affected after the PE-ALD. This cross-section is carefully analyzed with EDS

mapping (Figure 5-2). No sharp transition between the TiO_2 layer (Ti signal) and the alumina membrane is observed. This indicates that Ti is distributed throughout the $\gamma\text{-Al}_2\text{O}_3$ layer surface and a slight penetration of titanium oxide into the layer. A clear distinction between the layers is slightly blurred by sample drift during the elemental mapping. The permeation of gases through the pores confirms that the deposited layer is still porous. Moreover, the diffusion of TiO_2 inside the pores during the PE-ALD process could increase the adhesion of the deposited layer to the support.

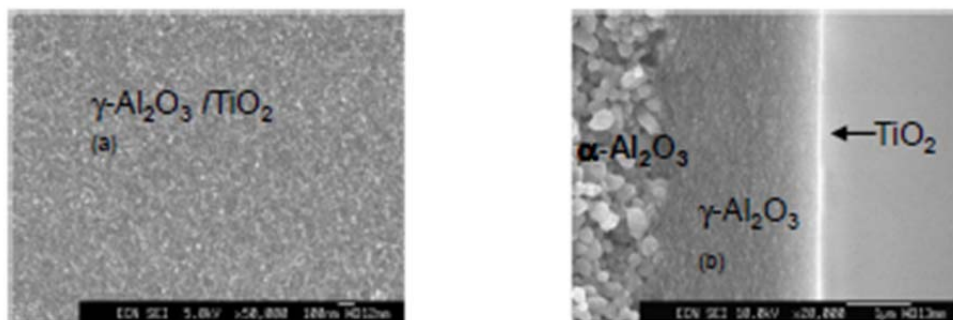


Figure 5-1: SEM pictures of an upper top-surface (a) and a cross section (b) of a $\gamma\text{-Al}_2\text{O}_3$ membrane modified with PE-ALD of titania.

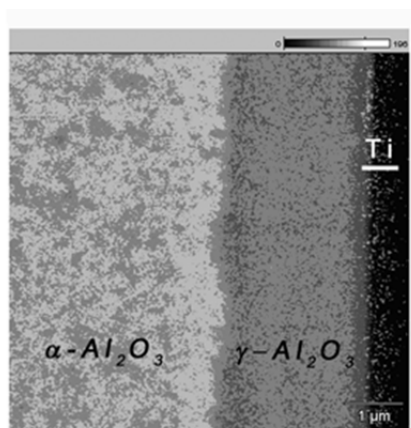


Figure 5-2: X-ray mapping of elemental constituents within a cross section of $\gamma\text{-Al}_2\text{O}_3$ membrane modified with PE-ALD of titania.

5.3.2 Pore size analysis

Figure 5-3 shows the measured He permeance as a function of the pore Kelvin radius during permoporometry experiments for the γ -Al₂O₃ membrane and modified PE-ALD ones. The Kelvin radius of the pores have been calculated from the range of the relative vapor pressure P/P_0 of H₂O where the pores are blocked with H₂O vapor. In the γ -Al₂O₃ membrane (Figure 5-3a), the observed hysteresis between the adsorption and desorption branches indicated the capillary condensation of H₂O in the Kelvin radius range of 1.3-2 nm. The He permeance reaches the steady state at $P/P_0 \sim 0.6$, which corresponds to the pore Kelvin radius of ~ 2 nm. It is clear that the γ -Al₂O₃ membrane has a pore size distribution approximately with pores' radius of 2 nm and high quality (no presence of larger defects). After PE-ALD (Figure 5-3b), a large drop in He permeance is observed and reaches a steady state at $P/P_0 \sim 0.3$ (Kelvin radius ~ 0.7 nm), without any hysteresis loop. Further increase of the relative vapor pressure P/P_0 (> 0.3) leads to a He permeance which is below the system measurement limit of $6.5 \times 10^{-8} \text{ mol.m}^{-2}.\text{s}^{-1}.\text{Pa}^{-1}$ at 343 K. It should be noted that permoporometry is originally developed for the characterization of pores with radius $> 1 \text{ nm}$ ^[9], where the mechanism of capillary condensation can occur in such pores. Due to the small kinetic size and the high vapor pressure of water, it is still appropriate for measuring pore size in the range from 0.6 to 3 nm ^[9]. This implies that the modified PE-ALD membrane has a pore size distribution mainly with pores' radius of $\sim 0.7 \text{ nm}$, in good correlation with the obtained gas permeation results in the next section.

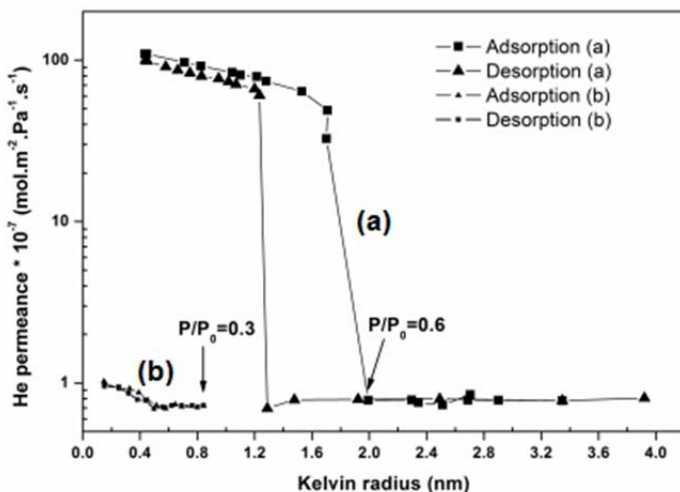


Figure 5-3: He permeance as a function of the pore Kelvin radius for $\gamma\text{-Al}_2\text{O}_3$ membranes (a) and one modified the PE-ALD of titania (b) obtained by permporometry.

5.3.3 Membrane permeation properties

Figure 5-4 shows the H_2 and CO_2 permeance of the $\gamma\text{-Al}_2\text{O}_3$ and modified PE-ALD membranes. Initially, the $\gamma\text{-Al}_2\text{O}_3$ membrane has higher permeance for both gases. The permeance of these gases decreases with about one order magnitude after PE-ALD. As presented in Figure 5-4a, H_2 and CO_2 permeances through the $\gamma\text{-Al}_2\text{O}_3$ membrane decrease with temperature, which is in agreement with the Knudsen diffusion mechanism. It is quite different in the modified PE-ALD membrane (Figure 5-4b), only the H_2 permeance slightly increases with temperature and not that of CO_2 . The result implies that the transport of H_2 through the modified PE-ALD membrane is activated as its permeance increases as a function of temperature. The CO_2 permeance decreased as a function of temperature, which indicates a negative activation effect for CO_2 due to its adsorption on the pore wall. An apparent activation energy of $\sim -6 \text{ kJ.mol}^{-1}$ for CO_2 is calculated from the CO_2 permeance data in the K temperature range 298-448K using the Arrhenius-type relationship^[10]. The negative value is probably attributed to a slight adsorption capacity of CO_2 on the wall of the pores, which was observed for sol-

gel derived silica ^[11]. When the temperature increases, the average molecular velocity increases and the adsorption of CO₂ molecules at the surfaces of the pores becomes weaker. The desorbed CO₂ amount increases with temperature and this effect dominates over the activated diffusion of CO₂, which results in the decrease of the CO₂ permeance in the experimental range of temperatures. The behavior of H₂ and CO₂ permeances with the opposite temperature dependence reveals the increased H₂ selectivity with increasing permeation temperature. An apparent activation energy of ~1 kJ.mol⁻¹ is calculated from the H₂ permeance data recorded in the 298-448 K temperature range. This positive energy value is low for a surface diffusion mechanism and also lower than most reported values of about 2-16 kJ.mol⁻¹ in silica membranes ^[12, 13]. The observation of such a low activation energy was also reported by Prabhu and Oyama ^[14], who calculated an activation energy of 1.9 kJ.mol⁻¹ in high-temperature CVD of silica membrane (Nanosil). They explained that the low activation energy was due to the diffusion of atomic hydrogen species through the membrane. In our case, the low activation energy may be the result of the main contribution of repulsive interactions between hydrogen and the adsorbed-OH groups on the surface of TiO₂, among other effects on the transport mechanism of H₂ through the modified PE-ALD membrane

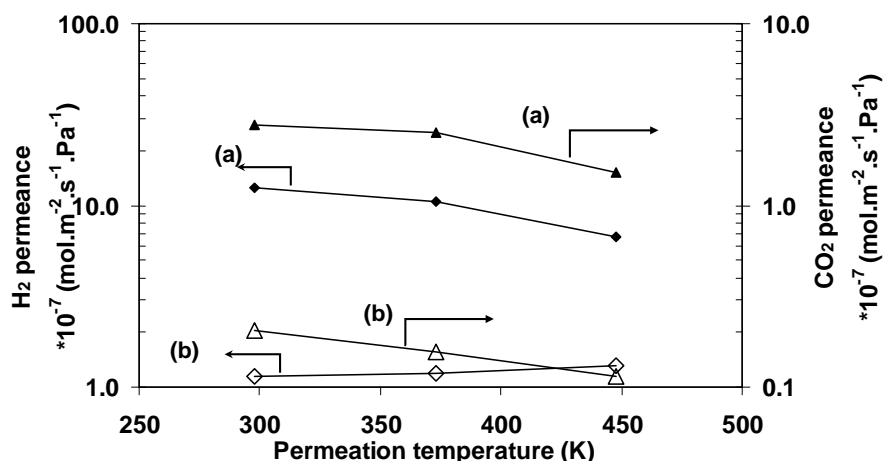


Figure 5-4: Permeance of pure gases with different temperatures at 10⁵ Pa pressure difference for a γ-Al₂O₃ membrane (a) and a γ-Al₂O₃ membrane modified with PE-ALD of titania (b).

Figure 5-5 shows the comparison between H_2 selectivity, i.e., the permselectivity in the single gas permeation (the ratio of H_2 and CO_2 permeance) and separation factor in a H_2/CO_2 binary mixture. In the $\gamma-Al_2O_3$ membrane (Figure 5-5a), the H_2 selectivity is close to the value of the ratio of the reciprocal square roots of molecular weight of CO_2 and H_2 , i.e., the value of 4.69. Meanwhile, the separation factor value is small (~ 2). This result indicates that Knudsen diffusion is the dominant transport mechanism in the $\gamma-Al_2O_3$ membrane. As shown in Figure 5-5b for the modified PE-ALD membrane of titania, the departure from the ideal Knudsen diffusion may be due to the contribution of other mechanisms to the gas transport through this membrane. In a H_2/CO_2 binary mixture, as occurred in the single gas permeation when the temperature increases, the desorbing CO_2 can inhibit the H_2 diffusion through the pores, which results in the lower H_2 permeance. The separation factor of H_2/CO_2 in the binary gas mixture has the highest value of around 5.8 at 450 K. This separation factor is smaller than the permselectivity (~ 10) due to the larger H_2 permeance without the disturbing of CO_2 in the single gas permeation. It is quite difficult to predict membrane selectivity in a gas mixture, because its components can interact with each other. Since H_2 has a smaller size (2.98 Å) and molecular weight (2 g.mol⁻¹) than CO_2 (3.3 Å and 44 g.mol⁻¹), it may be expected that the H_2 diffusion becomes even more pronounced compared to CO_2 diffusion when temperature increases. This situation can lead to a slight increase of H_2 selectivity with increasing temperature.

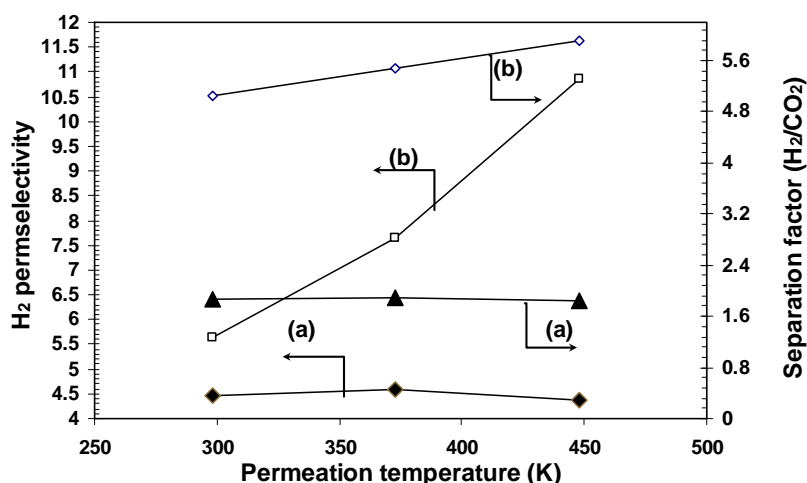


Figure 5-5: H₂ selectivity in single gas and separation factor for binary H₂/CO₂ for a γ -Al₂O₃ membrane (a) and for a γ -Al₂O₃ membrane modified with PE-ALD of titania (b).

Table 5-1 represents the comparison of the permeation properties of the modified PE-ALD with those of other microporous membranes, such as silica, zeolite, and metal-organic frameworks (MOFs) in the temperature range of 473 K-723 K. The data are taken from the recent literature [6-9, 11-13, 17, 22-24] and focused on H₂ selectivity for the purpose of membrane application in a water-gas shift process, where the products contain primarily H₂ and CO₂ [15]. Whereas silica-based membranes exhibit relatively a high H₂ permeance, a high permselectivity, and a separation factor up to 50, their hydrothermal stability needs to be improved by modifying the surface with Co [16], Nb [17], or C [18]. Zeolite membranes have a higher hydrothermal stability than microporous silica membranes, but their inter-crystallite pores need to be reduced in order to have high H₂ separation factor. Small pores and adsorption sites are formed by the catenation of frameworks in MOFs and may exhibit enhanced gas adsorption and high selectivity for H₂ [19]. On the other hand, it seems that MOFs are unlikely to compete with zeolites due to their limited long-term stability at high temperature applications (>773 K) and high costs. The PE-ALD titania membrane prepared in this work has high H₂ permeance in the same range of silica membranes and a reasonable separation factor. Given the material used, the membrane might be considered

hydrothermally stable enough to be used at high temperatures (>673 K). However, the hydrothermal stability properties will be further assessed in future work.

Table 5-1: Comparison of H₂ permeance and permselectivity/ separation factor of titanina membrane (this work) with literature results of silica, zeolites, and MOFs.

Membrane type	H ₂ permeance 10 ⁻⁸ mol.m ⁻² .s ⁻¹ .Pa ⁻¹	CO ₂ permeance 10 ⁻⁸ mol.m ⁻² .s ⁻¹ .Pa ⁻¹	Permeation temperature °C	Pressure difference 10 ⁵ Pa	H ₂ /CO ₂ permselectivity	Separation factor	Ref.
Silica (sol-gel)	2.10-4.80	0.35-0.90	200	1-3	5.33-6.00	6.15-6.60	[6]
Cobalt-silica	0.90	0.07	100-250	3	45-160	2-50	[7]
Niobia-silica	3.80-0.45	0.08	200	4	40-70	-	[8]
Silica (sol-gel)	209	13	400	1-3	15.50	-	[9]
Silica (CVD)	16	0.03	500	2.02	170-590	-	[11]
Silica (sol-gel + CVD)	7.10	0.14	300	0.35-1.38	50	-	[12]
Silica (CVD)	5	0.045	500	1	1200	-	[13]
ZSM-5 & SAPO-34							
Zeolites	10-100	5-0.43	200-400	1.38	2-230	1.40-47	[17]
MFI Zeolites	18.60-27.50	1-10	450	1.01	2.78-17.50	2.56-10.80	[22]
DDR Zeolite	3.50	0.90	300	2	3.50	2.20	[23]
ZIF-7 (MOFs)	4.55	0.33	220	1	13	13.60	[24]
Titania	12.50	1.15	175	1-3	10.87	5.80	-

5.4 Conclusions

Hydrogen selective membranes were prepared using a combination of processes involving the plasma-enhanced atomic layer deposition of titanium dioxide on sol-gel derived γ -alumina membranes. The thin titanium dioxide layer was relatively porous while at the same time the initial pore size of the membrane was successfully reduced. The enhancement in H_2/CO_2 selectivity of the modified membrane can be attributed to the reduction in pore size. This membrane exhibits H_2/CO_2 permselectivity of about 10 and a reasonable separation factor of about 5.8 for H_2 in a H_2/CO_2 mixture at 448 K. Under the experimental conditions used, the thicknesses of deposited layers can be easily controlled by adjusting the cycle numbers. Besides improvement of the performance of the composite membrane, this characteristic of thickness control can be extended to the modification of other types of membranes for designing H_2 selective membranes.

Acknowledgements

The authors wish to thank Stanford University for supporting the research through the Global Climate Energy Project (GCEP) and the sponsors of GCEP. We gratefully acknowledge Prof. Dr. M.C.M. van de Sanden and C.A.A. vanHelvoirt (Eindhoven University of Technology) for arranging and carrying out the ALD experiments and Prof. Dr. F. Kapteijn (Delft University of Technology) and his co-workers (Dr. J. Gascon and Dr. A. E. Martinez) for providing access to equipment for membrane characterization.

References

- [1] George, S. M., "Atomic Layer Deposition: an overview", *Chemical Reviews*, Vol. 110, No. 1, 2010, pp. 111-131.
- [2] Potts, S. E., Keuning, W., Langereis, E., Dingemans, G., van de Sanden, M. C. M., and Kessels, W. M. M., "Low temperature plasma-enhanced atomic layer deposition of metal oxide thin films", *Journal of the Electrochemical Society*, Vol. 157, No. 7, 2010, pp. 66-74.
- [3] Bernardo, P., Drioli, E., and Golemme, G., "Membrane gas separation: a review/state of the art", *Industrial & Engineering Chemistry Research*, Vol. 48, No. 10, 2009, pp. 4638-4663.
- [4] Elam, J. W., Routkevitch, D., Mardilovich, P. P., and George, S. M., "Conformal coating on ultrahigh-aspect-ratio nanopores of anodic alumina by atomic layer deposition", *Chemistry of Materials*, Vol. 15, No. 18, 2003, pp. 3507-3517.
- [5] Campaniello, J., Engelen, C. W. R., Haije, W. G., Pex, P. P. A. C., and Vente, J. F., "Long-term pervaporation performance of microporous methylated silica membranes", *Chemical Communications*, No. 7, 2004, pp. 834-835.
- [6] Ockwig, N. W. and Nenoff, T. M., "Membranes for hydrogen separation", *Chemical Reviews*, Vol. 107, No. 10, 2007, pp. 4078-4110.
- [7] McLeary, E. E., Jansen, J. C., and Kapteijn, F., "Zeolite based films, membranes and membrane reactors: Progress and prospects", *Microporous and Mesoporous Materials*, Vol. 90, No. 1-3, 2006, pp. 198-220.
- [8] Hong, M., Falconer, J. L., and Noble, R. D., "Modification of zeolite membranes for H₂ separation by catalytic cracking of methyl-diethoxysilane", *Industrial & Engineering Chemistry Research*, Vol. 44, No. 11, 2005, pp. 4035-4041.
- [9] Tsuru, T., Hino, T., Yoshioka, T., and Asaeda, M., "Permporometry characterization of microporous ceramic membranes", *Journal of Membrane Science*, Vol. 186, No. 2, 2001, pp. 257-265.
- [10] Barrer, R. M., "Porous crystal membranes", *Journal of the Chemical Society, Faraday Transactions*, Vol. 86, No. 7, 1990, pp. 1123-1130.

- [11] de Vos, R. M. and Verweij, H., "Improved performance of silica membranes for gas separation", *Journal of Membrane Science*, Vol. 143, No. 1-2, 1998, pp. 37-51.
- [12] Gu, Y. F., Hacıoğlu, P., and Oyama, S. T., "Hydrothermally stable silica-alumina composite membranes for hydrogen separation", *Journal of Membrane Science*, Vol. 310, No. 1-2, 2008, pp. 28-37.
- [13] Gopalakrishnan, S. and da Costa, J. C. D., "Hydrogen gas mixture separation by CVD silica membrane", *Journal of Membrane Science*, Vol. 323, No. 1, 2008, pp. 144-147.
- [14] Prabhu, A. K. and Oyama, S. T., "Highly hydrogen selective ceramic membranes: application to the transformation of greenhouse gases", *Journal of Membrane Science*, Vol. 176, No. 2, 2000, pp. 233-248.
- [15] Barelli, L., Bidini, G., Gallorini, F., and Servili, S., "Hydrogen production through sorption-enhanced steam methane reforming and membrane technology: A review", *Energy*, Vol. 33, No. 4, 2008, pp. 554-570.
- [16] Battersby, S., Smart, S., Ladewig, B., Liu, S. M., Duke, M. C., Rudolph, V., and da Costa, J. C. D., "Hydrothermal stability of cobalt silica membranes in a water gas shift membrane reactor", *Separation and Purification Technology*, Vol. 66, No. 2, 2009, pp. 299-305.
- [17] Boffa, V., ten Elshof, J. E., Garcia, R., and Blank, D. H. A., "Microporous niobia-silica membranes: Influence of sol composition and structure on gas transport properties", *Microporous and Mesoporous Materials*, Vol. 118, No. 1-3, 2009, pp. 202-209.
- [18] Duke, M. C., da Costa, J. C. D., Lu, G. Q., Petch, M., and Gray, P., "Carbonised template molecular sieve silica membranes in fuel processing systems: permeation, hydrostability and regeneration", *Journal of Membrane Science*, Vol. 241, No. 2, 2004, pp. 325-333.
- [19] Li, Y. S., Liang, F. Y., Bux, H. G., Yang, W. S., and Caro, J., "Zeolitic imidazolate framework ZIF-7 based molecular sieve membrane for hydrogen separation", *Journal of Membrane Science*, Vol. 354, No. 1-2, 2010, pp. 48-54.

- [20] T. Tsuru, T. Hino, T. Yoshioka, M. Asaeda, Permporometry characterization of microporous ceramic membranes, *J. Membr. Sci.* 186 (2001) 257-265.
- [21] R. M. Barrer, Porous crystal membranes, *J. Chem. Soc. , Faraday Trans.* 86 (1990) 1123-1130.
- [22] A. K. Prabhu, S. T. Oyama, Highly hydrogen selective ceramic membranes: application to the transformation of greenhouse gases, *J. Membr. Sci.* 176 (2000) 233-248.
- [23] X. H. Gu, Z. Tang, J. H. Dong, On-stream modification of MFI zeolite membranes for enhancing hydrogen separation at high temperature, *Microporous Mesoporous Mater.* 111 (2008) 441-448.
- [24] M. Kanezashi, J. O'Brien-Abraham, Y. S. Lin, K. Suzuki, Gas permeation through DDR-type zeolite membranes at high temperatures, *AIChE J.* 54 (2008)1478-1486.

Chapter 6

Atomic layer deposition of TiO₂ films on planar dense and porous substrates

Abstract

This chapter describes the atomic layer deposition (ALD) of TiO₂ using the home-built ALD reactors installed during the research period. ALD of TiO₂ from TiI₄ and H₂O onto a porous substrate has been investigated. In particular, the control of TiO₂ deposition on porous supports is carried out for the development of membranes. The study on the gas permeation characteristics of the membranes modified with ALD is presented. In addition, an in-situ investigation of the growth rate is performed after the end of each ALD cycle using Ti[N(CH₃)₂]₄ and H₂O as precursors. The cycle by cycle layer growth is determined with spectroscopic ellipsometry (SE). The model used is based on the Bruggeman Effective-Media Approximation (EMA). Atomic Force Microscopy (AFM) analysis and Scanning Electron Microscopy (SEM) are used to study the structural and texture properties of the TiO₂ films deposited by ALD.

6.1 Introduction

Titanium dioxide (TiO_2) has found application in solar cells, gas sensors, and photocatalytic coatings, owing to its interesting optical properties and chemical stability in hostile environments ^[1]. For membrane applications, titania membranes have also attracted interest because of their superior chemical resistance, compared to other membrane materials, including γ -alumina and silica ^[2]. Different methods have been employed to synthesize TiO_2 membranes such as sol-gel ^[2-4], chemical vapor deposition (CVD) ^[5], and atomic layer deposition (ALD) ^[6, 7]. As a synthesis method from a gas phase, ALD seems to be an ideal method to deposit TiO_2 on porous substrates. ALD proceeds through self-limiting reactions between chemical precursors and substrates. Its self-limiting reactions provide several advantages over other deposition methods such as good film quality, accurate thickness control, excellent conformity, and uniformity over large areas.

Precursor properties play an important role in ALD. Different precursors have their own pros and cons. The TiCl_4 and H_2O process was exploited to become one of the first ALD processes for TiO_2 deposition ^[5]. Notably, the deposition temperature applied is in the range of 180-600 °C, yielding a growth rate of 0.05-0.1 nm/cycle. The commonly used TiCl_4 may result in Cl-contamination of the grown films. In addition, the reaction by-product HCl is a corrosive gaseous product. An option instead of using TiCl_4 is to employ another Ti halide, for example TiI_4 ^[7]. Because the metal-I bond is weaker than the metal-Cl bond, the annealing process after ALD reduces the halide content more effectively. A growth rate of 0.06-0.2 nm/cycle is observed ^[7]. Another alternative is to use metal-organic precursors such as tetrakis(dimethylamino) titanium (TDMAT, $\text{Ti}[\text{N}(\text{CH}_3)_2]_4$) ^[6, 8, 9]. TDMAT has a high enough vapor pressure and a relatively high thermal decomposition temperature above 150°C compared to other Ti precursors. A growth rate of 0.03 to 0.21 nm/cycle within the temperature range of 50-200 °C has been observed ^[6, 8, 9].

In this work, we systematically investigated the ALD of TiO_2 using the $\text{TiI}_4/\text{H}_2\text{O}$ and TDMAT/ H_2O processes. The aim of this work is to improve the separation properties

of titania membranes by combining the sol-gel and ALD processes. Hence, a two step synthesis approach is presented, which includes sol-gel derived TiO₂ membranes and ALD of TiO₂ onto these membranes. Gas permeation measurements are carried out to determine the effectiveness of gas separations with the resulting porous membranes. The thin films of TiO₂ are also deposited on dense silicon substrates. Spectroscopic ellipsometry (SE) is used to determine the growth rate of the TiO₂ deposit on the Si substrates. This is expected to be beneficial in optimizing the deposition processes and future thin film requirements would become easier to fulfill.

6.2 Experimental

6.2.1 Mesoporous titania membrane preparations

Prior to the ALD modification, the sol-gel derived TiO₂ membranes were prepared. The membranes were prepared by depositing mesoporous TiO₂ layers on commercial porous α -Al₂O₃ supports (Pervatech, The Netherlands). The preparation has also been carried out on γ -Al₂O₃/ α -Al₂O₃ supports, whose surfaces are smoother than the α -Al₂O₃ ones. This reduces support-derived defects. The α -Al₂O₃ supports are of 2 mm thickness and have a diameter of 25 mm and an average pore size of 100 nm at the top layer. The γ -Al₂O₃ layer has an average pore size of 4 nm and was synthesized in our laboratory (see chapter 3). The supports were dip-coated with a sol of TiOOH for a few seconds (\sim 5 s). The TiOOH sol was synthesized by the sol-gel route using an amphiphilic tri-block copolymer as a template under acidic conditions ^[10]. This is based on an evaporation-induced self-assembly (EISA) process (see Chapter 2). In this study the tri-block copolymer Pluronic® P123 (EO₂₀PO₇₀EO₂₀, EO=ethylene oxide, PO=propylene oxide, BASF) was added to ethanol (C₂H₅OH, MERCK Chemicals, max 0.01% H₂O). After 30 min of stirring, titanium tetraisopropoxide (TTIP, Sigma Aldrich, 99.999%) was added to the solution and subsequently hydrochloric acid (HCl, Sigma Aldrich, 37%) was added. The mixture was stirred for 2 h. The final sol has a pH of about 1 and the molar ratio of 1 TTIP : 0.017 P123 : 15 C₂H₅OH : 1.8 HCl : 5.4 H₂O. The sol was aged for at least 8 h at 5 °C in order to obtain a stable sol solution.

After coating, films are aged for one day at $-15\text{ }^{\circ}\text{C}$ and then dried in air at room temperature ($\sim 4\text{ h}$). Finally, calcination is performed in air using a step-wise heat treatment of $40\text{ }^{\circ}\text{C}$ (6 h), $120\text{ }^{\circ}\text{C}$ (6h), and $400\text{ }^{\circ}\text{C}$ (1 h). The heating rate is $1\text{ }^{\circ}\text{C}\cdot\text{min}^{-1}$.

6.2.2 ALD of TiO_2 using TiI_4 and H_2O precursors

TiO_2 films were deposited in a hot-wall flow-type ALD-I reactor (Figure 6-1). The system consists of a $50 \times 50 \times 66\text{ mm}$ deposition chamber and the solid and liquid precursor lines with their own entrances into the chamber as schematically presented in Figure 6-2. A three-zone furnace (Carbolyte Furnace) was used to heat the system, where the first zone was used to heat the solid precursor, while the second and third zones were used to heat the deposition chamber. The pressure inside the reactor is controlled by a MKS type 152© automatic pressure controller, typically at $0.2 \cdot 10^3$ - $2 \cdot 10^3\text{ Pa}$ during the precursor pulses. The temperatures are monitored by the K-type (Nickel-Chromium, the temperature range of 200 - $1250\text{ }^{\circ}\text{C}$) thermocouples.

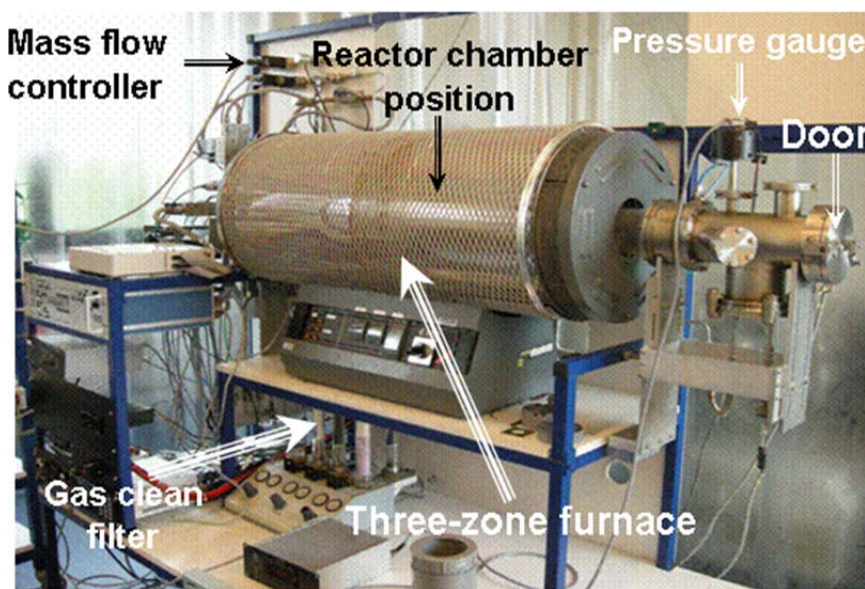


Figure 6-1: Photograph of the home-built ALD-I reactor.

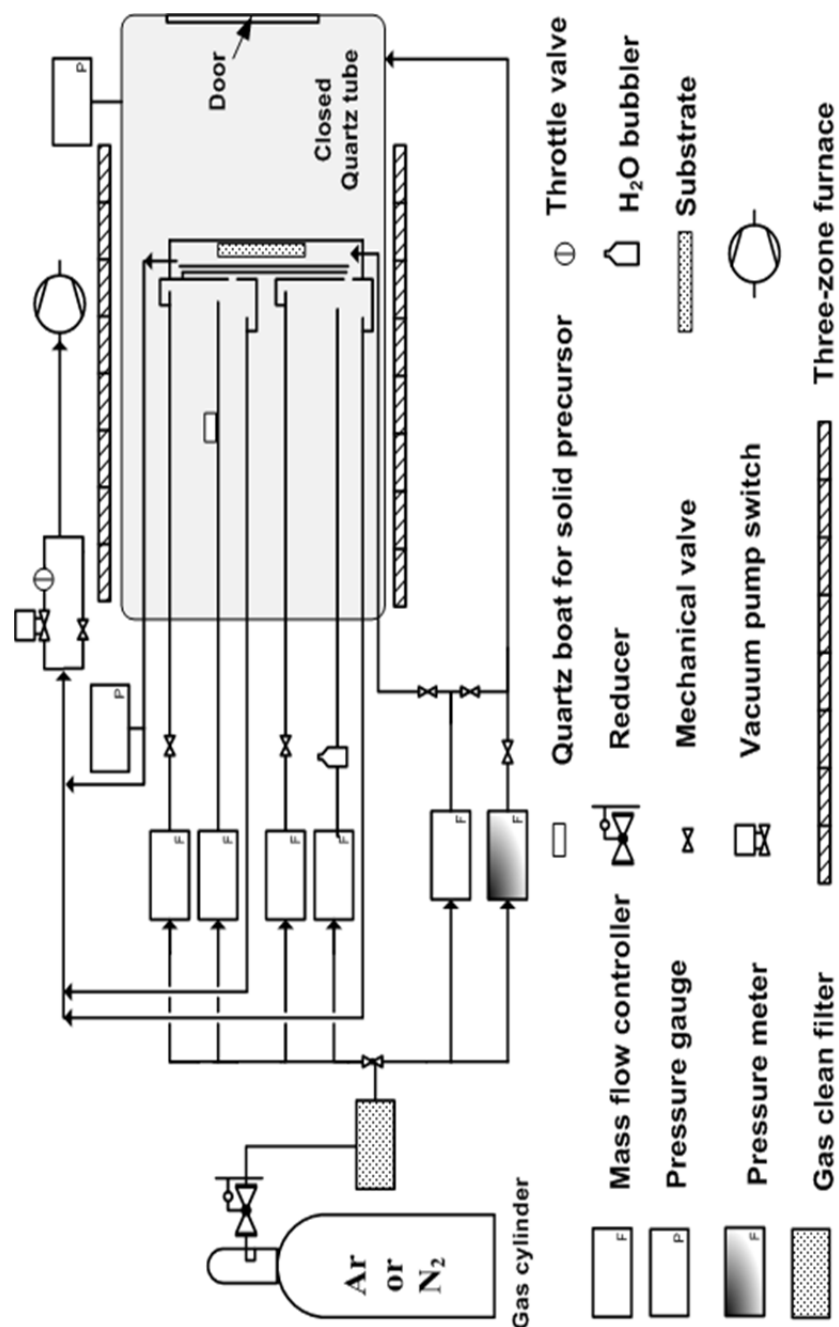


Figure 6-2: Schematic presentation of the home-built ALD-I reactor

TiI_4 (anhydrous powder, 99.99%, Sigma-Aldrich) was evaporated from a quartz boat kept at $\sim 115^\circ\text{C}$ in the carrier gas (Ar, 99.99%). Its vapor was transported into the deposition chamber by a virtual valve (see Figure 6-3). This is done by directing two inert gas (Ar) flows into the deposition chamber. One is a carrier gas flowing over the TiI_4 source and the other one a valving gas. When the virtual valve is in its closed state, the valving gas is on and the carrier gas is off. The flow direction of the valving gas divided into two parts, i.e., one directed to the deposition chamber and the other flow toward the vacuum line, setting the diffusion barrier to block the TiI_4 precursor to reach the deposition chamber. The TiI_4 precursor can only be transported to the reactor chamber by switching the valving gas off and the carrier gas on. This is the open state of the virtual valve. The virtual valve of the water precursor line operates in a similar way. Water vapor was introduced into the reaction zone through the deionized water (resistivity: 18 $\text{M}\Omega\cdot\text{cm}$) bubbler at room temperature. A typical cycle time was employed, i.e., a TiI_4 pulse of 2 s, an Ar (N_2) purge of 5-10 s, a H_2O pulse of 5 s, and an Ar (N_2) purge of 5-10 s. The flow rate of the carrier and purge gas was varied from 0 to 30 sccm (standard cubic centimeters per minute). It should be noted that these cycle parameters were optimized after many introductory experiments.

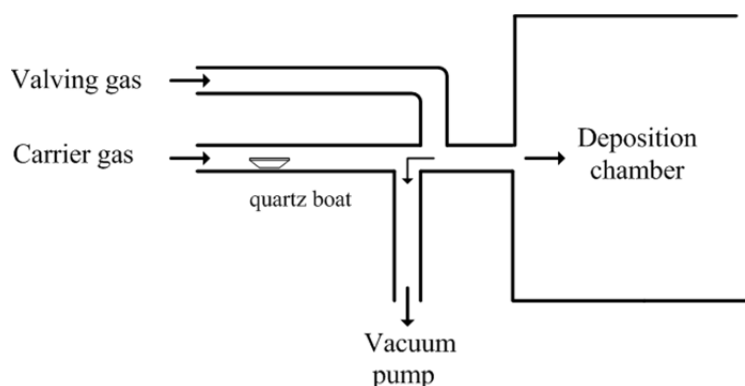
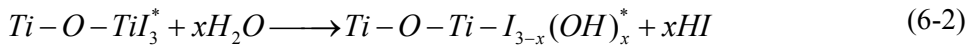


Figure 6-3: Schematic presentation of the virtual valve.

The advantage of the virtual valve is that one is able to use it at high temperatures ($>100^\circ\text{C}$) instead of expensive high-temperature mechanical valves. Solid precursors

such as TiI₄ with low volatility need to be heated at high-temperatures in order to have a sufficient vapor pressure. However, the whole solid source-virtual valves enclosed into the quartz tube with a large volume makes the process complicated in case of (minor) leakage presence. Due to this characteristic of the reactor design, it is quite challenging to keep the deposition chamber leak-free because the movement between the virtual valves and the deposition chamber occur during the process. During operating, a higher pressure (100-500 Pa) is applied along the quartz tube, which ensures that the virtual valves and the deposition chamber are pressed together slightly. Before introduction into the reaction chamber, all samples are cleaned with an organic solution (C₂H₅OH and deionized water) in an ultrasonic bath. Then the samples were heated at 400 °C for at least one hour before the deposition. Corning glass supports (50 x 50 x 20 mm) and mesoporous titania membrane supports (2 mm thickness and diameter of 25 mm) are used as ALD substrates.

The reaction mechanism can be described as follows ^[7]:



where the asterisks denote the surface species.

6.2.3 ALD of TiO₂ using TDMAT and H₂O precursors

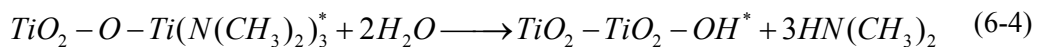
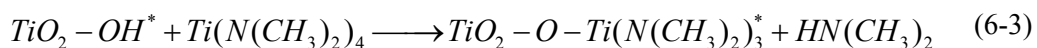
TiO₂ films were deposited in a flow-type ALD-II reactor (Figure 6-4). Only mechanical valves are used in this system as schematically presented in Figure 6-5, which make the reactor simpler and more practical than the ALD-I reactor. The deposition chamber is a vertical load-lock chamber to accommodate a sample size up to 50 mm in diameter. It has an inlet at one end and the exhaust at the other, and two windows with optical access to spectroscopic ellipsometry. The spectroscopic ellipsometer is Woollam M-2000 ellipsometer, which consists of a broad band 75 W Xe-lamp (250-1000 nm), a polarizer, an analyzer, and a charge-coupled device (CCD)-based detection system. The sample is heated using a resistive heating plate, providing temperatures up to around 500 °C. A mechanical pump with a throttle valve at the

exhaust maintains control of the reactor pressure, with pressure stabilization steps prior to precursor pulse steps. Mechanical (solenoid) valves connected to precursor bubblers control the amount of precursor being delivered during each pulse. Precursor vapor and purge gas were introduced into the deposition chamber from the inlet for a fixed amount of time separately and sequentially by means of on/off control of solenoid valves. To control source injection and purge time, the valve on/off time was varied from 1-30 s. Each precursor, i.e., TDMAT or H₂O, has a separate line with a mass flow controller and can use a carrier gas (Ar, 99.99%).

The TDMAT was held in a stainless steel bubbler maintained at 60°C to provide a vapor pressure of ~133.3 Pa. During the TDMAT pulse without carrier gas, the precursor vapor was transported into the deposition chamber due to the difference in pressure. Water was held in a stainless steel bubbler maintained at 25°C to provide a vapor pressure of ~3169 Pa and operated similar to the TDMAT pulse. The feed lines were held at 80 °C in order to prevent the condensation of the precursors. The flow rate of the purge gas was varied from 20 to 300 sccm. The deposition temperature was maintained at 100 °C.

The Si (100) substrates with approximate dimensions of 40 mm × 40 mm × 1 mm were prepared for the deposition as follows. Before introduction into the reaction chamber, an organic wet cleaning (C₂H₅OH, H₂O₂ and deionized water) was carried out in an ultrasonic bath, followed by air drying in a dust-free room. In order to evaporate alcohol and water adsorbed in porous alumina supports, these samples were heated in the reactor at 200 °C for at least one hour before deposition at 100 °C.

Although the details of the reaction mechanism of ALD of TiO₂ from TDMAT and H₂O have not been studied, the general deposition reaction can be separated into two half reactions as follows^[8]:



where the asterisks denote surface species.

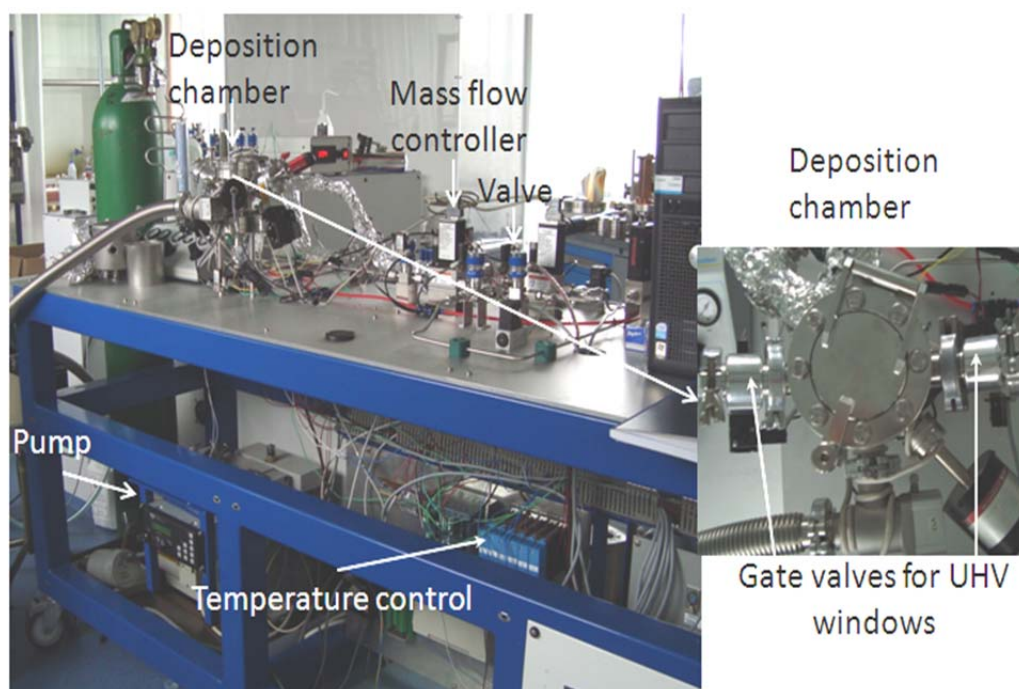


Figure 6-4: Photograph of the home-built ALD-II reactor.

In summary, the ALD-II reactor was designed when the ALD-I reactor had been operational, therefore, adjustments to improve the design was made. The relevant differences of this reactor can reveal some benefits as follows:

- The system has a small volume and the availability of a load lock, which is easy to mount sample.
- A spectroscopic ellipsometer is mounted for process development and monitoring. This becomes valuable when there is a need to study in-situ.
- Precursor sources with mechanical valve system are used. Mechanical valves enable simple control of the amount of the precursor being delivered in each pulse.

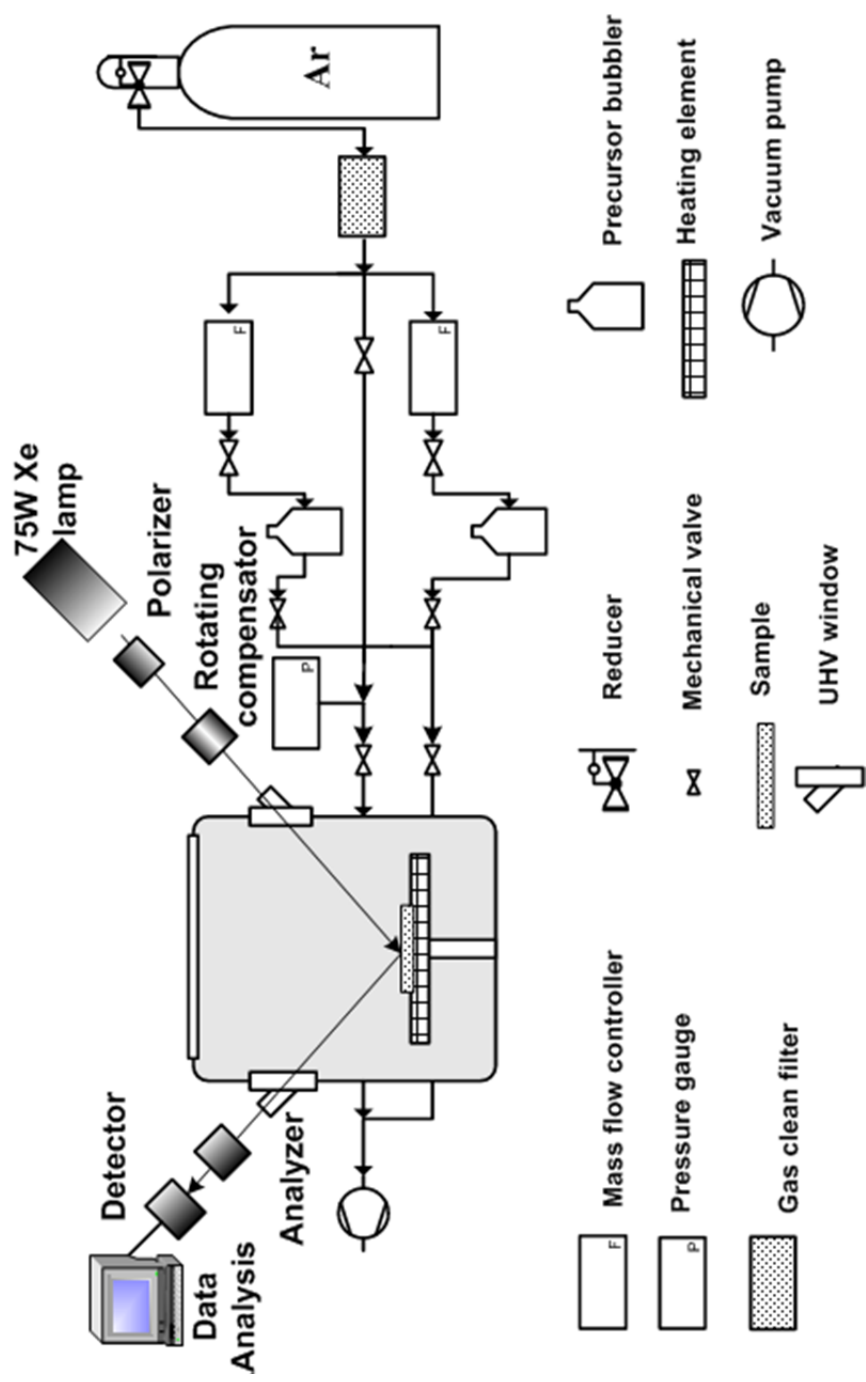


Figure 6-5: Schematic presentation of home-built ALD-II reactor and spectroscopic ellipsometry components.

6.2.4 Porosity analysis and structural characterization

Nitrogen adsorption-desorption measurements were performed with unsupported membranes only in an Autosorb 1-B physisorption set-up (Quantachrome Instruments). The metal oxide phase of the unsupported membranes were investigated by X-ray diffraction (Bruker D8 Advance XRD with Co K α - radiation, $\lambda = 1.54178 \text{ \AA}$) analysis on powders. The weight loss and thermal evolution of the unsupported membranes were analyzed during thermal gravimetric analysis (TGA) and differential thermal analysis (DTA). The TGA/DTA system is the NETZSCH STA 409 PC/PG with a heating ramp of $1^\circ\text{C}.\text{min}^{-1}$.

6.2.5 Gas permeation

Single-gas permeation tests were carried out at room temperature by passing a single gas (He, H₂, CO₂, or N₂), or a H₂/CO₂ mixture (50:50/v:v) through a membrane, i.e., the porous Al₂O₃ /TiO₂. The permeate flow of gas (or gases) was measured with a soap meter. In this test, a total pressure on the feed side was kept in the range of $2 - 5 \times 10^5$ Pa and the permeate side was kept constant at atmospheric pressure. The permeation temperature is limited to 175°C due to the use of low-temperature O-ring seals in the equipment. Error estimates were in most cases within 5% of the calculated permeance. The permeance Per ($\text{mol m}^{-2}\text{s}^{-1}\text{Pa}^{-1}$) of the gas permeating through the membrane is defined as:

$$\text{Per} = \frac{J}{\Delta P A} \quad (6-5)$$

where J is the gas flow through the membrane ($\text{mol}.\text{s}^{-1}$), $\Delta P = P_f - P_p$ is the pressure difference (Pa), P_f and P_p are the pressures in the feed side and permeate side, respectively, and A is the exposed area of the membrane (m^2).

The gas compositions in the H₂/CO₂ mixture were analyzed by gas chromatography (Varian Micro-GC4900) with a flame ionization detector (FID) and a thermal conductivity detector (TCD). The separation factor $\alpha_{\text{H}_2/\text{CO}_2}$ is expressed as a function of the molar fractions by the following equation:

$$\alpha_{\text{H}_2/\text{CO}_2} = \frac{y_{\text{p,H}_2}}{x_{\text{r,H}_2}} \frac{x_{\text{r,CO}_2}}{y_{\text{p,CO}_2}} \quad (6-6)$$

where $y_{\text{p,H}_2}$ and $y_{\text{p,CO}_2}$ are the molar fractions of H_2 and CO_2 at the permeate side and $x_{\text{r,H}_2}$ and $x_{\text{r,CO}_2}$ are the molar fractions of H_2 and CO_2 at the retentate side.

6.2.6 Atomic Force Microscopy

Atomic force microscopy (AFM) was performed with a scanning probe microscope (NTMDT Ntegra) in the tapping mode in order to determine the surface roughness of the TiO_2 films. The cantilever was made out of Si with a nominal tip apex radius of 10 nm. After scanning, the images were flattened with order 2. This implies that a least-squares fit is made to the data in the scanned area using a second-order polynomial. The resulting best fit is then subtracted from the image. Flattening was done to remove curvature and slope from an image. The surface roughness can be quantified by the root-mean-squared roughness (R_{RMS}), which is defined as the standard deviation of the AFM data:

$$R_{\text{RMS}} = \sqrt{\frac{\sum_{n=1}^N (Z_n - \bar{Z})^2}{N-1}} \quad (6-7)$$

where Z_n is the height of the n^{th} data, \bar{Z} is the mean height and N is the number of data within the given area.

6.2.7 Spectroscopic ellipsometry (SE)

Ellipsometry measurements of the TiO_2 films deposited on the Si wafer are routinely used to determine the thickness and optical constants of the films ^[11]. Its application for studying thin film synthesis reveals that is a fast technique, especially for in-situ measurements where the film thickness and the growth rate per ALD cycle are monitored during the process ^[12]. The film thickness can be measured in the range of a monolayer of atoms to several microns. The growth rate per ALD cycle is one of the most important process parameters during the process. SE measures the change of

polarization of the light upon reflection from (or transmission through) a sample. After reflection, a linear polarized light beam generally becomes elliptical. The measurement is performed by determining the ratio ρ of the complex Fresnel coefficients, R_p and R_s , respectively in the directions parallel and perpendicular to the plane of incidence, as defined [16]:

$$\rho = \tan(\Psi) e^{i\Delta} = \frac{R_p}{R_s} \quad (6-8)$$

where Ψ and Δ are the ellipsometric angles. The angle of incidence is fixed at 75 °. After the end of each ALD cycle ellipsometry scans were taken during 2 s. The SE data Ψ and Δ are fitted with a model using Woollam WVASE32 software ©. The model consists of a dense substrate, Si, a native SiO₂ layer, and a TiO₂ layer exposed to the ambient air. Approximately 2 nm is used as the thickness of native oxide on Si in the model and is kept fixed during the data analysis. The thickness of the TiO₂ layer is derived from a growth model based on the effective medium approximation (EMA) [13]. In the EMA, a high fraction of islands is assumed to form before coalescence is achieved under the growth conditions. The evolution of the TiO₂ islands is hence described by the growth of the EMA layer, characterized by a thickness and a fraction of voids, both changing with the cycle number.

6.3 Results and discussion

6.3.1 Sol-gel derived titania membrane

Figure 6-6 shows the XRD patterns of an unsupported titania membrane (after calcination in air at 400 °C and grinding the free-standing film). According to the wide-angle XRD pattern, titania is identified as the anatase phase. The low-angle XRD pattern shows only one peak (011) with the d-spacing value of 7.75 nm.

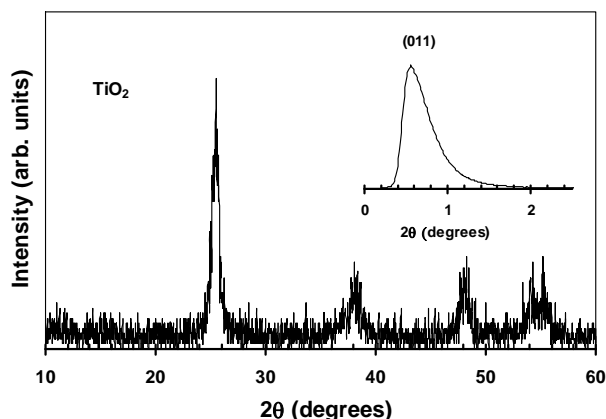


Figure 6-6: Low- and wide-angle XRD patterns of unsupported mesoporous titania, calcined in air for 1 h at 400 °C.

The mass loss and thermal evolution of titania during the calcination in air were analyzed using thermal gravimetric analysis (TGA) and differential thermal analysis (DTA). A heating rate of $1^\circ\text{C}\cdot\text{min}^{-1}$ was used and the data are shown in Figure 8. A mass loss of about 60% occurs and an exothermic peak is observed at 290 °C. This is due to the pyrolysis of the surfactant P123 and residual organic materials. This considerable mass loss, together with the XRD results, shows the optimum temperature for the titania calcination to be 400 °C for 1 h in air.

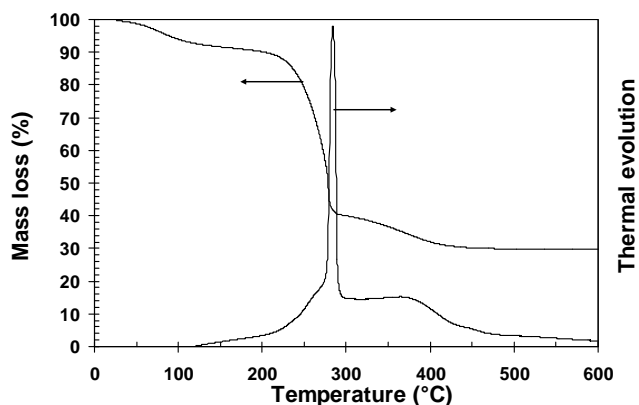


Figure 6-7: Mass loss and thermal evolution of mesoporous titania in an air flow during TGA/DTA analysis.

Figure 6-8 and Figure 6-9 present the nitrogen adsorption–desorption isotherm and pore size distribution of the unsupported TiO₂ membrane (free-standing film). The isotherm is typical type IV, characteristic of well-developed mesoporous materials. The BET surface of 188 m².g⁻¹ and pore volume of 0.273 cm³.g⁻¹ are high. The pore size distribution is narrow with a mean pore size of 4.5 nm, which is obtained from the Barrett, Joyner and Halenda (BJH ^[14]) model derived from the desorption branch. These results imply that the synthesized TiO₂ has good potential for application in fabricating mesoporous TiO₂ membranes, the pore size of which will be subsequently reduced further by ALD.

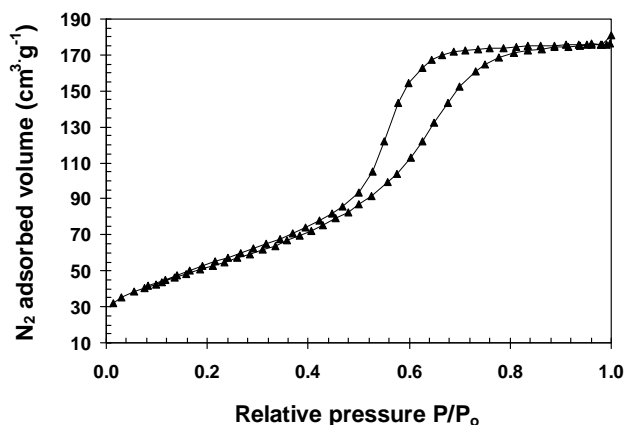


Figure 6-8: N₂ physisorption isotherm for unsupported mesoporous titania calcined in air at 400 °C.

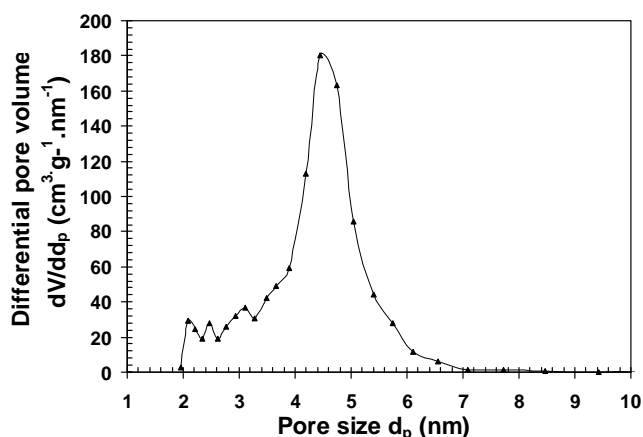


Figure 6-9: BJH pore size distribution of the unsupported mesoporous titania calcined in air at 400 °C (The line is a guide to the eye).

6.3.2 Gas separation behavior of modified membranes obtained via ALD of TiO_2 by using TiI_4 and H_2O as precursors

Figure 6-10 presents the permeance of single component gases (He , H_2 , CO_2 , and N_2) through mesoporous titania and titania membranes modified with 15 ALD cycles of TiO_2 deposition (~ 3 nm of thickness) in ALD-I reactor. A typical growth rate of TiO_2 on Corning glass is 0.036 nm/cycle. The gas permeances decrease with increasing molecular size of the permeating gas. The modified titania membrane exhibits a permeance one order of magnitude smaller than that of the unmodified membrane. This result is a strong indication that the pore structure of the membrane is modified by the ALD process. The permeance of H_2 is approximately two times higher than the value of CO_2 for the mesoporous titania. The gas transport through the mesoporous titania membrane occurs mainly by Knudsen diffusion, but there is a small contribution from viscous flow. In the case of the TiO_2 -deposited titania membrane, the permeance of H_2 is approximately four times higher than the value of CO_2 . Thus, the permselectivity of H_2/CO_2 of ~ 4 is close to the ideal permselectivity value based on the Knudsen diffusion mechanism. Hence the gas transport through the modified ALD membrane is mainly affected by the Knudsen diffusion. These results clearly show that with ALD it

is possible to reduce large pore diameters of titania and hence improve the H₂ selectivity. Knudsen diffusion is still dominant for the transport of H₂ and CO₂ in the modified titania membranes with 15 ALD cycles of TiO₂ deposition.

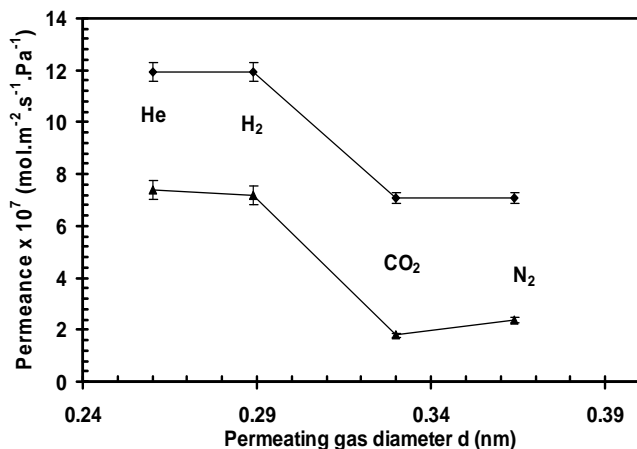


Figure 6-10: Relationship between permeance and the permeating gas diameters d from single gas permeation experiments at 25 °C and a pressure drop of 10^5 Pa of sol-gel derived titania (diamond symbols) and after modification with 15 ALD cycles (triangle symbols).

Although the deposition of TiO₂ is carried out more than 15 cycles, the measured H₂ selectivity after 30 ALD cycles is not higher, except a small decrease of the H₂ permeance with a factor of 2. It was visually observed that the deposition resulted in a non-uniform layer. Because of the reactor design, it is very difficult to control an effective transport of precursors over the sample in the flow channel. The inert gas leaks alongside the deposition chamber which perturbs the flow (see section 6.2.2).

6.3.3 Growth kinetics of the TDMAT/ H₂O process

In order to find out what kind of reactions take place during the deposition process at 100 °C, the evolution of film thickness with 50 cycles was evaluated by varying the TDMAT pulse times from 2 to 30 s and fixed parameters of 10s of TDMAT purge, 1 s of water pulse, and 60 s of water purge. Figure 6-11 presents the growth rate (the film thickness per cycle) vs. the TDMAT pulse time. The TiO₂ thickness measurements

were performed by ex-situ SE. Six measurements were obtained at random spots on each sample to verify the uniformity of the TiO_2 film. It is observed that a longer pulse time, i.e., longer than 2 s does not result in a higher growth rate. In addition, an ideal saturation curve is obtained when the TDMAT pulse time exceeds approximately 2 s. This observation indicates that the surface reactions are self-limiting at these pulse lengths. Although the H_2O pulse is not studied in detail, as it appears that there is no significant difference in growth rate between 1 s and 5 s of H_2O pulses. Since a high water dose requires much longer H_2O purge due to the high adsorption of water at the low deposition temperature $< 150\text{ }^\circ\text{C}$ ^[15], the 1 s of H_2O pulse is considered long enough for the water dose in this study.

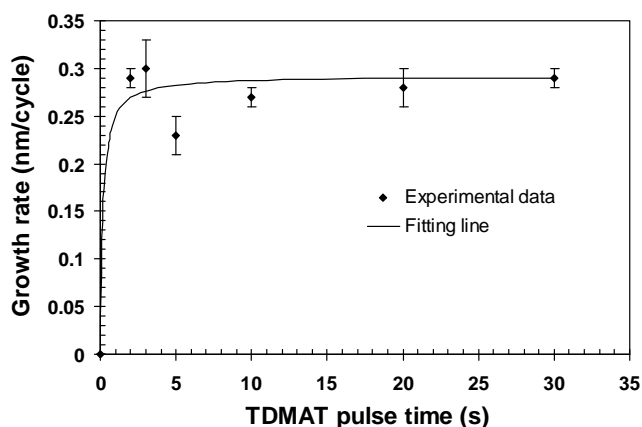


Figure 6-11: Growth rate of films deposited at 100 °C with 1 s H_2O pulse as a function of TDMAT pulse time and the fitting line assumes ideal saturation.

One of the typical features of ALD processes is the linear relationship of film thickness to the number of ALD cycles. Thus, growth linearity was cross-checked by in-situ measurements with SE. The depositions were carried out by varying the TDMAT pulse time from 5 to 30 s and fixed parameters of 10 s of TDMAT purge, 1 s of water pulse, and 60 s of water purge. As shown in Figure 6-12, the TiO_2 thickness showed a relatively linear relation with the number of cycles. A region of low growth rate is also observed, which is a characteristic of the nucleation delay (e.g., island persistence) during the first several cycles (~ 10 cycles). This is probably due to the number of

reactive sites –OH at the substrate Si/SiO₂ being lower than at the surface of the ALD-grown film. In the experiment of 1s of TDMAT pulse, the growth of the thickness is continuous, but is lower than those of the other longer pulse times. This in-situ observation, in combination with the above results (Figure 6-10) suggest that the investigated conditions belong to a non-ideal ALD growth mode. The non-ideal ALD displayed that the growth rate is not constant and the precursor molecules do not adsorb on the surface with perfect self-saturation. Such ALD growth mode has been reported in the work of Elam et al. ^[16] for TiN ALD from TDMAT and NH₃. According to their results, the growth rate of TiN did not saturate with increasing TDMAT exposure time and no “ALD window”, i.e., a temperature range at which the growth rate is constant, was observed. At the conditions used in this study, the TiO₂ growth rate varied from 0.23 to 0.3 nm/cycle (Figure 6-10), which was much higher than the reported values in the literature. There the growth rate was 0.03 to 0.05 nm/cycle within the temperature range of 50-150 °C ^[6, 8]. Maeng et al. ^[9] have obtained a high growth rate of 0.21 nm/cycle at 200 °C. They explained that the high growth rate might be caused by thermal decomposition of TDMAT at this high temperature. The non-ideal ALD growth characteristic of TDMAT was also mentioned in that work ^[9]. The higher growth rate in our study is possibly related to the deposition conditions in ALD. Since the thermal decomposition of TDMAT is known to be at about 150-180 °C ^[9], at a deposition temperature of 100 °C there is sufficient thermal energy for the precursor-surface reactions. Another benevolent factor can be the high adsorption of water at this temperature ^[15]. Thus, the concentration of the surface OH groups can be high, which leads to a large number of active sites resulting in a high growth rate. Another consideration is the use of carrier gas (dilution) to transport the precursor in other reports ^[6-9], which is not used in this study. No use of the carrier gas directly influences the precursor dose and a high probability for surface reactions to occur at the active sites. This may lead to readsorption of the reactants and consequently more than one monolayer per ALD cycle. Having a closer look at the published data, it appears very difficult to compare the results due to the differences of reactor designs and process conditions.

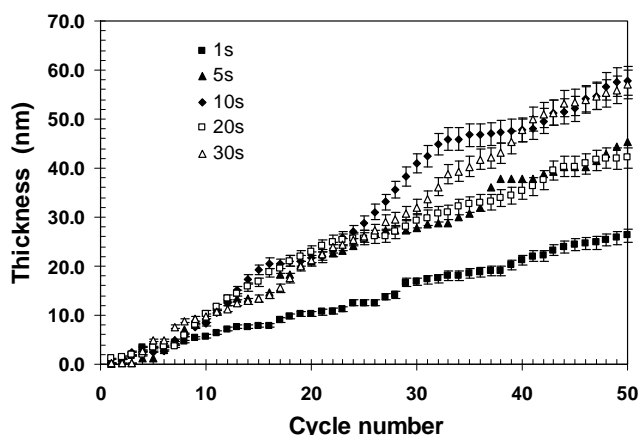


Figure 6-12: The relationship of film thicknesses deposited at 100 °C with 1 s H₂O pulse and different TDMAT pulse times to the cycle numbers.

Cross-sectional SEM micrographs of the TiO₂ films grown at 100 °C with 1 s H₂O pulse and different TDMAT pulse times (1-30 s) after 50 cycles are shown in Figure 6-13. Smooth layers of deposited TiO₂ with a well defined thickness profile can be observed for 5 s and 30 s of TDMAT pulses. The other samples are thinner and rougher. As shown in Figure 6-13, the thicknesses derived from in-situ SE using the EMA model are overestimated, in comparison with the ones determined by SEM. This can reflect the temperature dependence of the measured ellipsometric parameters, which are functions of the refractive indices. In-situ SE measurements were carried out at the deposition temperature (100 °C) and the sample drifted during the deposition, hence the temperature causes the refractive indices change lower. As a consequence, it is difficult to accurately determine the “real” thickness by this in-situ SE. Further investigations will be necessary to clarify this temperature affect and other factors.

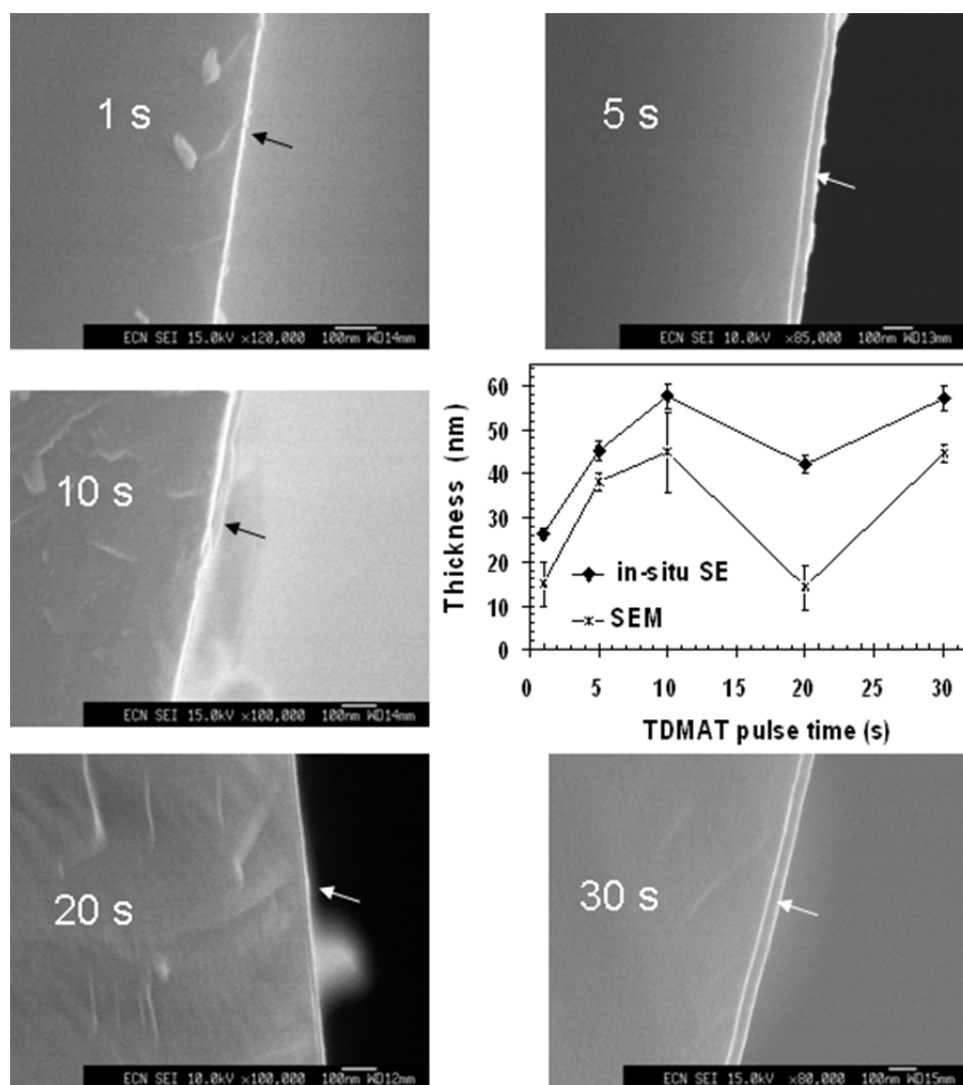


Figure 6-13: Cross-sectional SEM micrographs (the bar is 100 nm) and comparison of thicknesses measured by in-situ SE and SEM on films as deposited at 100 °C with 50 ALD cycles, 1 s H_2O pulse and different TDMAT pulse times (1-30 s).

AFM analysis of TiO_2 deposited on Si (100) reveals that the surface morphology of the TiO_2 layers is rather homogeneous. Figure 6-14 shows the AFM image of a TiO_2 layer (after 100 cycles) deposited at the conditions of 10 s TDMAT pulse, 10 s of TDMAT

purge, 1 s of water pulse, and 60 s of water purge. The R_{RMS} for a $1\ \mu\text{m} \times 1\ \mu\text{m}$ area is about 0.439 nm.

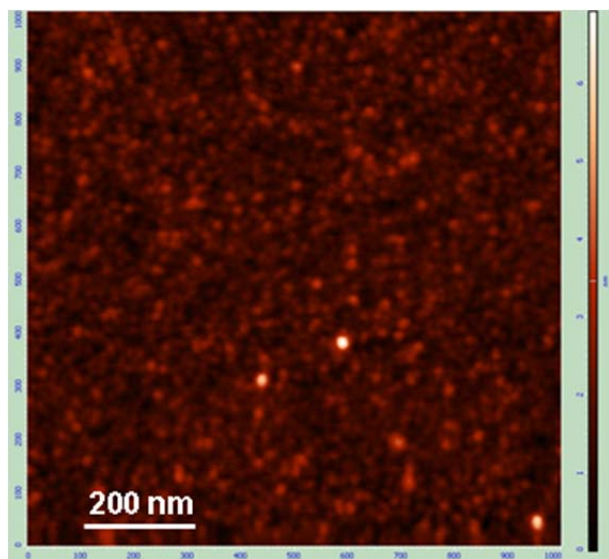


Figure 6-14: AFM image of TiO_2 (100 ALD cycles) deposited on dense Si (100) at 100°C .

6.3.4 Gas separation behavior of modified membranes via ALD of TiO_2 by using TDMAT and H_2O as precursors

Using the same ALD procedure described above for silicon using 30 s of TDMAT pulse, TiO_2 was deposited on sol-gel derived titania membranes. The permeance of H_2 and CO_2 at 10^5 Pa pressure difference for a titania membrane (a) and a titania membrane modified with ALD (b) are shown in Figure 6-15. The data are plotted versus the inverse square root of the temperature. The Knudsen-type permeation mode predicts that gas permeance will have an inverse square root dependency on molecular weight and temperature^[17]. For the sol-gel derived titania membrane, a linear behavior is observed for both gases, which is expected for Knudsen diffusion. The H_2 permselectivity and separation factor over CO_2 for this sol-gel derived membrane are ~ 4.51 and 2.64, respectively. After modification with 30 ALD cycles the permeance of the gases decreased and the temperature dependence of the H_2 permeance is different. The permeance through the modified ALD membrane increases with increasing temperature, while a slightly increase is observed for CO_2 . The change of slope in the

H₂ permeance is due to a change of the predominant transport mechanism, i.e., an activated diffusion mechanism. The permeance displays the temperature dependence of $1/T$, which is stronger than the $1/\sqrt{T}$ characteristic of Knudsen diffusion. The activation energy of H₂ permeance can be obtained by fitting the experimental gas permeance data to an Arrhenius expression:

$$F = F_0 \exp\left(\frac{-E_a}{RT}\right) \quad (6-9)$$

where F is the permeance ($\text{mol m}^{-2}\text{s}^{-1}\text{Pa}^{-1}$), F_0 is the pre-exponential factor ($\text{mol m}^{-2}\text{s}^{-1}\text{Pa}^{-1}$), E_a is the activation energy (J.mol^{-1}), R is the gas constant ($\text{J.mol}^{-1}\text{K}^{-1}$), and T is the permeation temperature (K). An activation energy of $\sim 7.75 \text{ kJ.mol}^{-1}$ is obtained for H₂, while the activation energy for CO₂ is 0.78 kJ.mol^{-1} . This can be related to the presence of micropores ($< 2 \text{ nm}$) in the membrane after ALD. The H₂ permselectivity increased to values in the range $6.71 - 10.91$ and the separation factor is approximately 5.52 .

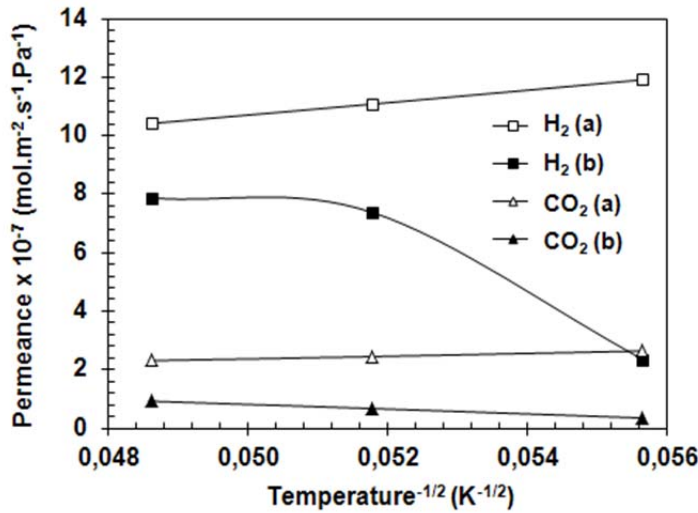


Figure 6-15: Permeance of H₂ and CO₂ with different temperatures at 10⁵ Pa pressure differences for a titania membrane before (a) and after modification with 30 ALD cycles (b).

The surface structure of the titania membrane after ALD is shown in Figure 6-16. It is observed that the surface structure of the membrane consists of aggregate particles. At first glance the surface structure appears to be the same before and after ALD, but careful examination reveals that it is smoother after ALD. This implies that there is lateral diffusion of titania deposited within the pores of the membrane. The grain size is approximately the same, but the roughness of the surface structure decreased after ALD. The calculated R_{RMS} values are 5.4 nm and 3.9 nm for the titania surface before and after ALD deposition.

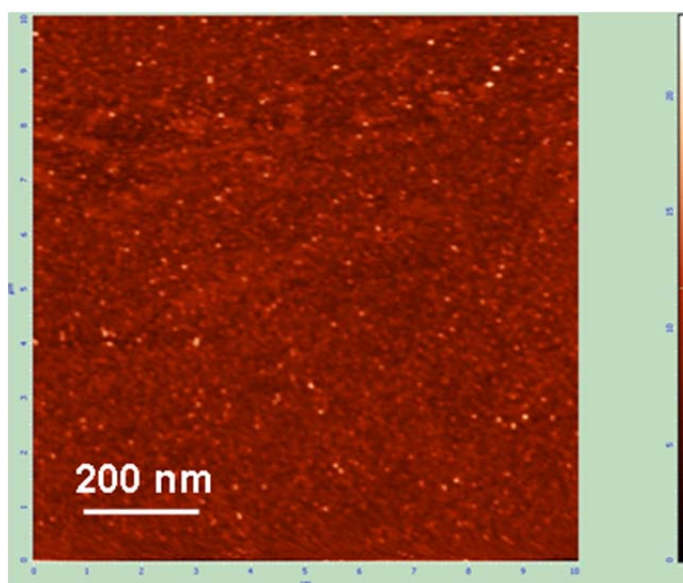


Figure 6-16: AFM image of the surface of a titania membrane after modification with 30 ALD cycles.

6.4 Conclusions

A crack-free mesoporous titania membrane supported on alumina was successfully fabricated via the sol-gel route using the tri-block copolymer P123 as a mesostructure-directing template. The controlled synthesis route resulted in a titania membrane with desired structural properties such as homogenous surface, large surface area ($188 \text{ m}^2\text{g}^{-1}$), and a small meso-pore size distribution around 4.5 nm.

Permeation of the gases through this membrane is mainly controlled by the Knudsen diffusion mechanism. The prepared membrane can be used further for the ALD modification in order to reduce the initial pore size. The results of this study indicated that the investigated ALD depositions improves the H₂ selectivity and separation properties of the membrane. The higher values of H₂ permselectivity and separation factor in the modified membranes are a good indication that smaller pore sizes have been produced after ALD. However, one has to recognize that this strongly affects to the gas permeance (low flux) and has to be optimised. The situ-SE measurements have shown to be valuable when monitoring film growth during ALD. The preliminary SE results of TiO₂ ALD films deposited on Si wafers has demonstrated the ability for this characterization technique to effectively engineering deposition. The results obtained indicate that the thickness analysis of TiO₂ structures using the EMA model are somewhat different from SEM and in any case should be used with caution. Further studies need to be devoted to optimize the process, as well as the modeling of the SE results. In the ALD-I reactor the large-dead volume at the cost of possible leakages has serious drawbacks. In contrast to the ALD-I reactor, the ALD-II reactor has a small volume and improved design. However, the use of TDMAT precursor may be limited for the TiO₂ ALD because of the non-ideal ALD growth characteristics of TDMAT/H₂O process.

Acknowledgements

The authors wish to thank Stanford University for supporting the research through the Global Climate and Energy Project (GCEP) and the sponsors of GCEP. We gratefully acknowledge Prof. Dr. F. Kapteijn (Delft University of Technology) and his co-workers for providing access to equipment for membrane characterization and M.D.A. Rietkerk and M. Roos (ECN) for gas permeation measurements and SEM, respectively. Thanks are due to Dr. R. van de Krol and A. Didden for providing access to the equipment ALD-II.

References

- [1] Chen, X. and Mao, S. S., "Titanium dioxide nanomaterials: Synthesis, properties, modifications, and applications", *Chemical Reviews*, Vol. 107, No. 7, 2007, pp. 2891-2959.
- [2] Chang, C. H., Gopalan, R., and Lin, Y. S., "A comparative-study on thermal and hydrothermal stability of alumina, titania and zirconia membranes", *Journal of Membrane Science*, Vol. 91, No. 1-2, 1994, pp. 27-45.
- [3] Van Gestel, T., Sebold, D., Kruidhof, H., and Bouwmeester, H. J. M., "ZrO₂ and TiO₂ membranes for nanofiltration and pervaporation - Part 2. Development of ZrO₂ and TiO₂ topayers for pervaporation", *Journal of Membrane Science*, Vol. 318, No. 1-2, 2008, pp. 413-421.
- [4] Kreiter, R., Rietkerk, M. D. A., Bonekamp, B. C., van Veen, H. M., Kessler, V. G., and Vente, J. F., "Sol-gel routes for microporous zirconia and titania membranes", *Journal of Sol-Gel Science and Technology*, Vol. 48, No. 1-2, 2008, pp. 203-211.
- [5] Aarik, J., Aidla, A., Mandar, H., and Uustare, T., "Atomic layer deposition of titanium dioxide from TiCl₄ and H₂O: investigation of growth mechanism", *Applied Surface Science*, Vol. 172, No. 1-2, 2001, pp. 148-158.
- [6] Lim, G. T. and Kim, D. H., "Characteristics of TiO_x films prepared by chemical vapor deposition using tetrakis-dimethyl-amido-titanium and water", *Thin Solid Films*, Vol. 498, No. 1-2, 2006, pp. 254-258.
- [7] Kukli, K., Aidla, A., Aarik, J., Schuisky, M., Harsta, A., Ritala, M., and Leskela, M., "Real-time monitoring in atomic layer deposition of TiO₂ from TiI₄ and H₂O-H₂O₂", *Langmuir*, Vol. 16, No. 21, 2000, pp. 8122-8128.
- [8] Xie, Q., Jiang, Y. L., Detavernier, C., Deduytsche, D., Van Meirhaeghe, R. L., Ru, G. P., Li, B. Z., and Qu, X. P., "Atomic layer deposition of TiO₂ from tetrakis-dimethyl-amido titanium or Ti isopropoxide precursors and H₂O", *Journal of Applied Physics*, Vol. 102, No. 8, 2007.

- [9] Maeng, W. J. and Kim, H., "Thermal and plasma-enhanced ALD of Ta and Ti oxide thin films from alkylamide precursors", *Electrochemical and Solid-State Letters*, Vol. 9, No. 6, 2006, pp. G191-G194.
- [10] Richman, E. K., Brezesinski, T., and Tolbert, S. H., "Vertically oriented hexagonal mesoporous films formed through nanometre-scale epitaxy", *Nature Materials*, Vol. 7, No. 9, 2008, pp. 712-717.
- [11] Tompkins, H. G. and Irene, E. A., *Handbook of Ellipsometry*, William Andrew Publishing, Norwich NY, 2005.
- [12] Langereis, E., Heil, S. B. S., Knoops, H. C. M., Keuning, W., van de Sanden, M. C. M., and Kessels, W. M. M., "In situ spectroscopic ellipsometry as a versatile tool for studying atomic layer deposition", *Journal of Physics D:Applied Physics*, Vol. 42, No. 7, 2009.
- [13] Fujiwara, H., *Spectroscopic Ellipsometry: Principles and Applications*, John Wiley and Sons 2007, pp. 1-388.
- [14] Barrett, E. P., Paul, L. G., and Halenda, P. P., "The Determination of Pore Volume and Area Distributions in Porous Substances. I. Computations from Nitrogen Isotherms", *Journal of the American Chemical Society*, Vol. 73, No. 1, 1951, pp. 373-380 .
- [15] Hausmann, D. M., Kim, E., Becker, J., and Gordon, R. G., "Atomic layer deposition of hafnium and zirconium oxides using metal amide precursors", *Chemistry of Materials*, Vol. 14, No. 10, 2002, pp. 4350-4358.
- [16] Elam, J. W., Schuisky, M., Ferguson, J. D., and George, S. M., "Surface chemistry and film growth during TiN atomic layer deposition using TDMAT and NH₃", *Thin Solid Films*, Vol. 436, No. 2, 2003, pp. 145-156.
- [17] Burggraaf, A. J., "Transport and separation properties of membranes with gases and vapours, *in* *Fundamentals of inorganic membrane science and technology*, edited by A. J. Burggraaf and L. Cot Membrane Science and Technology, Elsevier B.V., Amsterdam, 1996, pp. 331-434.

Chapter 7

Summary and Outlook

Abstract

This chapter presents the obtained results in retrospect and the outlook for further research. The main goals of the research described in this thesis are: i) to synthesize microporous membranes using a combination of sol-gel and Atomic Layer Deposition (ALD) processes, ii) to investigate the gas separation properties of these membranes with a focus on hydrogen separation. This work demonstrated that membranes modified with ALD exhibited significantly enhanced H₂ selectivity over CO₂. Furthermore, the proposed processing scheme shows potential for the development of composite membranes using other porous substrates.

7.1 Summary

Carbon capture and storage (CCS) can significantly contribute to the reduction of the emission of the greenhouse gas CO₂. Capture by means of CO₂ sorption or membrane-based separation processes is a promising way for achieving decarbonization of fuel or flue gas cleaning. In the field of separation and also purification of hydrogen, membrane separation technology has been and still is a focal point for Research and Development (R&D) due to its promising energy-efficiency, inherent selectivity and continuous operation. Research is being devoted to the development of membranes for H₂ separation from CO and CO₂ containing gas mixtures with high permeance and selectivity for conversion to electricity via fuel cells or directly in gas turbines. Currently, most membranes are being developed to separate H₂ from the underlying reaction mixtures obtained via coal gasification, steam-methane reforming, and water gas-shift processes. The key advantage of membrane separation, but also sorbent-based separation, is the possibility to go beyond the thermodynamic conversion limits set by the equilibrium constant of these H₂ production reactions. The in-situ separation of H₂ from the gas mixture through membranes shifts the equilibrium toward higher production of H₂ by preventing the back reaction. At the same time a stream of CO₂ is produced, pure enough for storage in geological reservoirs (empty oil and gas fields or deep saline aquifers) or for use in enhanced oil or gas recovery processes.

Inorganic microporous membranes are considered promising for H₂ separation in high-temperature H₂ production processes because of their high thermal and chemical stability. A brief review of the state-of-the-art inorganic membranes for H₂ separation in Chapter 1 reveals that the currently investigated microporous membranes with good performance in separating gas mixtures of H₂/CO₂, such as silica membranes, cannot be used at elevated temperatures and in the presence of high pressure steam due to hydrothermal instability. The major objective of this thesis is dedicated to fabricate and study a microporous non-silica based membrane system, consisting of an α -alumina macroporous support, a mesoporous intermediate layer, and a microporous γ -Al₂O₃, or TiO₂ top layer as illustrated in Figure 4 of Chapter 1, for H₂ separation from a gas

mixture with CO and CO₂. Thanks to a stacked layer architecture, it is possible to operate this membrane system in pressure gradients of up to 40 bars over the membrane assembly. We have studied the possibility to incorporate Al₂O₃, TiO₂, and ZrO₂ into the envisioned structure using the synthesis concept of a combination of sol-gel and Atomic Layer Deposition (ALD) processes.

The first aim of the research presented in this thesis was to develop a mesoporous membrane which could be easily modified with the ALD technique to become microporous. As is presented in Chapter 2, mesoporous membrane properties can be improved by combining sol-gel processing with evaporation-induced self-assembly (EISA), instead of a conventional sol-gel route. While in the sol-gel route the development of a porous structure is based on particle packing or polymerization, which yields materials with high tortuosity, the EISA route in principle yields materials with a lower tortuosity and a much higher porosity than is possible in randomly packed structures; in some cases even linear channels can be produced. A procedure for the synthesis of (semi-)crystalline, mesoporous γ -Al₂O₃ membranes by the colloidal sol-gel technique was established (Chapter 3). The obvious way for reducing the hydrothermal instability of silica would be replacing part of the silica by the much more stable alumina. The influence of mixing up to 64 mol% alumina on the microstructure of hybrid alumina-silica membranes was investigated. It was demonstrated that the hybrid material shows fingerprints of both the meso- and microporous nature of its constituents. This study suggests that a hybrid alumina-silica separating layer could never be chemically stable, because separate phases of γ -alumina and silica are still present on an extended scale, that can even be observed with XRD. It furthermore implies that the efforts of researchers ^[1-4] to make physical mixtures of silica and another oxide are doomed to fail. In Chapter 4, the procedure for mesoporous ZrO₂ membrane synthesis by combining the sol-gel method with the EISA process is presented. Calcination at high temperature (500 °C) leads to disorder or structural rearrangement, accompanied by layer cracking. However, the mesoporous structure is still retained in the zirconia membrane. The combination of the sol-gel with the EISA process was further developed to obtain mesoporous TiO₂ membranes, which

is described in Chapter 6. Different from mesoporous ZrO_2 , the ordered structure of TiO_2 in a thin film was conserved upon calcination at 400 °C.

The second important aim of this study was the use of the ALD process to tune the pore size of the mesoporous interlayer down to the kinetic diameter of the gasses to be separated. In Chapters 4, 5, and 6, ALD was demonstrated to be a viable technique for tuning mesopores of sol-gel derived membranes. In addition, ALD showed itself to be quite useful as a technique for defect repair (Chapter 4). The proposed processing scheme has potential to be extended to the development of composite membranes using other porous substrates.

The foremost goal of the ALD related membrane research was to provide enhanced H_2 selectivity of the synthesized membranes. Tests on the H_2/CO_2 separation were carried out on these synthesized membranes. The H_2 permeance and H_2/CO_2 selectivity of these membranes are $\sim 1\text{-}2 \times 10^{-7} \text{ mol.m}^{-2}.\text{s}^{-1}.\text{Pa}^{-1}$ and $\sim 5.8\text{-}10.9$ at 175 °C and 10^5 Pa pressure difference, respectively (Chapters 5 and 6). It was shown that ALD can elegantly be coupled with the sol-gel synthesis to fabricate microporous membranes on a large scale. The membranes should have target values of the H_2 permeance of the order $10^{-7} \text{ mol m}^{-2} \text{ s}^{-1} \text{ Pa}^{-1}$ and a H_2/CO_2 selectivity > 50 at $>400 \text{ °C}$ and $0.35 \times 10^5 \text{ Pa}$ [5]. The synthesized membranes clearly need to be further optimized for a viable application of H_2 separation from the reformat products.

7.2 Outlook

The following initiatives could extend the current results to improved quality of membranes for H_2 separation at elevated temperature and pressure:

- More fundamental studies should be performed to understand supported self – assembled mesoporous membrane layers. A technique that would directly enable to observe the orientation of the pores of the EISA process to the support should be explored. In fact, the real orientation of the cylindrical pores in this work could not be unambiguously defined in supported layers whereas in unsupported powders it could. Although Al_2O_3 -, TiO_2 -, and ZrO_2 -based materials are known to be more stable than

silica, more research is needed in this area, especially proving the enhanced stability against hydrothermal attack.

- In the gas permeation measurements of the supported membranes, temperatures higher than 175 °C could not be used due to the use of low-temperature O-ring seals in the membrane module. Since the H₂/CO₂ selectivity in binary gas mixtures is expected to significantly increase with temperature up to the envisaged operational temperature of about 450°C in e.g. water gas-shift reactions, it is worthwhile to modify the membrane module in such a way that higher temperature and hydrothermal conditions can be achieved. This will help to examine the stability and selectivity characteristics of the membranes. Furthermore, the described synthesis technology needs to be applied also on tubular membranes, which have large effective surface area and simple high-temperature sealing, and are the preferred geometry in large-scale commercial and industrial membrane applications.

- ALD offers a unique methodology for coating all the surfaces of mesoporous membranes in order to reduce the pore size in a controlled manner. However, a variety of pore step coverage mechanisms exist and investigations of thin-film deposition onto porous membranes would not be complete without closer consideration of these mechanisms. The deposition can take place inside the pores, form a partial cover over the pore entrances, or form particles within the pores of the membranes. Unfortunately, cross-sectional SEM images could not confirm the nature of ALD modification inside the pores, as our investigational technique (EDX) is limited to the determination of the depth penetration of the deposited material into the pores. It is, therefore, necessary to optimize cross-sectional TEM analysis, which will help to understand the penetration depth of the precursors into the pores.

- In situ ellipsometric measurements performed in the designed ALD system can provide optical information yielding numbers for the thickness, and density of a membrane layer. By monitoring the change of the optical characteristics of the membrane layer during the solvent vapor (water or alcohol) adsorption and desorption,

the information can even be used to calculate the porosity and pore size distribution of the membrane in a similar way as described for the permoporometry technique.

References

- [1] Gu, Y. F. and Oyama, S. T., "Permeation properties and hydrothermal stability of silica-titania membranes supported on porous alumina substrates", *Journal of Membrane Science*, Vol. 345, No. 1-2, 2009, pp. 267-275.
- [2] Fotou, G. P., Lin, Y. S., and Pratsinis, S. E., "Hydrothermal Stability of Pure and Modified Microporous Silica Membranes", *Journal of Materials Science*, Vol. 30, No. 11, 1995, pp. 2803-2808.
- [3] Yoshida, K., Hirano, Y., Fujii, H., Tsuru, T., and Asaeda, M., "Hydrothermal stability and performance of silica-zirconia membranes for hydrogen separation in hydrothermal conditions", *Journal of Chemical Engineering of Japan*, Vol. 34, No. 4, 2001, pp. 523-530.
- [4] Kanezashi, M. and Asaeda, M., "Hydrogen permeation characteristics and stability of Ni-doped silica membranes in steam at high temperature", *Journal of Membrane Science*, Vol. 271, No. 1-2, 2006, pp. 86-93.
- [5] DOE, U. S., Department of Energy, Technical plan-hydrogen production, energy efficiency and renewable energy. 2007.

Samenvatting en vooruitblik

Synopsis

In dit hoofdstuk worden de behaalde resultaten en de opties voor toekomstig onderzoek beschreven. De hoofddoelen van het in dit proefschrift beschreven onderzoek zijn i) het maken van microporeuze membranen gebruikmakend van een combinatie van sol-gel synthese en Atomaire Laag Depositie (ALD), ii) het bepalen van de gaspermeatie-eigenschappen van deze membranen met de focus op de waterstof afscheiding. Dit onderzoek laat zien, dat met ALD gemodificeerde membranen een significant hogere selectiviteit hebben ten opzichte van CO₂ dan onbehandelde membranen. Bovendien laat het voorgestelde productieschema zien dat er groot potentieel bestaat voor de ontwikkeling van composiet membranen op andere poreuze substraten.

7.3 Samenvatting

Afvang en opslag van koolstof dioxide, CO₂, kan in belangrijke mate bijdragen tot de reductie van het broeikasgas CO₂. Afvang door middel van sorptie, of op membraanscheiding gebaseerde processen zijn veelbelovende opties om brandstof koolstof vrij te maken of om CO₂ uit het verbrandingsgas te halen. Op het gebied van afscheiding en zuivering van waterstof, is membraantechnologie nog steeds hoofddoel van onderzoek en ontwikkeling (O&O) vanwege mogelijke hoge energie-efficiëntie, inherente selectiviteit, en continu bedrijf.

Het onderzoek is geweid aan de ontwikkeling van membranen voor het verwijderen van H₂ uit gasmengsels met CO en CO₂ met hoge permeantie en selectiviteit voor conversie naar elektriciteit via brandstofcellen of direct in een gasturbine.

Op dit moment worden de meeste membranen ontwikkeld om H₂ te halen uit de reactie-mengsels, die verkregen worden uit kolenvergassing, stoom-methaan reformatie en water-gas-shift processen. Het belangrijkste voordeel bij membraanscheiding maar ook scheiding met sorbents, is de mogelijk om voorbij de evenwichtsconversie te komen door via het wegvangen van een productgas de terugreactie onmogelijk te maken. Tegelijkertijd wordt een CO₂ stroom geproduceerd die zuiver genoeg is voor opslag in geologisch reservoirs (lege olie- en gasvelden, diepe zoute aquifers), of gebruik in verhoogde olie en gaswinningprocessen.

Anorganische membranen worden als veelbelovend beschouwd voor waterstofafscheiding uit hoge-temperatuur processen vanwege hun hoge thermische en chemische stabiliteit. Een kort overzicht van de huidige stand van zaken op het gebied van anorganische membranen voor H₂ afscheiding in hoofdstuk 1 leert dat in principe goed scheidende microporeuze membranen, zoals die gebaseerd op silica, niet toepasbaar zijn bij hoge temperatuur en in aanwezigheid van stoom op druk, in verband met slechte hydrothermale stabiliteit.

Het hoofddoel van het in dit proefschrift beschreven onderzoek is het maken van microporeuze membraansystemen, die niet op silica zijn gebaseerd, maar bestaan uit een α -alumina macroporeus support, een mesoporeuze tussenlaag en een microporeuze

top laag van $\gamma\text{-Al}_2\text{O}_3$ of TiO_2 zoals weergegeven in Figuur 4 van hoofdstuk 1, voor H_2 afscheiding uit een mengsel met CO en CO_2 . Dankzij de gelaagde structuur kunnen deze membranen gebruikt worden tot 40 bar transmembraan druk. De mogelijkheid bestaat om Al_2O_3 -, TiO_2 -, en ZrO_2 op te nemen in het beoogde membraanconcept door gebruik te maken van een syntheseconcept gebaseerd op een combinatie van sol-gel en ALD processen. Het eerste wat gedaan moest worden is het ontwikkelen van een mesoporeus membraan dat gemakkelijk met ALD gemodificeerd kon worden tot een microporeus membraan. Zoals aangegeven in Hoofdstuk 2 kunnen de membraaneigenschappen verbeterd worden door een combinatie van sol-gel en verdamping-geïnduceerde zelforganisatie (EISA) toe te passen in plaats van de conventionele sol-gel route. Waar in de sol-gel route de vorming van een poreuze structuur is gebaseerd op deeltjespakking of polymerisatie, leidend tot materialen met hoge tortuositeit, wordt in de EISA route hogere porositeit en lagere tortuositeit gevonden dan mogelijk is voor willekeurig gepakte structuren; in sommige gevallen kunnen zelfs lineaire poriën worden gevormd. Voor het bereiden van (semi)kristallijne $\gamma\text{-Al}_2\text{O}_3$ membranen werd een procedure vastgesteld voor het colloïdale sol-gel proces (Hoofdstuk 3). Een voor de handliggende methode voor het reduceren van de hydrothermale instabiliteit is het vervangen van silica door het veel stabielere alumina. De invloed van het mengen van silica met tot 64 mol % alumina op de microstructuur is onderzocht. Het bleek dat zich geen nieuwe verbinding vormde tussen silica en alumina en dat de ‘vingerafdrukken’ van beide deze zin loopt niet materialen, zowel qua Röntgenpatroon als qua porositeitstype, respectievelijk micro- en mesoporeus. Dit betekent dat op basis van deze mensels nooit een hydrothermaal stabiel hybride membraan kan worden gemaakt en dat pogingen van andere onderzoekers ^[1-4] om silica met een stabiel oxide te mengen gedoemd zijn te mislukken. In Hoofdstuk 4 wordt de procedure om een zirconia membraan te maken door combinatie van de sol-gel methode en de EISA methode gepresenteerd. Calcinatie van het verkregen product bij hoge temperatuur (500°C) leidde echter tot wanorde en reorganisatie van de membraanlaag met scheurvorming tot gevolg. De zirconia laag blijft wel mesoporeus.

Dezelfde methode is verder uitgewerkt voor mesoporeuze titania membranen, zoals beschreven in Hoofdstuk 6. Deze laag bleef in tact bij calcineren bij 400 °C.

Het tweede belangrijke doel van deze studie was het gebruiken van het ALD proces om poriegrootte van de mesoporeuze tussenlaag te verkleinen tot de kinetische diameter van de te scheiden gassen. In Hoofdstukken 4, 5 en 6 wordt getoond dat ALD inderdaad een werkende techniek is om dit te bereiken. Ook voor reparatie van defecten bleek ALD zeer bruikbaar (Hoofdstuk 4). Het voorgestelde processchema heeft het potentieel in zich om uitgebreid te worden naar de ontwikkeling van composietmembranen gebruikmakend, van andere poreuze substraten.

Het belangrijkste doel van het ALD-gerelateerde onderzoek was het verhogen van de selectiviteit voor waterstof. Experimenten met deze membranen voor de H₂/CO₂ scheiding leverden een H₂ permeantie en H₂/CO₂ selectiviteit van respectievelijk $\sim 1\text{--}2 \times 10^{-7} \text{ mol.m}^{-2}.\text{s}^{-1}.\text{Pa}^{-1}$ en $\sim 5.8\text{--}10.9$ bij 175 °C and 10⁵ Pa drukverschil (Hoofdstukken 5 en 6). Het is aangetoond dat ALD op elegante wijze kan worden gekoppeld aan de sol-gel methode voor de fabricage van microporeuze membranen op grote schaal. De eisen qua permeantie en H₂/CO₂ selectiviteit liggen op $10^{-7} \text{ mol m}^{-2} \text{ s}^{-1} \text{ Pa}^{-1}$ en > 50 , respectievelijk ^[5]. Er is dus nog duidelijk een noodzaak om de membranen te optimaliseren voordat ze in de afscheiding van waterstof uit reformaatmengsels op zinvolle wijze kunnen worden toegepast.

7.4 Vooruitblik

De volgende initiatieven kunnen de huidige resultaten brengen tot verbeterde kwaliteit van membranen voor H₂ afscheiding bij hoge temperatuur en druk:

- Er is meer fundamenteel onderzoek nodig om op een drager aangebrachte zelfassemblerende mesoporeuze membraanlagen te begrijpen. Een techniek waarmee direct de oriëntatie van met het EISA proces gemaakte poriën kan worden vastgesteld zou moeten worden onderzocht. Deze oriëntatie kon in de gedragen membraanlagen thans niet eenduidig worden vastgesteld, maar in de ongedragen lagen wel. Hoewel Al₂O₃, TiO₂, en ZrO₂ gebaseerde materialen bekend staan om hun verhoogde stabiliteit

ten opzichte van silica, moet meer onderzoek op dit gebied worden uitgevoerd, met name ten aanzien van de hydrothermale stabiliteit.

- In de gebruikte permeatie metingen aan gedragen membranen konden geen temperaturen hoger dan 175 °C gebruikt worden vanwege het materiaal van de gebruikte O-ring afdichtingen. Omdat verwacht wordt dat verhoogde temperatuur leidt tot verhoogde H₂/CO₂ selectiviteit in binaire mengsels, zou het geschikt maken van de apparatuur voor de reële, hydrothermale condities bij 450°C waardevol zijn voor vervolgonderzoek. Daarnaast moet de beschreven synthesesetchnologie aangepast worden voor buisvormige membranen, die een hoog effectief oppervlak hebben en eenvoudig af te dichten zijn bij hoge temperatuur. Buizen zijn de voorkeurs geometrie in commerciële industriële membraantoepassingen op grote schaal.

- ALD biedt unieke mogelijkheden om oppervlakken van een poreus membraan op gecontroleerde wijze te bedekken met focus of poriegroottereductie. Er bestaat echter een aantal mechanismen waardoor dit bewerkstelligd kan worden, welke nader onderzocht moeten worden. De depositie kan plaatsvinden in de porie, of gedeeltelijk de porieopening bedekken, of kleine deeltjes vormen in de poriën van het membraan. Helaas konden SEM beelden van de doorsneden van de lagen geen uitsluitsel geven over de daadwerkelijke situatie en EDX was niet in staat om de penetratie in de poriën vast te stellen. Dit noopt tot het optimaliseren van de analyse van doorsneden met TEM.

- *In-situ* ellipsometrie uitgevoerd aan de nieuw ontworpen ALD opstelling geeft waardevolle optische informatie waaruit kwantitatieve waarden voor laagdikte en –dichtheid verkregen kunnen worden. Combinatie met de verandering van optische karakteristieken door absorptie en desorptie van een damp zou het mogelijk moeten maken om porositeit en poriegrootteverdeling te bepalen, analoog aan de in dit proefschrift beschreven permoporometrie methode.

Referenties

- [1] Gu, Y. F. and Oyama, S. T., "Permeation properties and hydrothermal stability of silica-titania membranes supported on porous alumina substrates", *Journal of Membrane Science*, Vol. 345, No. 1-2, 2009, pp. 267-275.
- [2] Fotou, G. P., Lin, Y. S., and Pratsinis, S. E., "Hydrothermal Stability of Pure and Modified Microporous Silica Membranes", *Journal of Materials Science*, Vol. 30, No. 11, 1995, pp. 2803-2808.
- [3] Yoshida, K., Hirano, Y., Fujii, H., Tsuru, T., and Asaeda, M., "Hydrothermal stability and performance of silica-zirconia membranes for hydrogen separation in hydrothermal conditions", *Journal of Chemical Engineering of Japan*, Vol. 34, No. 4, 2001, pp. 523-530.
- [4] Kanezashi, M. and Asaeda, M., "Hydrogen permeation characteristics and stability of Ni-doped silica membranes in steam at high temperature", *Journal of Membrane Science*, Vol. 271, No. 1-2, 2006, pp. 86-93.
- [5] DOE, U. S., Department of Energy, Technical plan-hydrogen production, energy efficiency and renewable energy. 2007.

Acknowledgments

The past five years are like a journey, which I have had the joys and moments shared with colleagues, financial supporters (GCEP sponsors), friends, and my family. They have helped me in many different ways to make it a memorable experience. I will cherish the days spent at MECS.

I would like to sincerely thank my promotor Prof. Dr. Joop Schoonman for giving me the opportunity to pursue a Ph.D. under his guidance. Dr. Wim Haije, thank you very much for being more like a daily supervisor. With your input and those weekly discussions, you encouraged me to continue my research and ensured that I finished.

I am grateful to Prof. Dr. Freek Kapteijn, who allowed me to access to the equipments for membrane characterizations. A special notes to thanks to his (former) co-workers: Sander Brouwer, Johan Groen, Alberto M. Joaristi, Jorge Gascon, Enrique R. Fernandez, and Willy Rook.

To Prof. Dr. Bernard Dam, thank you so much for giving me the chance to stay in your group during my writing period and valuable advices for oral presentations.

I would like to thank Prof. Dr. M.C.M. van de Sanden and Prof. Dr. W.M.M. Kessels for arranging the ALD experiments in their group. A special note to thanks to their co-workers: C.A.A. van Helvoirt and V. Longo.

During my PhD project, the work was not going as planned (which was often the case), there were my colleagues and friends to help me to get right back on the track. I want to thank Ruben Abellon for helping me in many experiments and Marcel Bus for the AFM instructions. Unfortunately, I was not able to carry out as many experiments with ALD equipment as I had planned, but I would like to thank Joost Middelkoop for all the effort to install the equipment. I also want to thank my MECS colleagues for all the joyful moments we had, including coffee breaks and “borrel” time. I also appreciate all the nice times of Italian lunch (Loic, Mario, Ugo, Corrado, David, Yan), Chinese lunch (Elise, Fanny, Wang, Antonia), and the many barbecues, outings, and parties with Vietnamese friends (Vcid members). It will be a long list if I name you all, but

especially to thank Trinh M. Tuan, Nguyen M. Hoang, Nguyen V. Phu, Nnuyen T. Chi, Le H. Trung, and Nguyen V. Phuong for all the nice hanging out. Virginie & Alain, I cannot thank you enough for your continuous support and your kindness. Elise and Max, thanks for all your friendship.

During the past years, I spent very little time with my family. France is not so far, but is neither nearby. I am extremely grateful to my family for their monumental, unwavering support, and encouragements, and finally, to my dear late grand-mother, you are always in my heart! Kava, thanks for believing in me and encouraging me despite the distance.

For all the people I have not mentioned here, but who were always with me throughout the journey, thank you in all my endeavors.

Tran Thi Hoang Yen

Delft, September 2011

List of publications

The thesis is based on the following publications:

T.H.Y. Tran, H. Schut, W.G. Haije, and J. Schoonman, Structural characterization and porosity analysis in self-supported porous alumina-silica thin films, *Solid Thin Films*, 2011 (Chapter 3)

T.H.Y. Tran, W.G. Haije, V. Longo, W.M.M. Kessels, and J. Schoonman, Plasma-enhanced atomic layer deposition of titania on alumina for its potential use as a hydrogen-selective membrane, *Journal of Membrane Science*, 2011 (Chapter 5)

T.H.Y. Tran, W.G. Haije, M. de Niet, J. R. van Ommen, and J. Schoonman, Hydrogen separation properties of a sol-gel derived zirconia membrane with pore sizes tuned using atomic layer deposition of alumina, *International Journal of Hydrogen Energy*, submitted 2011 (Chapter 4)

T.H.Y. Tran, W.G. Haije, and J. Schoonman, Application of a sol-gel based nanostructured ceramic membrane for hydrogen separation in CO₂ capture purposes, *Nova Science Publishers Inc.*, Hauppauge New York, USA, 2010 (Chapter 2 and 6)

T.H.Y. Tran, K. Stoitsas, V.C. Feuillade, W. Haije, and J. Schoonman, Advanced Membrane Reactors in Energy Systems, *Ceramic Materials in Energy Systems for Sustainable Development*, Ed. L.Gauckler, Italy, 2009.

Oral presentations

T.H.Y. Tran, W. Haije, J. Schoonman, and B. Dam, Advanced Membrane Reactors in Energy Systems, Network Young Membrains (NYM), Montpellier, France, September 3-4, 2009.

T.H.Y. Tran, K. Stoitsas, W. Haije, and J. Schoonman, Pore-Size Control of Ceramic Membranes by Atomic Layer Deposition for Hydrogen Separation. International Conferences on Inorganic Membranes (ICIMs), Tokyo, Japan, August 18-22, 2008.

J. Schoonman and T.H.Y. Tran, Materials Science for the Protection of the Environment. Brasov Romania. BRAMAT 2008, February 25-28, 2009.

K. Stoitsas, T.H.Y. Tran, , W. Haije, and J. Schoonman, Synthesis, characterization and Separation Potential for H₂/CO₂ mixtures of Alumina and Silica Membranes (Before the modification with Atomic Layer Deposition). Annual Meeting Lunteren: Chemistry of the Solid State & Materials Science and Crystallography & Structural Research, Lunteren, The Netherlands, April 14-15, 2008.

J. Schoonman, T.H.Y. Tran, K. Stoitsas, V. Feuillade, and W. Haije, Advanced Membrane Reactors in Energy Systems. FORUM 2008. Ceramic Materials in Energy Systems for Sustainable Development. Chianciano Terme, Italy. July 5-8, 2008.

J. Schoonman, T. Tran, and K. Stoitsas, Clean Fossil Fuels: Advanced Membrane Reactors. Functional Nanoscale Materials and Devices for Chem., Bio Sensors, Photonics, and Energy Generations and Storage. NATO-Advanced Study Institute. Sinaia, Romania, June 4-15, 2007. (Invited Lecture and proceeding paper).

K. Stoitsas, J. Schoonman, and T.H.Y. Tran, Development of Membrane Materials for Advanced Reactors for Carbon-Free Fossil Fuel Conversion, Exxon Mobil Symposium, Brussels, Belgium, December 2007.

K. Stoitsas, T.H.Y. Tran, A. Weibel, and J. Schoonman, Development of Membrane Materials for Advanced Reactors for Carbon-Free Fossil Fuel Conversion, GCEP Symposium, Stanford University, September 18- 20, 2006.

Poster presentations

T.H.Y. Tran, W. Haije, and J. Schoonman, Atomic Layer Deposition (ALD) in mesoporous zirconia, Annual Meeting Lunteren: “Chemistry of the Solid State” & “Materials Science and Crystallography & Structural Research”, Lunteren, The Netherlands, April 20-21, 2009.

T.H.Y. Tran, K. Stoitsas, W. Haije, and J. Schoonman, Gas permeation characteristics of g-alumina Membranes Modified by Atomic Layer Deposition. International

Conferences on Inorganic Membranes (ICIMs), Tokyo, Japan, August 18-22, 2008. (Poster and extended abstract).

T.H.Y. Tran, K. Stoitsas, W. Haije, J. Schoonman, Gas permeation characteristics of γ -alumina membranes modified by Atomic Layer Deposition, Annual Meeting Lunteren: “Chemistry of the Solid State & Materials Science” and “Crystallography & Structural Research”, Lunteren, The Netherlands, April 14-15, 2008.

T.H.Y. Tran, K. Stoitsas, W. Haije, J. Schoonman, Preparation and characterization of alumina-silica composite membranes for modification by Atomic Layer Deposition technique, Annual Meeting Lunteren: Chemistry of the Solid State & Materials Science and Crystallography & Structural Research, Lunteren, The Netherlands, April 20-21, 2008.

T.H.Y. Tran, K. Stoitsas, W. Haije, and J. Schoonman, Monodisperse porous support system for Atomic Layer Deposition for pore size tuning of H_2 -selective porous membranes. GCEP Symposium, Stanford University, October 1-3, 2007.

Curriculum Vitae

Tran Thi Hoang Yen was born in Da Lat, Vietnam on December 6th, 1979. After graduating from the Biology major at Bui Thi Xuan high school (Vietnam), she started her studies at the University of “UFR des Sciences et Techniques”, Besançon (France). In 2001 she achieved a two-year sciences and technologies’ degree. In 2002 she obtained a B.Sc. in chemistry. In 2004 she obtained M.Sc. in chemistry (formulation and surface treatment). At this point she would like to continue her studies and to experience a different culture. Since 2006 she has been working towards her PhD degree at MECS, TU Delft, The Netherlands. During her PhD studies she presented her work at several conferences (Stanford GCEP Symposium, USA; ICIMs, Tokyo; NYM, France) and published outcomes of research in international journals (Solid Thin Films, Journal of Membrane Science, Nova Science Publishers). The results of the research carried out during her PhD studies are described in this thesis.